SHEAR WAVE SPLITTING
IN THE CENTRAL RIO GRANDE RIFT, NEW MEXICO

by

Serdar Ozalaybey

Submitted in Partial Fulfillment of the
Requirements for the Degree of
Master of Science
in Geophysics

New Mexico Institute of Mining and Technology

Socorro, New Mexico

December, 1990

ABSTRACT

SKS phases, digitally recorded at Socorro (WTX) and at Albuquerque (ANMO), have been analyzed for shear wave splitting to study shear wave polarization anisotropy in the central Rio Grande rift, New Mexico. The analysis showed that the direction of anisotropy differs significantly at both stations, with the fast direction NE–SW at WTX, and approximately N–S at ANMO. Neither fast direction reflects the present day east–west extension inferred from fault–plane solutions, alignment of basaltic cones and other indicators of stress for the Rio Grande rift. The NE–SW fast direction at WTX may be due to the strain–induced upper mantle alignment of olivine minerals inherited from the mid–Oligocene early rift extension. The fast direction may also be caused by the absolute plate motion direction of the North American Plate (~NE–SW) estimated for the Socorro region. The Socorro accommodation zone is another alternative explanation for the observed anisotropy at WTX. At ANMO, approximately the N–S fast direction may be caused by the tectonics of the Rio Grande rift and the rotation of the Colorado Plateau. If this is causing the anisotropy, then the fast direction may be reflecting a transitional change in the regional extension direction to the north of ANMO, from the present day extension direction to the extension across the Jemez lineament trending NNW–SSE. The fast direction might also be related to near N–S trending strike–slip wrench faults near ANMO.

ACKNOWLEDGMENTS

I would like to thank Dr. John W. Schlue for suggesting this project and his time and advice throughout this study.

TABLE OF CONTENTS

INTRODUCTION

Rifts occur in diverse tectonic environments that result from the continuous two dimensional evolution of the multi–plate mosaic of the Earth as well as from the interaction between the mantle process and the overlying lithosphere (Sengor and Burke, 1978). Although the mechanism of rifting and resulting surface structures may vary with fundamentally different tectonic environments, there are two main hypotheses for rifting : passive and active mantle hypotheses. In the passive mantle hypothesis, the horizontal movement of plates and their interaction give rise to differential stresses within the lithosphere that result in rifting. For example, these stresses may be generated at plate margins by ridge push or trench pull (Turcotte and Emmerman, 1983). The active mantle hypothesis requires an initial small convection in the mantle whose horizontal extent is about a few hundred kilometers that directly affects the overlying lithosphere and induces rifting (Mc Kenzie and Weiss, 1975). The sequence of events in the former hypothesis is rifting–uplifting–volcanism whereas in the latter one it is doming–volcanism–rifting. Because both sequences lead to identical structures, the relative sequence of events and so the type of rifting is a difficult question to answer once a mature rift has formed (Sengor and Burke, 1978). Figure 1 illustrates simplified block diagrams showing the evolution of a mature rift valley and the complexity of the rifting process.

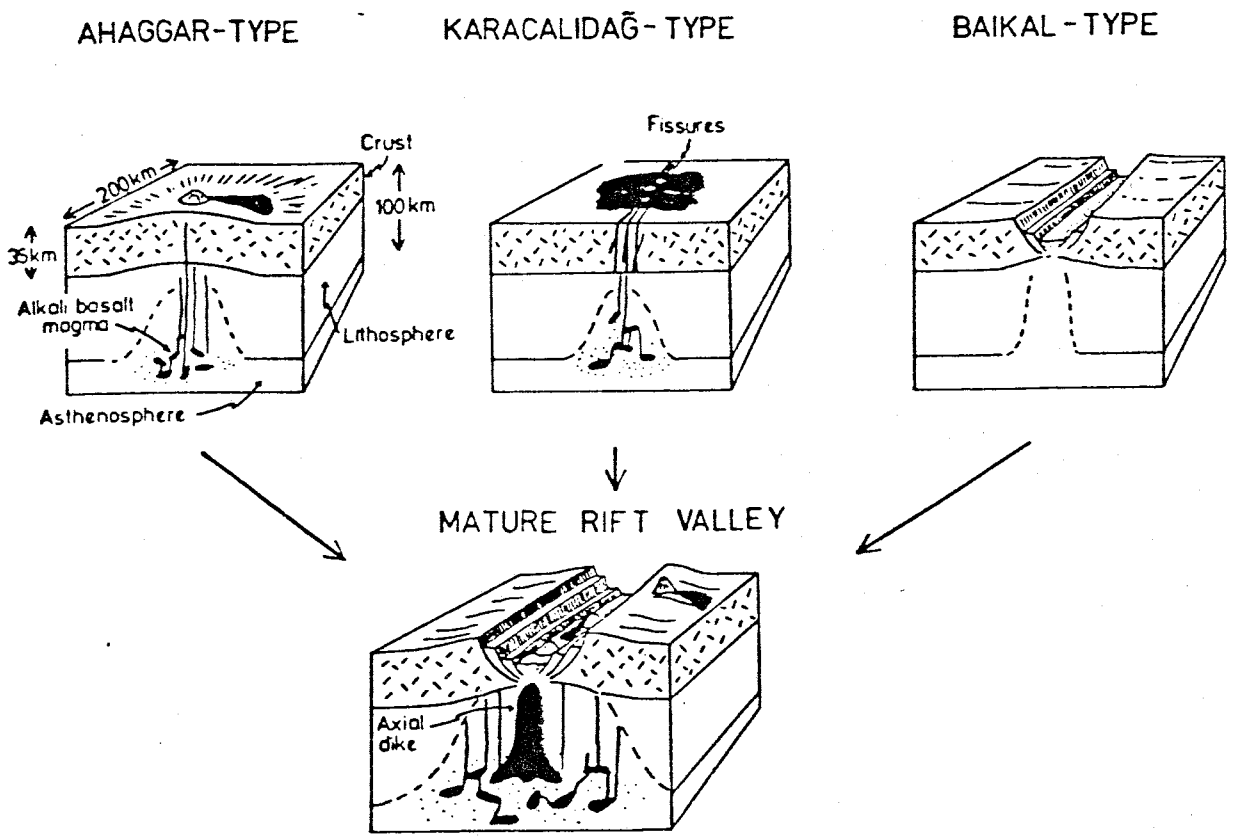

Fig. 1. Idealized and simplified block diagrams showing the evolution of a 'mature rift valley' from three different initial configurations. In Ahaggar-type rift valley evolution mantle is active and induces uplift and subsequent rifting. In this case volcanism is likely to predate rifting. In the Baikal-type mantle is passive and there is no pre-rifting doming or volcanism. Karacalidag-type was added to the diagram to illustrate a complexity: horizontal extension forms fissures through which magma wells up prior to major downfaulting and rift formation. Hence, in the geological record the sequence of events in the formation of a Karacalidag-type rift will look like those of an Ahaggar-type rift, although the mode of rifting was that of a Baikal-type rift. The end products of all rift processes are likely to look very similar.

Figure 1. Simplified block diagrams showing the evolution of a mature rift valley and the complexity of the rifting process (after Sengor and Burke, 1978).

An important peculiarity of the continental crust is that the history of different tectonic regimes is recorded at the surface of the Earth; the fabric of faults and joints, metamorphism and magmatism (through dikes and cones etc.) survive as relics during subsequent tectonic revolutions (Illies, 1981). The most direct observations of mantle and crustal deformation related to rifting come from geomorphology and geochemical properties as revealed at the Earth's surface. However, the relationship between these first order observations and rifting cannot be always explained without geophysical research probing of the crust–lithosphere and the lithosphere–asthenosphere boundaries. Observations such as fault plane solutions of earthquakes and the distribution of seismic velocities provide constraints on the orientation of the principal stresses and mantle–crustal deformation with depth, while gravity, magnetic, and heat flow observations can be used to estimate the boundaries of rift zones.

Continental rifts may be formed by simple extension, by shear, or more generally by the superposition of different deviatory regional stress fields. Whether the origin of rifting is passive or active, the driving tectonics, in most of the continental rifts, causes doming and cracking of the lithosphere, together with deep–seated extensional fracture systems in the crust. This deformation of the crust and lithosphere then gives rise to graben structures and extensional normal faulting. The characteristic structural types of rift zones are shown in Figure 2.

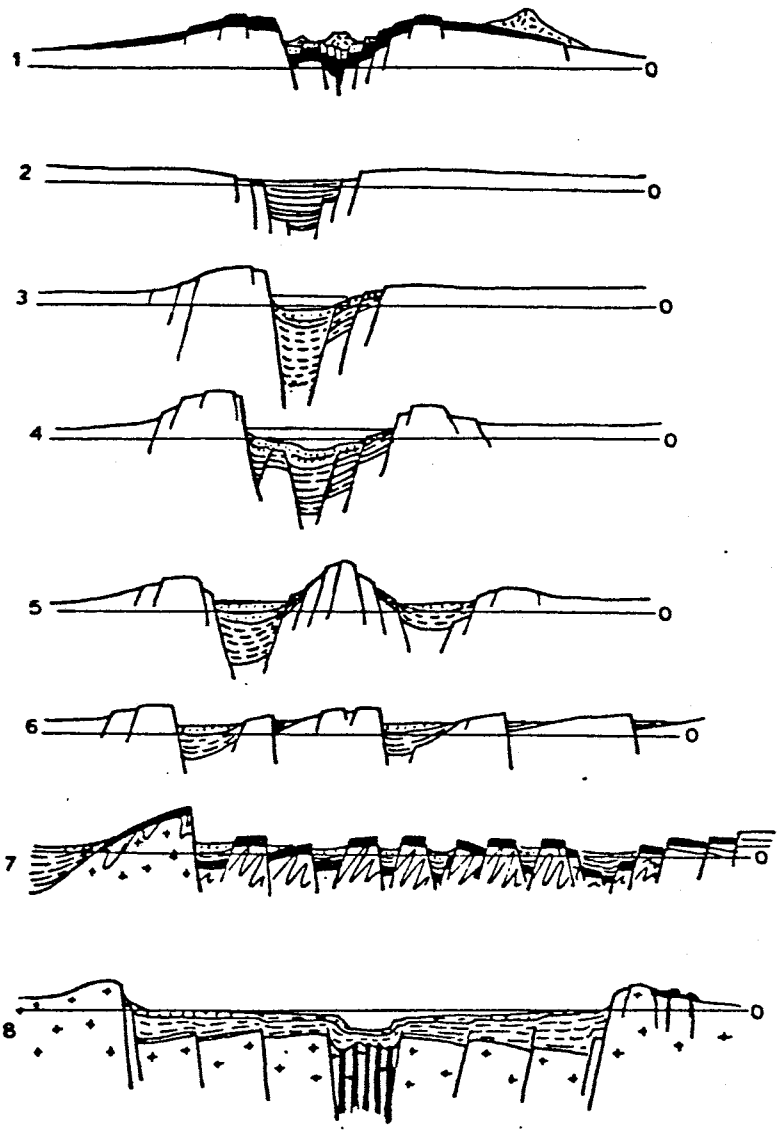

Fig. 2. The characteristic structural types of rift zones (the vertical scale of the cross-sections is exaggerated).
1 = arch-volcanic epiplatform rift zone (Kenyan rift zone according to B.H. Baker); 2–5 = crevice-like epiplatform rift zones: 2 = without marginal uplifts; 3 = with one marginal uplift; 4 = with two marginal uplifts; 5 = with internal uplift; 6 = zone of one-side tilted blocks; 7 = rift-like epiorogenic belt; 8 = intercontinental rift zone (rift zone of Red Sea according to C.L. Drake and R.W. Girdler).

Figure 2. The characteristic structural types of rift zones (after Milanovsky, 1972) .

Characteristic properties of these zones include high heat flow due to the rise of hot mantle materials as well as hydrothermal convections within the fissures, high seismicity levels associated with strain release due to stress accumulation at different depth levels and crustal extension, low seismic velocities in the upper mantle due to the lower rigidity of hotter–than–normal asthenosphere, relative uplift and magmatic activity, and negative gravity anomalies due to the thickness of unconsolidated sediments.

The deformation of the crust, lithosphere and the mantle due to rifting will result in spatial and temporal or directional variations in these properties listed above . Directional changes (anisotropy) along with spatial and temporal variations may be observed both in the crust and in the mantle. Anisotropy in the Earth's crust may dominantly be caused by stress–aligned fluid–filled cracks, microcracks, and preferentially oriented pore–space, known as extensive dilatancy anisotropy (EDA) (Crampin, 1984). Anisotropy in the mantle, on the other hand, appears to be mainly strain–induced . Strains associated with absolute plate motion, as in the oceanic upper mantle, as well as strains induced by the past and present internal deformation of the upper mantle by orogenic and rifting episodes, can cause the preferred orientations of upper mantle minerals such as olivine (Silver and Chan, 1990). This elastic anisotropy in rocks, which is a direct consequence of stress and strain relations, can be studied through elastic seismic waves. Anisotropy, in general, has two major effects on seismic wave propagation. First, the velocities of P waves (with longitudinal particle motion) and shear waves (with transverse particle motion)

may vary with the direction of propagation. This is called seismic velocity anisotropy or azimuthal anisotropy. Second, a pair of orthogonally polarized shear waves with different velocities along the same propagation direction may be generated from a single initial shear wave upon its passage through an anisotropic medium. This phenomenon is termed shear wave splitting by Crampin (1987). This second type of anisotropy effect on shear waves due to splitting will be referred as shear wave polarization anisotropy (or simply shear wave anisotropy) in this study.

There have been numerous successful studies of seismic velocity anisotropy of the upper mantle below the oceans using the measurements of P_n velocity from refraction surveys (e.g., Hess 1964; Raitt et al., 1969; Shearer and Orcutt, 1986) and both azimuthal and polarization anisotropy of long period surface waves (e.g., Forsyth, 1975; Schlue and Knopoff, 1977; Tanimoto and Anderson, 1985). The same techniques, however, have not been fully successful in studying anisotropy under the continents with a few exceptions (e.g., Bamford, 1977; Bamford et al., 1979; Vetter and Minster, 1981). Two problems in studying subcontinental anisotropy are the lack of appropriate earthquake sources sampling the upper mantle, and the shorter horizontal length scales of coherent deformation of the subcontinental mantle. The difficulty of studying continental anisotropy can be addressed by making use of shear wave polarization anisotropy due to shear wave splitting (described by Silver and Chan, 1988).

Shear waves provide an ideal tool for studying anisotropy through the phenomenon of shear wave splitting. A particular manifestation of seismic anisotropy which makes it ideal for studying upper mantle anisotropy is shear wave splitting, where an incident shear wave is polarized into two orthogonal directions travelling at different velocities with nearly identical paths. The polarization directions and the delay time between the two split shear arrivals may provide excellent lateral resolution of any anisotropy in the upper mantle, as well as constraints on the orientations of principal axes of strain and the depth extent of the anisotropy and its magnitude (Savage et al., 1990).

An ideal geometry is to use shear waves with near–vertical paths through the mantle. Shear waves most often used have been S waves directly above deep–focus earthquakes (e.g., Ando et al., 1983; Ando and Ishikawa, 1980; Bowman and Ando, 1987), ScS waves (shear waves reflected off the core–mantle boundary) (e.g., Ando, 1984; Fukao, 1984), and SKS waves (shear waves that travel through the mantle as an S wave and the outer liquid core as a P wave and then emerge as polarized S waves) (e.g., Vinnik et al., 1984, Kind et al., 1985; Silver and Chan, 1988; Savage et al., 1990; Silver and Chan, 1990) (see Figure 3).

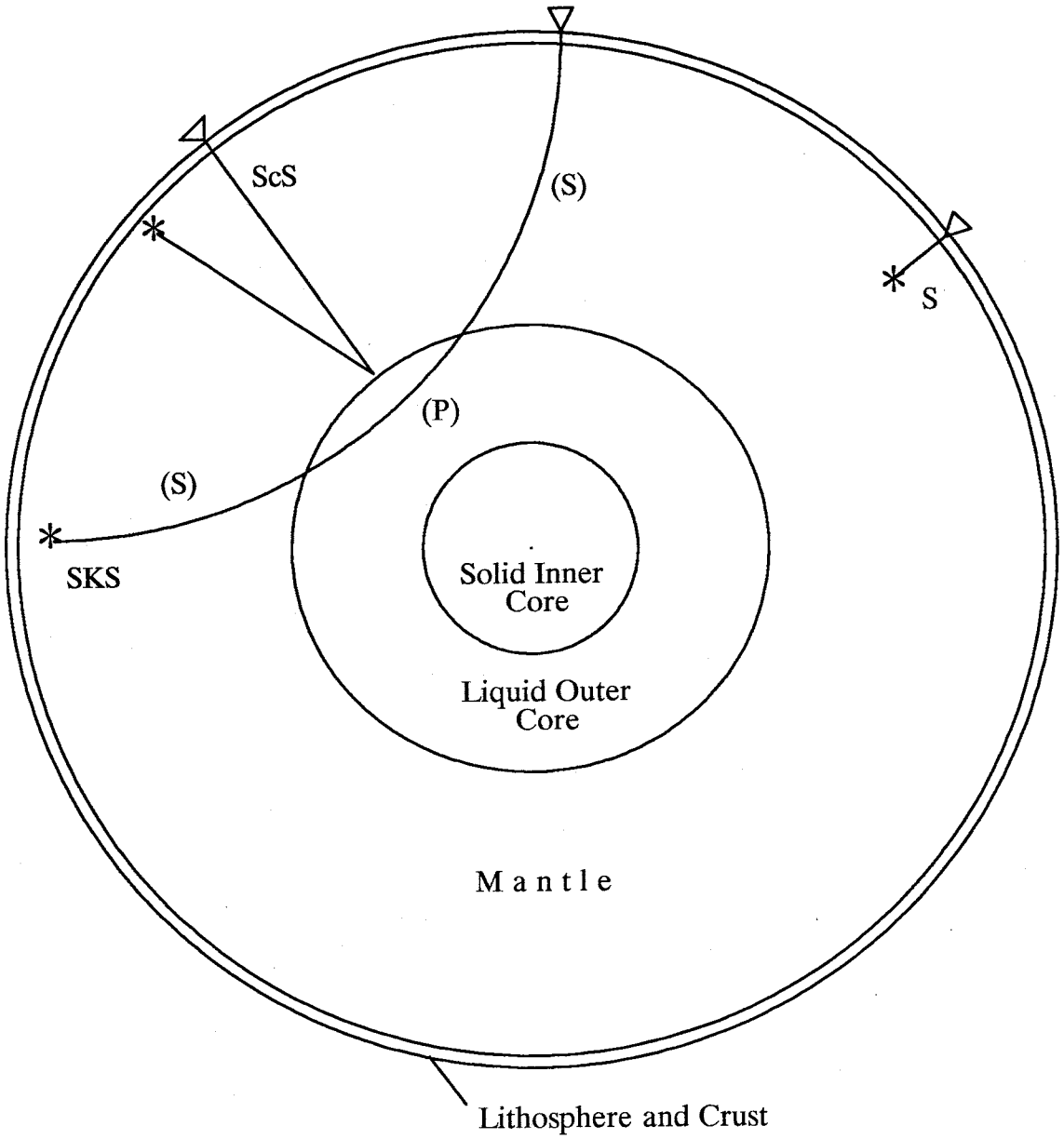

* Earthquake hypocenter

∇ Receivers

Figure 3. Schematic diagram showing shear waves S, ScS, and SKS with near vertical angle of incidence beneath the receivers .

It is clear that the study of shear wave polarization anisotropy through SKS splitting has become an important tool in studying continental anisotropy. We have chosen to analyze shear wave polarization anisotropy in the Rio Grande rift in order to clarify and understand the mechanism and dynamics of the continental rifting, in particular, the current stage of rifting in the Rio Grande rift. The objective of this study is, therefore, to determine the characteristics of SKS splitting beneath two stations in the central Rio Grande rift. The stations are located at Socorro (WTX) and Albuquerque (ANMO), New Mexico. To achieve our objective, digitally–recorded three component SKS waveforms have been examined for shear–wave splitting. In the following sections, I will give a brief geological and geophysical background of the Rio Grande rift followed by a detailed theory of shear wave splitting and the presentations of splitting measurements from each station. The final part of this study is the discussion and interpretation of observed SKS wave polarization anisotropy beneath the two stations and its relation to past and present tectonic processes of the Rio Grande rift.

GEOLOGICAL AND GEOPHYSICAL BACKGROUND

The Rio Grande rift is an extensional tectonic feature with en echelon rift valleys, extending south from Leadville, Colorado into Northern Mexico (Chapin, 1971) (Figure 4). The present day Rio Grande rift separates the Colorado Plateau and Basin and Range Provinces to the west from the Great Plains on the east (Figure 5). The Rio Grande rift began forming about 32 - 29 Ma and was intensely deformed by late Paleozoic and Laramide uplifts (Chapin and Seager, 1975). During the late Laramide (latest Palocene–earliest Eocene), the Colorado Plateau block was translated north–northeastward and experienced right lateral wrench faulting caused by a shift in the axis of horizontal compression from east–northeast to about N45°E (Chapin and Cather, 1983).

The rift can be divided into three segments. The northern segment, extending from Leadville to Alamosa, Colorado, is characterized by north - northwest trending grabens of Neogene age. This trend parallels the late Paleozoic and Laramide structural grain and exhibits a near–absence of synrift volcanism in the axial basins (Chapin, 1979).

The central part of the rift (from Alamosa to Socorro, New Mexico, which is the area of interest of this study), began to open about 29 Ma when the crust was subjected to regional extension. At this time, numerous normal faults trending approximately N10°W formed. This extensional fault zone allowed

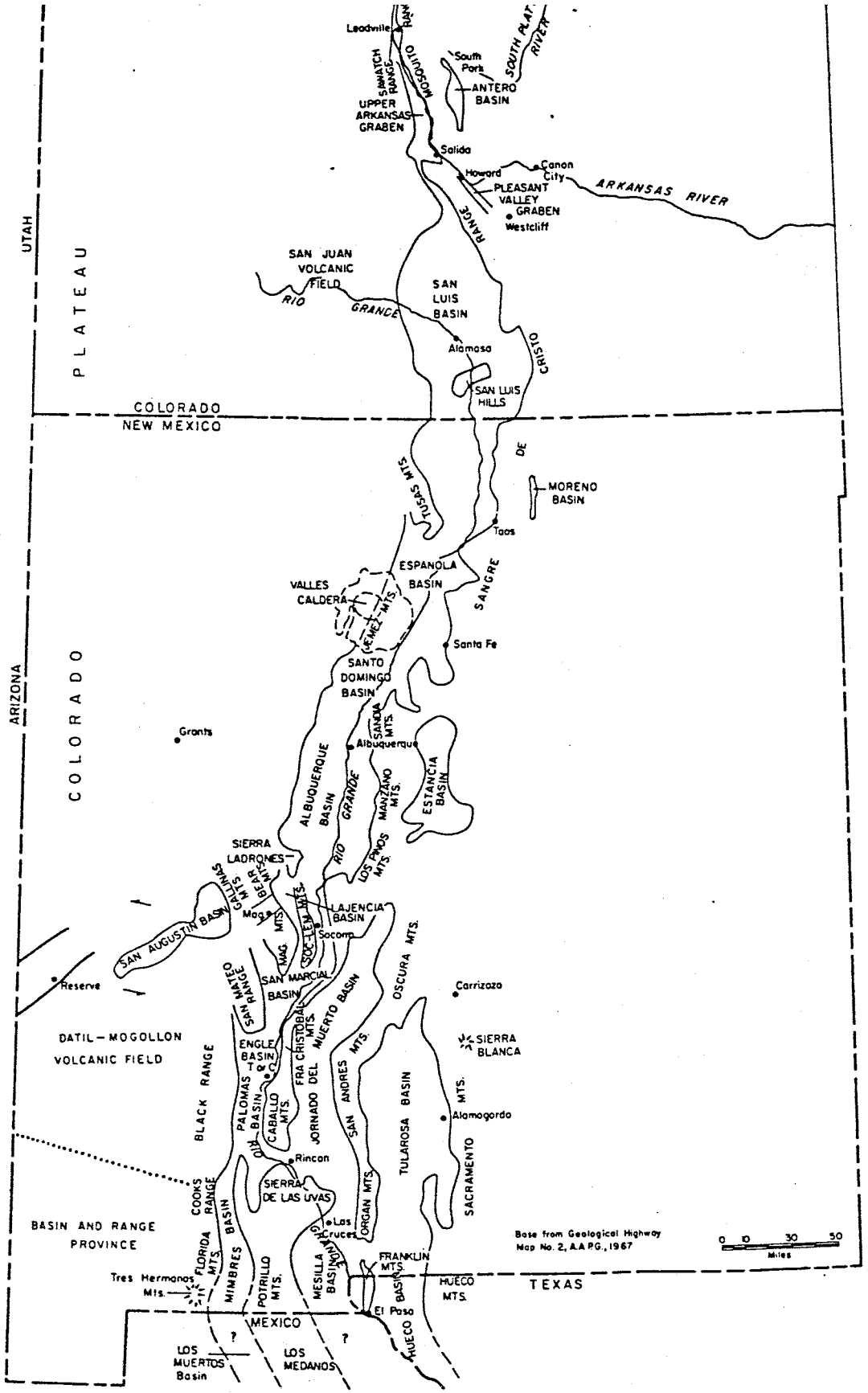

Figure 4. Generalized map of the Rio Grande rift (after Chapin, 1971) .

the intrusion of numerous dikes and the eruption of large volumes of basalt (Chapin,1975 and 1979). Early rift magmatism was relatively sparse within this segment, but late rift volcanism was voluminous (Chapin, 1979).

The southern segment of the Rio Grande rift (from Socorro to El Paso, Texas), widens into a north–trending series of parallel grabens and horsts. This segment is characterized by voluminous early and late rift magmatism. Magmatism has been widespread from southern Colorado to northern Mexico since 5 Ma (Chapin and Seager, 1975).

Combined paleostress determinations using dike trends, alignments of basaltic cones, and other geophysical and geological stress indicators such as fault plane solutions suggest that, on the east side of the Rio Grande rift (near the Southern Great Plains Province), the orientation of least horizontal principal stress has been N–S to NNE–SSW since at least 28 Ma (Aldrich et al., 1986), as opposed to the current approximately east–west extension for at least the central Rio Grande rift (Aldrich et al., 1986, Zoback and Zoback, 1980).

The region surrounding Socorro is one of the most geophysically studied regions of the Rio Grande rift. There exists a large, mid–crustal, sill–like magma body at an average depth of 19 km between Belen and Socorro (Sanford et al., 1973 and 1977) which may be bounded by an accommodation zone south of Socorro. The Socorro accommodation zone (SAZ), was first described as a deeply–seated transverse shear zone by Chapin et al. (1978), but more recently has been suggested to be relatively aseismic zone of weakness in an otherwise highly seismogenic zone, due to shearing in the crust (Sanford et al., 1990).

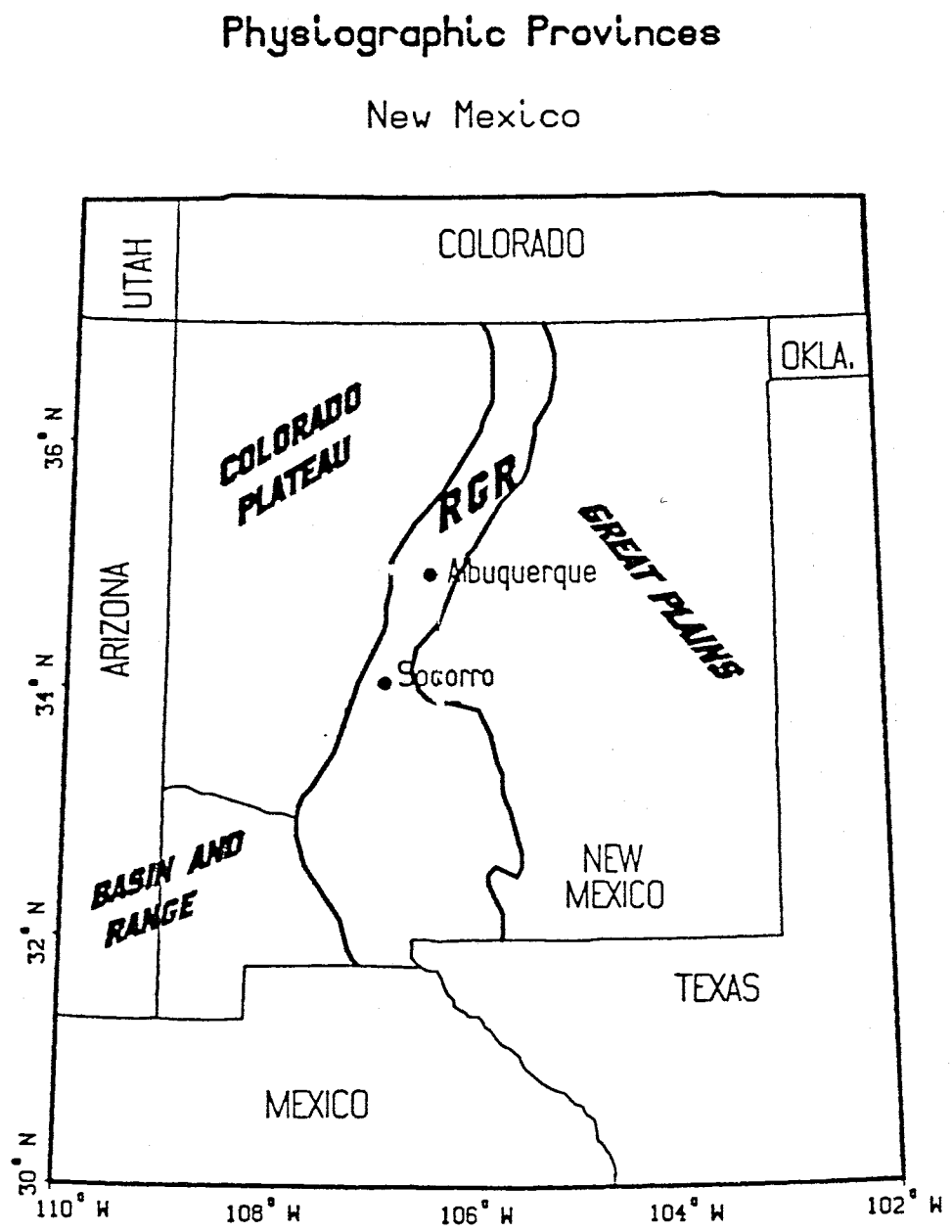

Figure 5. Physiographic provinces within the state of New Mexico (after Sinno et al., 1986).

In either case the SAZ appears to be a near–vertical structural discontinuity that trends parallel to the early rift extension directions and which may extend into the lower crustal plate (Chapin, 1989).

Various geophysical and geological data indicate that rifting is continuing at the present time. Observations include that of high heat flow (Reiter et al., 1975 and 1979), contemporary relative uplift (Larsen and Reilenger, 1983), a broad negative regional gravity anomaly considered evidence for a broad asthenospheric–lithospheric structure (Cordell, 1978), and other gravity results which have been interpreted as indicating an anomalous mantle upwarp at the base of the crust (Decker and Smithson, 1975). Other observations include high electrical conductivity at mid–crustal levels thought to be caused by basaltic magma upwelling from deeper sources (Hermance and Pederson, 1980), and micro–earthquake swarms in the Socorro region possibly indicating magma injection into the crust (Sanford and Einarsson, 1982).

REVIEW OF THEORY

Background

In isotropic, homogeneous and linearly elastic media, for wave propagation in any direction, there always exists two real body waves with mutually orthogonal and linear polarizations. The polarizations of such body waves are either parallel to the direction of propagation, for P waves, or perpendicular to it, for S waves. Figure 6 shows the polarizations of P and S waves on a plane wavefront Π, in a Cartesian coordinate system. The vector L describes a motion with velocity α corresponding to longitudinal (P) waves. The vectors M and N describe motion perpendicular to the direction of propagation with velocity β to corresponding transverse or shear (S) waves with its possible two components SH and SV respectively. The theoretical velocities α and β, for a given isotropic material with two independent elastic constants λ and μ (Lame' s constants) and the density of the material ρ, are given by :

$$\alpha = [(\lambda + 2 \mu) / \rho]^{1/2} \quad \text{and} \quad \beta = (\mu / \rho)^{1/2} .$$

The velocities α and β and their respective polarizations are constant and do not change with the direction of propagation in isotropic media.

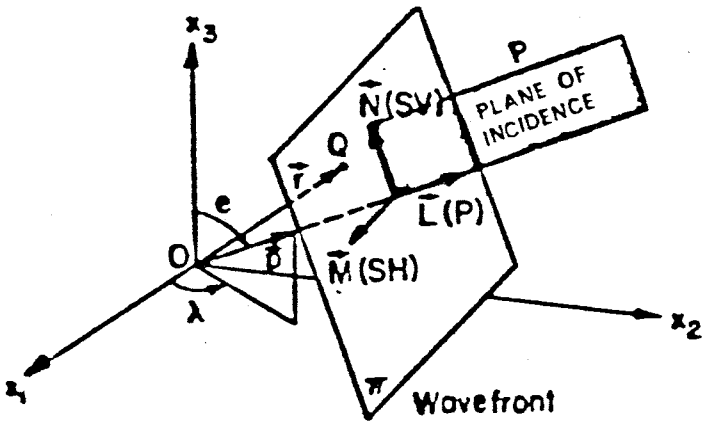

Figure 6. The polarizations of P and S waves in isotropic media (after Ben Menahem).

The behavior of body waves (as well as surface waves) in anisotropic media differs fundamentally from that in isotropic media. An anisotropic media, most generally, may be made up by a material that has its independent elastic constants arranged according to some form of symmetry system having its characteristic axes of symmetry and planes (eg. orthorombic, monoclinic, cubic , etc.). In such an anisotropic media, except along axis of symmetry , three real body waves with different velocities and mutually orthogonal polarizations may propagate for a given direction. The particle motions of the three body waves are not along the vectors L, M, and N (as shown in Figure 6), but are , in fact, fixed with respect to the anisotropy symmetry axes. Such body waves are called quasi-longitudinal and quasi-shear waves (Crampin, 1977). These quasi-body waves may be generated from body waves of any type (P, SV, or SH) upon incidence on a boundary between an isotropic lower and an anisotropic upper half space (Keith and Crampin, 1977a). The quasi-P wave has a greater velocity than the other two quasi-shear waves, as in the isotropic case. The quasi-shear waves traverse an anisotropic layer with different velocities resulting in a phase delay between the fast and slow quasi-shear waves; and upon re-entering into an isotropic medium each quasi-shear wave combines to generate S-wave motion containing a mixture of SV and SH polarization (Crampin, 1977). If the phase delays are sufficiently large compared to the period of the quasi-shear waves, the resultant S wave polarization will be anomalously different from that expected for isotropic S wave polarization. These deviations from isotropic wave motion result in various polarization anomalies which may be observed on three component seismograms of P and S waves, and may be used for detection of possible anisotropy.

The polarization anomalies caused by anisotropic layer(s) are, in general, controlled by a number of parameters. The dominant parameters controlling the magnitude of polarization anomalies are the degree of velocity anisotropy (fractional difference in velocity between the fast and slow directions), the thickness of the anisotropic layer(s), the direction of wave propagation with respect to the anisotropy symmetry axes, the angle of incidence, and the type of body wave that generates the quasi-body waves. A complete and detailed study of the reflected and transmitted body waves generated by P, SV, and SH waves incident from an isotropic lower half-space on a half-space of anisotropic material model can be found in Keith and Crampin (1977a); other detailed studies on seismic wave propagation and synthetic seismogram generation in anisotropic media can be found in Keith and Crampin (1977b and 1977c).

Shear Wave Splitting

Shear waves are very sensitive to the effects of anisotropy. Shear wave splitting, also known as shear wave bi–refringence or shear wave double–refraction, is based on the phenomenon that a shear wave propagating through an anisotropic region splits into two quasi–shear waves (or split shear waves) which travel at different velocities and with fixed mutually orthogonal polarizations (Crampin, 1985). These split shear waves propagate along nearly identical paths and upon re–entering an isotropic region, retain the fixed orthogonal directions and time delay due to the anisotropy along their raypath. Figure 7 illustrates the phenomenon of shear wave splitting schematically.

Two basic measurements, the time delay δt, and the fast polarization direction ϕ, can be made from the three component recordings of shear wave arrivals. The time delay, which is the differential arrival time between the two split shear waves, depends on the direction of propagation, the path length through the anisotropic region, and the degree of anisotropy, while the fast polarization direction, which is the polarization direction of the first arriving shear wave (or fast shear wave), is determined by the axes of anisotropy symmetries (Crampin, 1977).

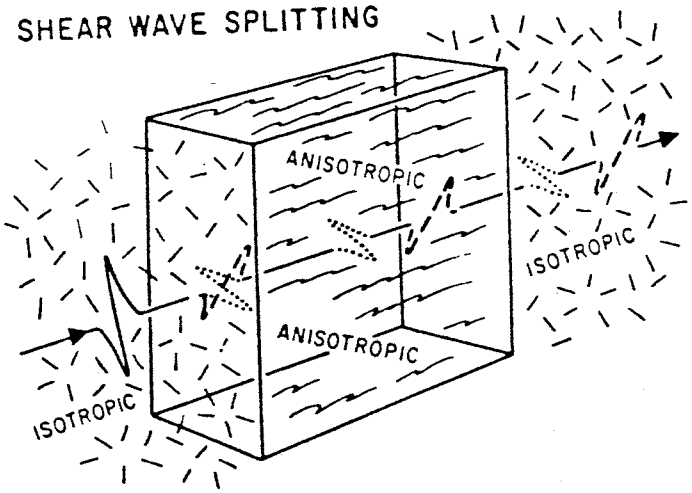

Figure 7. Shear wave splitting in anisotropic media (after Crampin,1981).

Factors Affecting Shear Wave Splitting

The ray paths and geometries used for shear wave splitting analysis are usually limited to shear waves which arrive at near–vertical incidence that are recorded on three component seismograms. This is because of the free surface effect on the recorded shear waves. It was first shown by Nuttli (1961) that the particle motion of an incident shear wave on the free surface could be altered substantially if the angle of incidence was greater than the critical angle i_c (Figure 8). The polarizations of shear waves arriving incident at angles greater than the critical angle are severely distorted by reflected S–to–P converted phases at the free surface, so that the original polarizations of shear waves can not be recovered. This angle defines a " shear wave window", within which the shear waveforms are not distorted by the free surface interactions (Booth and Crampin, 1985). Therefore, surface observations of shear wave splitting is limited to the shear waves incident at an angle inside this shear wave window. Rays within the shear wave window refract in the near surface layers to vertical or near vertical paths. Thus shear wave splitting analysis generally is conducted using only the horizontal seismogram components (Savage et al., 1990).

Shear wave splitting is best displayed on horizontal particle motion (polarization) diagrams. Polarization anomalies caused by shear wave splitting can be seen in these diagrams of the shear wave arrivals as departures from

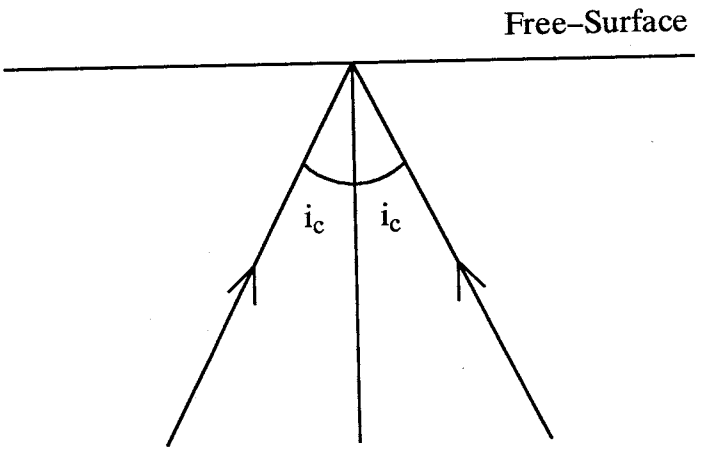

Figure 8. The cone delineated by the critical angle defines the shear wave window for splitting measurements.

The critical angle $i_c = \mathrm{Sin}^{-1}(V_s / V_p)$

where V_p and V_s are the near–surface velocities of P and S waves respectively. The critical angle is about 35^o for a Poisson's ratio of 0.25.

the direction of particle motion predicted by isotropic theory. That is, since the two split shear waves arrive at different times, the particle motion is not rectilinear and thus it is unlike the particle motion of shear waves which have travelled through an isotropic medium (Bowman and Ando, 1987). Thus the polarization anomalies as observed on the particle motion diagrams are the most indicative of shear wave splitting.

Shear waves with different wavelengths can sense different scales of anisotropy. For example, seismic wavelengths on the order of several tens of meters to several kilometers can be used to study crustal anisotropy, while wavelengths of several tens of kilometers can be used to study mantle anisotropy. Accordingly, the magnitude and characteristics of the polarization anomalies caused by shear wave splitting depend upon on the period of shear waves, the dimensions of anisotropic region, the degree of velocity anisotropy, and the direction of propagation with respect to axes of anisotropy. For crustal anisotropy, time delays can be as small as 2 msec/km (Booth et al., 1990), while for mantle anisotropy they can be around 1 second (Silver and Chan, 1988). If the time delay is small compared to the periods of split shear waves e.g., less than a quarter of the signal period (Booth et al., 1990), the polarization anomalies become less anomalous, masking the effects of splitting. Consequently, if the velocities of split shear waves become similar, or the period of a split shear wave increases, or the thickness of an anisotropic layer decreases, the time delay between the split shear waves is smaller, and therefore less anomalous motion is generated (Keith and Crampin, 1977b).

A linear trend for shear wave particle motion usually implies that the medium in which the wave has propagated is isotropic. However, linearity is also observed if the shear wave has an initial source polarization that coincides with the axis of symmetries of an anisotropic medium; no shear wave splitting will occur in this case. Therefore, information from linear particle motion is important to constraint the nature of anisotropy (Ando et al., 1983).

Laterally heterogeneous structures and scatterers may also cause irregularities and anomalies of the particle motions of shear waves. However, the effects of anisotropy can be easily distinguished from the effects of lateral heterogenity by polarization studies (Crampin, 1987). This comes from the fact that anisotropy causes shear wave splitting with fixed and orthogonally polarized shear wave arrivals, and therefore the polarization directions of fast shear waves from different azimuths will show uniform alignments that cannot be caused by lateral heterogenity.

Shear wave splitting may be caused by a single anisotropic layer or multiple regions of anisotropy along the ray path. If we assume that a single anisotropic layer of thickness L with isotropic shear velocity β_0 is responsible for the time delay δt observed for a shear wave incident along a vertical ray path, then these parameters can be related by the following approximate equation (Silver and Chan, 1988) :

$$\delta t = L \epsilon / \beta_0 \qquad (1)$$

where ϵ ($<<1$) is the fractional difference in velocity between the fast and

slow polarization directions. From this relationship, it is evident that the delay time is directly proportional with the increasing thickness L or ϵ. The fast polarization direction (denoted by ϕ) is simply indicative of the geographic orientation of the fast velocity direction (slow velocity direction perpendicular to it). It should be emphasized that the fast polarization direction reflects only the anisotropic fabric of the last significant anisotropic path traversed, while the time delay (δt) will be the cumulative effect of anisotropy along the entire ray path (the effects of anisotropy that split a previously split leading shear wave at a later stage in its ray path) (Savage et al., 1990). Thus, for multiple regions of anisotropy, the relationship between the splitting parameters and anisotropy can become quite complicated.

Shear Wave Splitting Through SKS Phases

The teleseismic seismic shear wave phase SKS propagates as an S wave from an earthquake to the core–mantle boundary (CMB), through the liquid outer core as a P wave, and again as an S wave from the CMB to the receiving station (see Figure 3). Because SKS has been converted from a P wave to an S wave at the CMB, it will be polarized in the vertical plane of propagation for a spherically symmetric, isotropic Earth (Silver and Chan,1988). Thus, on the receiver side, SKS emerges from the CMB as a radially polarized SV shear wave possessing a nearly vertical mantle path.

The phase SKS has many advantages for the study of upper mantle anisotropy, particularly continental anisotropy, compared to other shear phases such as ScS and S. First, the observed anisotropy using SKS splitting is confined to the receiver side of the path due to the P to S conversion at the CMB. For ScS and S wave splitting, the anisotropy can be on the source side as well (Kind et al., 1985). SKS, with its near–vertical ray path through the mantle on the receiver side is, therefore, sensitive only to splitting produced by anisotropy for the leg underneath the station. Secondly, since SKS is initially radially polarized SV (in the horizontal plane pointing from event to the station) on the receiver side, anisotropy is more easily detected than with the other shear phases,since their initial source polarizations may not be well known. Thus, if an effective anisotropic path is travelled between the CMB and the station by SKS, it will be split and will give rise to

detectible energy on the horizontal transverse component of motion (the transverse component is orthogonal to the radial component). As the effects of anisotropy and lateral heterogenity can be distinguished on polarization diagrams, the transverse component energy provides an excellent diagnostic for the presence of anisotropy (Silver and Chan, 1990). Third, the best distance range for SKS splitting measurements is 85°–110°, where SKS is both well isolated from ScS and S and sufficiently energetic. This allows the study of stable continental interiors, which are typically devoid of earthquakes and are not otherwise sampled by seismic sources (Silver and Chan, 1988). Finally, at these distances, SKS has a nearly vertical ray path due to the steep refraction angle at the CMB, so that the polarization anomalies are well within the shear wave window.

ANALYSIS OF SKS ARRIVALS

Method

Four methods generally have been used to resolve the shear polarization direction and time delay resulting from shear wave splitting. In the method used by Ando et al. (1983), the original horizontal seismograms are rotated to various azimuths. The polarization direction of the fast shear wave is the azimuth at which the fast and slow shear wave arrivals have the largest time separation and the amount of time separation is the time delay measured directly from the orthogonal seismograms generated at that azimuth. In a second method (e.g., Crampin et al., 1985; Booth et al., 1990), the polarization diagrams on the horizontal plane of radial and transverse components are displayed for a succession of small time intervals starting from the onset of the fast shear arrival. Then the fast polarization direction is determined from the linear or near linear particle motion of the first shear arrival. The time delay is also measured from the polarization diagrams by counting sample intervals between the onset of the leading fast shear wave and an abrupt change in polarization which is taken to indicate the arrival of the slow shear wave. A third method, by Bowman Ando (1987), maximizes the cross-correlation function between the fast and slow components to determine the time delay. In the aspect ratio method of Shih et al.(1989), the ratio of the projection of particle displacements onto a pair orthogonal axes (aspect ratio) is maximized as a function of azimuth. The fast polarization direction is the azimuth of the most linear particle motion at which the maximum aspect ratio occurs.

All of the methods above have relative strengths and weakness in measuring shear wave splitting parameters. The success of the each method is directly proportional to the amount of time separation (time delay) between the split arrivals. Since the time delays are usually of the order of a fraction of a second, these methods are only applicable to high frequency records of local events (Vinnik et al., 1989) .

The method which will be used to measure the splitting parameters from SKS arrivals in this study is described by Silver and Chan (1988). This method takes full advantage of the unique features of SKS in order to resolve the splitting parameters from the horizontal component seismograms of the SKS. The idea is to analyze the horizontal transverse component of the SKS. In the absence of anisotropy, for a laterally homogeneous Earth, the transverse component T(t) will be identically zero for a noise-free SKS seismogram, since SKS is strictly polarized as SV in the radial direction upon leaving the CMB on the receiver side. This is one of the important features of SKS which will be utilized as a constraint in finding the splitting parameters (Silver and Chan,1988). (See Figure 9 for a definition of radial and transverse directions and the projections of original horizontal seismograms onto these directions). In the presence of anisotropy, for near-vertical propagation, assuming transverse isotropy with a horizontal axis of symmetry, the radial and transverse components are related by

$$R(t) = s(t)\,\mathrm{Cos}^2\beta + s(t-\delta t)\,\mathrm{Sin}^2\beta \qquad (4)$$

$$T(t) = -1/2\,[s(t) - s(t-\delta t)]\,\mathrm{Sin}\,(2\beta) \qquad (5)$$

where β is the angle between the fast and radial directions and s(t) is the radial waveform in the absence of anisotropy. These equations show that for δt small,

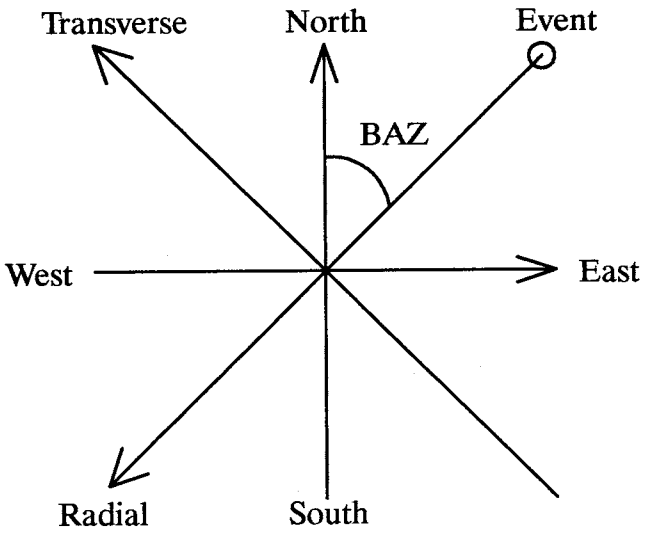

Figure 9. Schematic diagram showing radial and transverse directions on the horizontal plane with respect to the recording coordinate system. Arrows denote positive motion directions. The radial component R, and transverse component T, are obtained by vectorially rotating the original horizontal component seismograms into the theoretical ray back azimuth direction :

$$R(t) = -[X(t)\ \mathrm{Cos\ BAZ} + Y(t)\ \mathrm{Sin\ BAZ}] \quad (2)$$

$$T(t) = [X(t)\ \mathrm{Sin\ BAZ} - Y(t)\ \mathrm{Cos\ BAZ}] \quad (3)$$

where X(t) and Y(t) are the North–South (N–S) and the East–West (E–W) horizontal component seismograms respectively. BAZ is the ray back–azimuth measured clockwise from North.

the transverse component will be approximately equal to the time derivative of the radial component. It can also be seen from equation (5) that T(t) will be near zero if the anisotropy is small ($\delta t \sim 0$) or if the anisotropy is strong but the back azimuth is along the fast or slow polarization direction ($\beta = 0^o$, 90^o, 180^o,360^o) (Silver and Chan,1988; Vinnik et al., 1989).

In making splitting measurements, a $(\phi,\delta t)$ pair will be found that most successfully removes the effects of anisotropy from the transverse component of SKS. This can be done by minimizing energy $E_t(\phi, \delta t)$ on the corrected transverse component $T_c(t)$. For an N-point digital time series, this may expressed as

$$E_t(\phi, \delta t) = 1/N \sum_{i=1}^{N} (T_c)^2 \Delta t = \text{Minimum} \qquad (6)$$

where Δt is the time sampling interval. In using Silver and Chan's method (1988), $E_t(\phi, \delta t)$ will be evaluated for many candidate values of ϕ and δt in order to locate the minimum energy associated with the fast polarization direction ϕ and the time delay δt. In performing the minimization, ϕ is referenced to north (clockwise positive) and it will be varied from -90^o to 90^o in 1^o increments. δt will be varied from 0 to 3s in 0.05s increments.

Data

The three component, digital, broad-band teleseismic shear waveforms used in this study were recorded at the Albuquerque Seismic Observatory (ANMO) and the Socorro temporary seismic station(WTX). Station parameters are given in Table 1. Station WTX provided data recorded both by intermediate period instruments and by broad-band recorders. The broad-band system at WTX consists of Wide-Band Ranger Kinemetrics seismometers. The Wide-Band Ranger seismometers have a natural frequency of 20 Hz and a dynamic range of 125 dB. The velocity amplitude response for these seismometers is flat from 0.02 Hz to 50 Hz. The intermediate period seismometers have a peak frequency centered around 0.2 Hz and are capable of recording for a frequency band ranging from 0.08 Hz to 12 Hz. All data were sampled at 20 Hz and recorded by a Reftek recorder.

For a period of about five months from April to August 1990, a total of 9 teleseismic events (5 recorded at ANMO and 6 at WTX) were found to be useful for SKS splitting measurements. The hypocenters of these events were obtained from the U.S. Geological Survey Preliminary Determination of Epicenter Listings. A listing of the events and the stations recording them are included in Table 2.

The theoretical travel times for identification of SKS and S phases on the seismograms were calculated using a travel-time polynomial developed by Hales and Roberts (1970).

TABLE 1. Station Parameters

Station	Latitude (deg)	Longitude (deg)	Elevation (m)
ANMO	**34.95N**	**106.46W**	**1740**
WTX	**34.07N**	**106.95W**	**1555**

TABLE 2. Event Parameters

Event	Date yy/mm/dd	Origin Time (hr:min) utc	Magnitude	Depth (km)	Latitude (deg)	Longitude (deg)	Recorded at
90133	**90/05/13**	**04:23**	**6.0**	**30**	**40.26S**	**176.14E**	**WTX**
90148	**90/05/28**	**11:28**	**5.8**	**497**	**20.75S**	**178.07W**	**WTX**
90150	**90/05/30**	**10:40**	**6.7**	**90**	**45.87N**	**26.66E**	**WTX**
90177	**90/06/26**	**12:08**	**5.8**	**593**	**21.97S**	**179.52W**	**WTX,ANMO**
90191	**90/07/10**	**03:18**	**5.8**	**69**	**10.29S**	**161.14E**	**WTX,ANMO**
90203	**90/07/22**	**09:26**	**5.9**	**565**	**23.45S**	**179.92E**	**WTX**
90217	**90/08/05**	**01:34**	**5.9**	**516**	**29.51N**	**137.59E**	**ANMO**
90217	**90/08/05**	**17:42**	**5.6**	**10**	**1.01S**	**13.96W**	**ANMO**
90229	**90/08/17**	**13:07**	**5.9**	**33**	**11.20S**	**161.99E**	**ANMO**

(Information taken from the U.S. Geological Survey Preliminary Determination of Epicenter Listings).

In Figures 10a, 10b, and 10c, an example of splitting measurements is shown. Three component seismograms of SKS (vertical, radial, and transverse top to bottom,respectively) for station WTX and event 90203 is shown in Figure 10a. SKS and S arrivals are labelled. Transverse SKS component energy is present indicating possible anisotropy.

In Figure 10b, the original (uncorrected) radial and transverse component seismograms (the top two traces,respectively) are shown together with corrected transverse and radial components (the bottom two traces,respectively). Transverse SKS component energy has been removed by using the estimated splitting parameters $\phi = 45^{o}$ and $\delta t = 0.65s$ for this event.

Figure 10c shows a superimposed plot of the fast (solid) and slow (dotted) components of SKS. The left plot is the original uncorrected horizontal component seismograms rotated to the estimated fast (ϕ) and slow ($\phi + 90^{o}$) directions. On the right is the corrected overplot of fast and slow components. The correction was applied by advancing the slow component in time by $\delta t = 0.65s$. Bottom plots are the corresponding particle motion diagrams. The vertical axis of particle motion is along the fast direction. Near elliptical particle motion (lower left) becomes almost linear after the correction is applied (lower right).

The complete set of measurements is given in Appendix 1 for WTX and in Appendix 2 for ANMO.

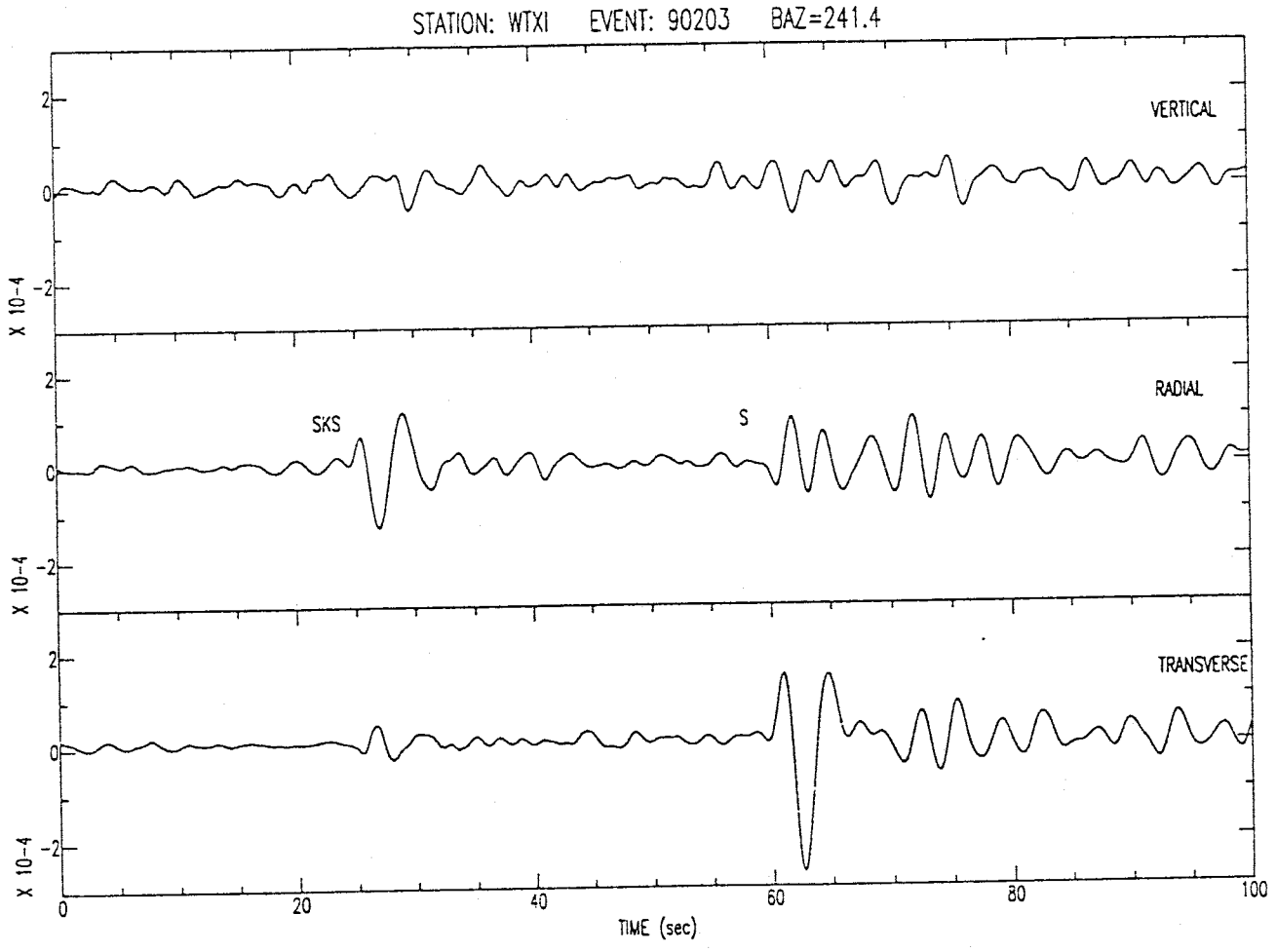

Figure 10a. Three component seismogram of S–arrivals for station WTX and event 90203 (90/07/22) from intermediate–period seismometers. Approximate arrival times of SKS and S are indicated on radial component. Note significant SKS energy on transverse component.

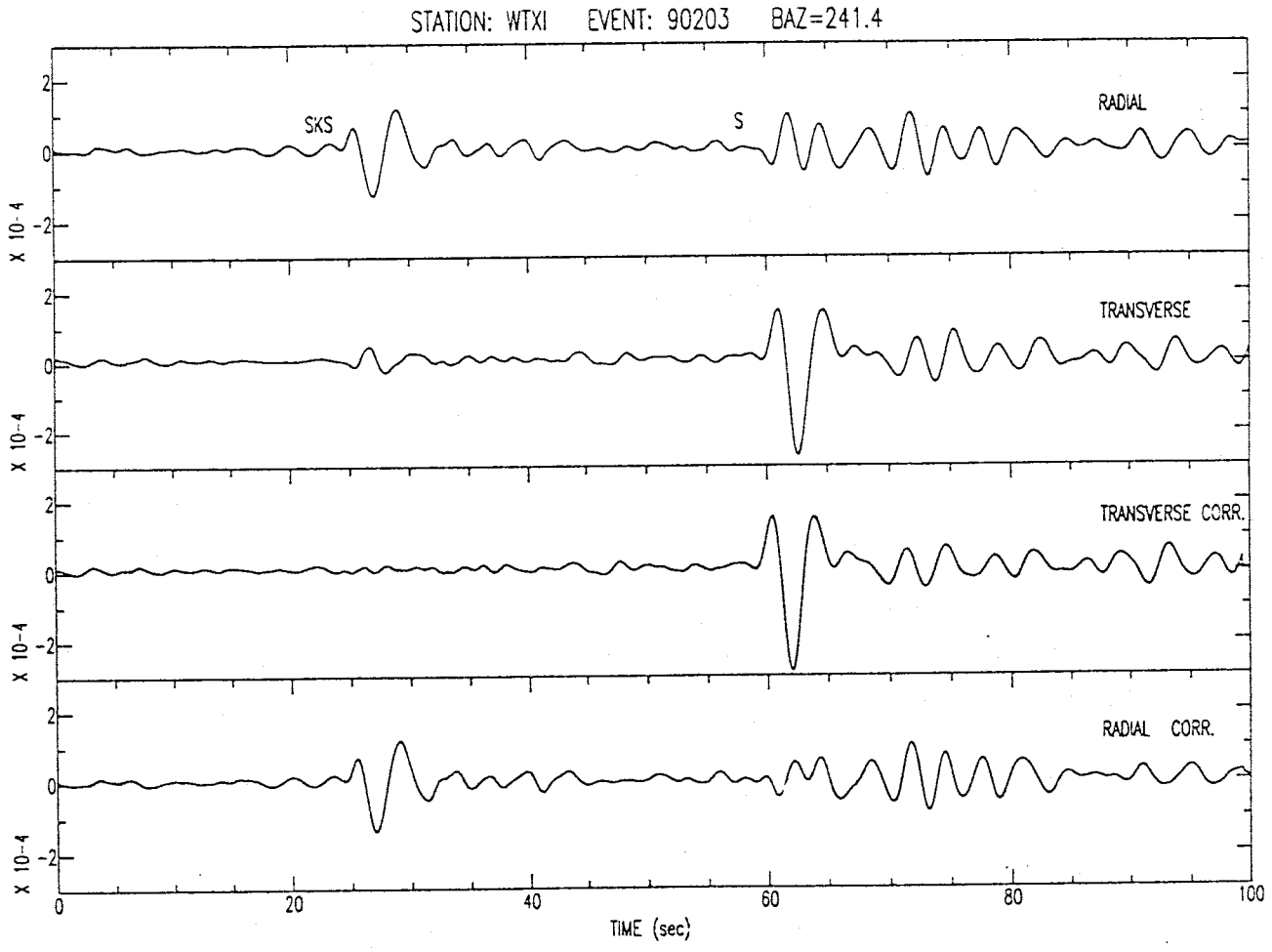

Figure 10b. Original radial and transverse components top two traces and corrected transverse and radial components bottom two traces respectively for event 90203 shown in Figure 10a. Note that in corrected seismogram, SKS transverse component has been removed.

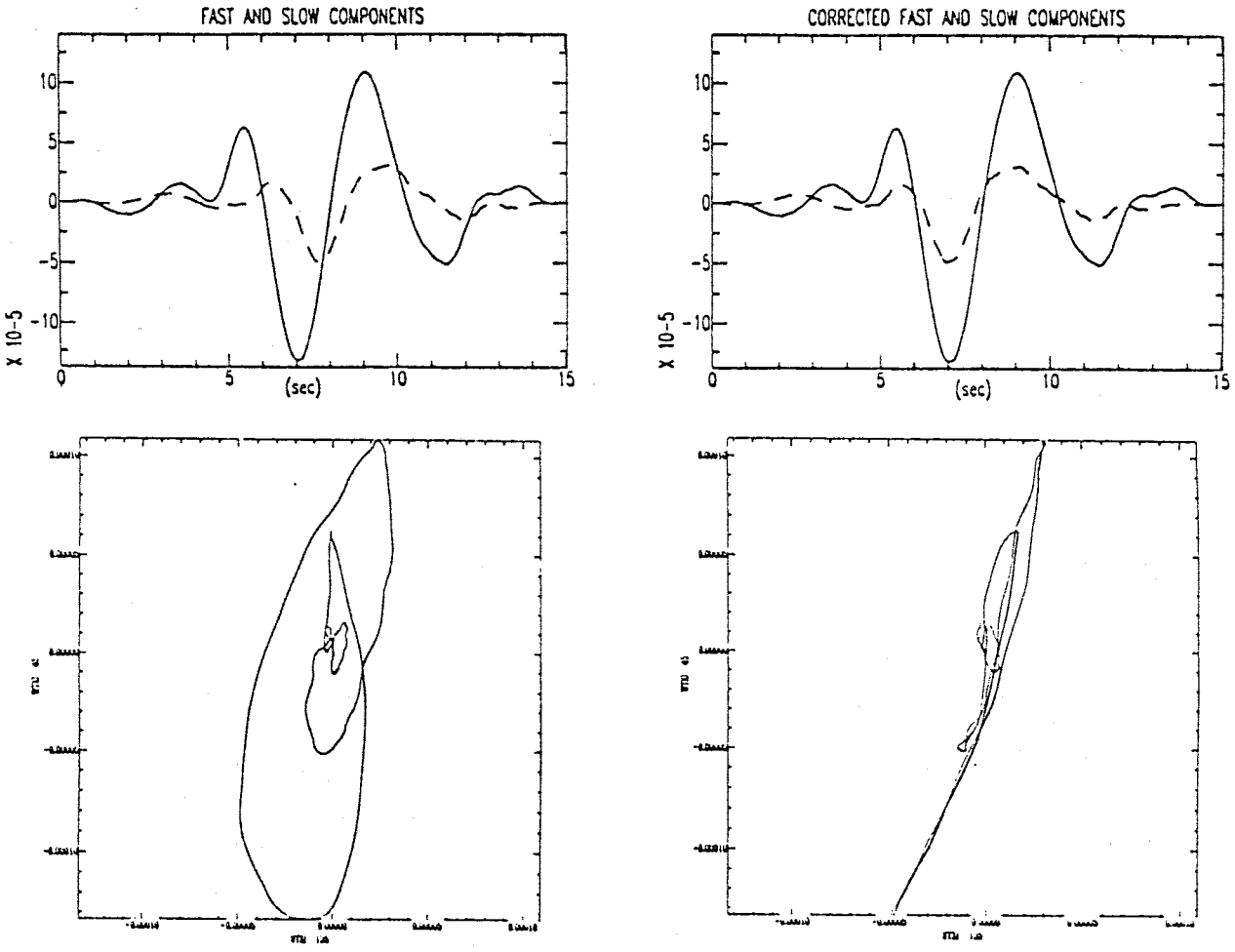

Figure 10c. Top two traces: Overplot of fast (solid) and slow (dotted) components of SKS rotated to fast (45^0) and slow (135^0) for event 90203. Left is uncorrected and corrected (right). Correction was made by advancing slow component in time by $\delta t = 0.65$ s. Bottom: Particle motion diagrams for fast and slow components uncorrected (left) and corrected (right). Near elliptical particle motion is almost linear on corrected particle motion plot.

Results

Tables 3 and 4 contain the estimates of splitting parameters at each station. Quality factors were assigned to each splitting estimate based on signal–to–noise levels of the well recorded SKS radial components. Events that do not exhibit detectable splitting (i.e., transverse SKS components with little or no energy) are listed with time delays of 0.0s. For these events, ϕ was taken to be the same as the event back azimuth (BAZ) or BAZ$\pm$n 90^0 (n=1,2,3) whichever is more consistent with the well constrained estimates for other events.

TABLE 3. WTX Splitting Measurements

EVENT	Δ (deg)	BAZ (deg)	ϕ (deg)	δt (sec)	QUALITY
90133*	**102.4**	**229.7**	**50**	**0.00**	**A**
90148*	**86.8**	**242.4**	**62**	**0.00**	**A**
90150*	**90.0**	**30.4**	**55**	**1.65**	**C**
90150	**90.0**	**30.4**	**94**	**0.75**	**B**
90177	**88.7**	**242.5**	**53**	**1.00**	**A**
90191	**97.3**	**262.5**	**52**	**1.45**	**C**
90203*	**89.9**	**241.4**	**45**	**0.65**	**A**

(* intermediate-period)

TABLE 4. ANMO Splitting Measurements

EVENT	Δ (deg)	BAZ (deg)	ϕ (deg)	δt (sec)	QUALITY
90177	**89.4**	**242.6**	**-28**	**0.00**	**A**
90191	**97.7**	**262.9**	**20**	**0.80**	**C**
90217	**92.0**	**308.3**	**-28**	**0.60**	**A**
90217	**92.6**	**89.4**	**21**	**1.80**	**A**
90229	**97.3**	**262.0**	**16**	**0.85**	**B**

Estimated fast polarization direction (ϕ), clockwise from north, and time delay (δt). For events (Event) (year, day of year), at distance (Δ). Back-azimuth (BAZ) and quality of each estimate indicated (A, B and C from high to low).

The azimuthal coverage for both stations was not good, especially for back azimuths to the east and southeast. The azimuthal distribution of events was a little better for ANMO than for WTX. Scatter in splitting parameters and lack of a well distributed azimuthal coverage remain a problem which can only be overcome by using more events.

The resulting splitting estimates at WTX show consistent fast polarization directions oriented around NE–SW for events with a back azimuth range between 230°–260°. Event 90150, which is the only easterly back azimuth event at WTX, gave a near E–W fast direction. Although this raises a question for possible azimuthally–dependent shear wave splitting (i.e. the events from westerly back azimuths with near NE–SW fast direction and E–W fast direction from easterly back azimuth events), this is difficult to constraint with the presently available data set. The estimated splitting parameters for ANMO, with fewer events, show scattered fast polarization directions around N–S direction.

In order to obtain an average fast polarization direction and an average delay time for each station, a simple mean was calculated. The simple mean calculation of all measurements for WTX yields an average splitting pair $(\phi,\delta t) = (59 \pm 15^{\circ}, 1.1 \pm 0.40s)$ and for ANMO $(\phi,\delta t) = (0 \pm 23^{\circ}, 1.0 \pm 0.46s)$. Weighted means were also calculated using quality factors assigned to each individual estimate (Tables 3 and 4), but this did not change the average estimates by more than 1° for WTX and 4° for ANMO. The weighted mean for WTX (excluding the splitting parameters for event 90150, which had markedly different fast angle and a quality B) is $(\phi,\delta t) = (53 \pm 5^{\circ}, 1.2 \pm 0.40s)$. Because the weighted means are not significantly different from the simple means, the simple average splitting parameters given above will be used as the average splitting parameters for each station in the following interpretation and discussion.

Discussion and Conclusions

The shear wave splitting results define two anisotropies with comparable magnitudes (time delays) but significantly differing directions at WTX and ANMO. However, the observed anisotropy at each station can be explained by past and present tectonic processes of the Rio Grande rift together with nearby tectonic features.

We consider strain-induced preferred orientation of olivine in the upper mantle due to past and present rifting episodes within the Rio Grande rift as the cause of the observed anisotropy.

The analysis of the Cenozoic geologic history of the Rio Grande rift reveals at least two phases of extension. An early phase of extension began along the Rio Grande rift in the mid-Oligocene (32Ma) and may have continued to the early Miocene (about 18Ma). During this phase, low-angle (listric) faults, relatively shallow basins, and high volcanic activity were formed under a regional extensional stress field oriented approximately NE-SW (Morgan et al.,1986). A late phase of extension followed the early phase of extension after a long transition period during the middle Miocene when volcanism was absent. This late phase of extension began in the late Miocene (about 10-5 Ma) with minor extension (5-20% extension) continuing to the present. This phase is characterized by a clockwise rotation of the extensional stress field from NE-SW to an E-W or WNW-ESE direction. This late-phase extension resulted in the segmentation of earlier rift basins into narrower horsts and grabens, the formation of northerly trending modern rift uplifts and basins, and high angle faults (Aldrich et al., 1986, Morgan et al.,1986).

This change in the regional stress direction also resulted in a small clockwise rotation of the Colorado Plateau, as well as major volcanism on its southern tectonic boundary known as the Jemez lineament (Aldrich and Laughlin, 1984).

In summary, two major extensional regimes transitional with each other through Miocene have been present in the Rio Grande rift. Assuming that the former NE–SW regional extension, which had a relatively longer period (about 14 Ma) and much larger magnitude than the latter extensional regime, caused a permanent preferred alignment of olivine in the upper mantle oriented along the extension direction, it seems that the fast polarization direction of $\phi = 59 \pm 15^{o}$ and time delay $\delta t = 1.1 \pm 0.40$s observed at WTX are in reasonably good agreement with the early rift extension direction. The late–phase or present–day extension with WNW–ESE direction,however, appears to be inconsistent with the observed anisotropy directions. This may possibly indicate that the late–phase extension controlling present day surface structures of the Rio Grande rift may not have existed long enough or may not be strong enough to cause any major changes on the orientation of subcontinental mantle minerals inherited from the previous rifting episode.

The NE–SW fast direction at WTX may also be due to plate–motion related strain–induced anisotropy in the upper mantle caused by the absolute plate motion direction of the North American Plate (NE–SW) estimated for the Socorro region.

So far we have used the strain–induced olivine alignment model to explain the shear wave polarization anisotropy results. Another alternative is to analyze the present day crustal stress and related crustal deformation.

One possible candidate for producing the observed anisotropy direction at WTX is a near–vertical structural boundary that acts like a null plane between two domains of fault blocks tilted in opposite directions in the Socorro region (Chapin,1989). This boundary is called the Socorro accommodation zone (SAZ) by (Chapin,1989) and trends about N70°E near Socorro (Figure 11). The SAZ has leaked magmas episodically for at least 32 Ma and it, therefore, appears to be penetrating into the upper mantle. This strongly suggests that the SAZ is a major deep–seated crustal discontinuity. The SAZ, on the other hand, is a relatively aseismic zone in a well–monitored, highly seismogenic zone surrounding the Socorro region (Sanford et al., 1990).The SAZ also crosses early rift calderas without any noticeable offset of their boundaries, indicating that it has not undergone much strike–slip movement (Chapin,1989). From these observations, if we assume that the anisotropy at WTX is entirely caused by the SAZ, either the SAZ extends into the lithosphere causing a considerable thickness of anisotropy in the upper mantle or the SAZ is a very strongly anisotropic structure with lesser depth extent confined more or less to to the crust in order to produce the observed time delay $\delta t = 1.1 \pm 0.40$s at WTX. This interpretation is however, very speculative with poorly known characteristics of the SAZ.

The composite fault plane solutions of micro–earthquakes in the vicinity of the Socorro region give an average least principal horizontal stress direction oriented N70°E (Sanford et al., 1979). This information provides an additional constraint implying that the present–day crustal stress and the early phase extension direction have remained in agreement, at least in the Socorro region. Therefore, it may be reasonable to infer that the anisotropy beneath WTX is due to the strain–induced upper mantle olivine orientation related to the early–rift extension regime with present–day crustal contribution to it.

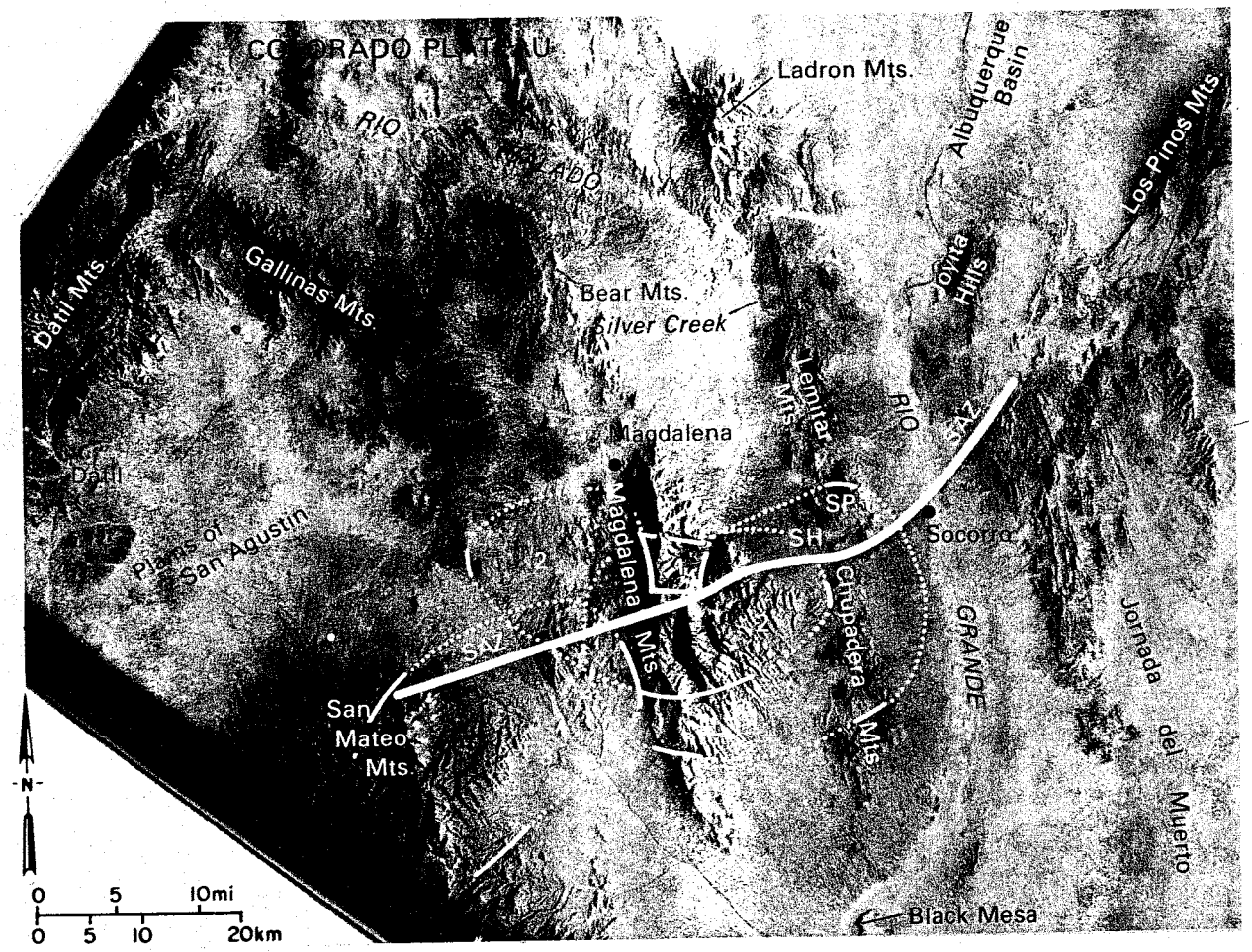

Figure 11. Skylab photograph of west-central New Mexico showing the location of the Socorro accommodation zone (SAZ) (after Chapin,1989).

The fast polarization direction $\phi = 0 \pm 23^{o}$ and time delay $\delta t = 1.0 \pm 0.46$s observed at ANMO, however, cannot be associated with any of the extensional regimes mentioned earlier. This would imply that sub–Moho materials beneath ANMO have experienced significantly different tectonic histories than the Rio Grande rift, so that upper mantle minerals have been oriented along nearly N–S to produce the observed fast polarization direction at ANMO. Although this conclusion cannot be well supported with other geophysical and geological data (which primarily indicate that both stations are essentially within the same tectonic province of the central Rio Grande rift), there is evidence for a different tectonic regime to the north of ANMO where a transitional tectonic boundary lies. This tectonic boundary is the southeastern boundary of the Colorado Plateau and is known as the Jemez lineament. The Jemez lineament is the most active tectonic feature in the southwestern United States; it has had recent basaltic volcanism during the last 4.5 Ma. A recent three–dimensional teleseismic P wave velocity inversion study provides clear evidence that directly beneath a 200 km long section of the Jemez lineament, there is a ~100 km wide, 1–2% low–velocity feature in the depth range of 50–160 km (Figure 12) (Spence and Gross, 1990). The interpretation of this low velocity feature is that a large magmatic source zone exists beneath the Jemez lineament but not beneath the Rio Grande rift. These results are best modeled by clockwise rotation of the Colorado Plateau about a pole located in northeastern Colorado (Figure 12). This rotation of Colorado Plateau relative to the North American plate caused by the change of the direction of spreading during the late Miocene and resulted in left slip along the Jemez lineament and extension across it (Aldrich and Laughlin, 1984). This tectonic regime, which substantially differs from the previous rifting episodes, predicts an average

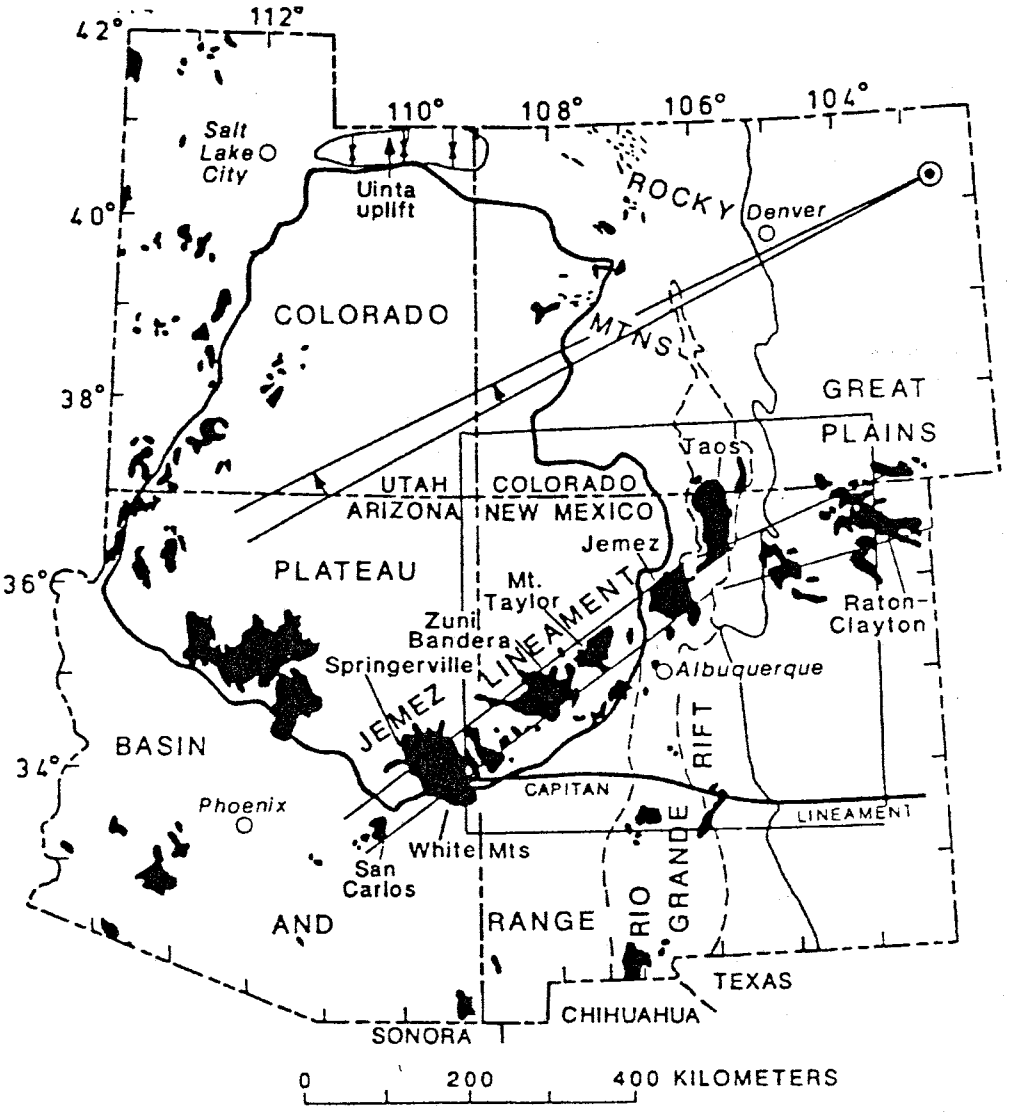

Figure 12. Regional map of the Rio Grande rift, the Jemez lineament, and the rotation of the Colorado Plateau indicated (after Spence and Gross, 1990).

extension direction of N35°W, which is perpendicular to the strike of the Jemez lineament. If the upper mantle beneath ANMO is affected by this tectonic regime, then station ANMO, located about 50 km southeast of the Jemez lineament, would show a fast angle direction parallel to this direction. Our estimate of a N–S (±23°) fast direction at ANMO is in fair agreement with a strain–induced olivine alignment model that is transitional between alignments caused by the tectonics of the Rio Grande rift (~E–W) and the Jemez lineament (~N35°W).

Finally, at ANMO the N–S orientation of the fast direction ($\phi = 0 \pm 23°$) is in fair agreement with the strike of Montosa fault zone N20°E. This fault is believed to be one of many along which up to 120 km right lateral strike–slip movement occurred during Eocene time. This movement was caused by a shift in the axis of regional compression in the southwestern United States from ENE to about N45°E during the late Laramide time (beginning 55Ma). This rotation brought the first order shear direction nearly parallel with the NNE trending southern Rocky Mountains in New Mexico and further allowed the translation of the Colorado Plateau approximately up to 100km along right–lateral wrench faults (Chapin and Cather, 1983). At least two major N–NNE trending, right–lateral wrench fault systems were active at the latitude of Santa Fe at this time. The Montosa fault may be related to one of these wrench fault systems known as the Picuris–Pecos fault system. Other strike–slip faults may exist under the alluvial fill of the Rio Grande rift. However, this remains a difficult question to resolve (Chapin and Cather,1983). The same arguments made for the SAZ apply to the Montosa fault zone for its potential to generate the observed anisotropy at ANMO.

REFERENCES

Aldrich, M. J., and A. W. Laughlin, A model for the tectonic development of the southeastern Colorado Plateau boundary, J. Geophys. Res., 89, 10207–10218, 1984.

Aldrich, M. J., C. E. Chapin, and A. W. Laughlin, Stress history and tectonic development model for the Rio Grande rift, New Mexico, J. Geophys. Res., 91, 6199–6212, 1986.

Ando, M., ScS polarization anisotropy around the Pacific ocean, J. Phys. Earth, 32, 179–196, 1984.

Ando, M., and Y. Ishikawa, S-wave anisotropy in the upper mantle under a volcanic area in Japan, Nature, 286, 43–46, 1980.

Ando, M., Y. Ishikawa, and F. Yamazaki, Shear wave polarization anisotropy in the upper mantle beneath Honsu, Japan, J. Geophys. Res., 88, 5850–5864, 1983.

Bamford, D., P_n velocity anisotropy in a continental upper mantle, Geophys. J. R. Astr. Soc., 49, 29–48, 1977.

Bamford, D., M. Jentsch, and C. Prodehl, P_n anisotropy studies in northern Britain and the eastern and western United States, Geophys. J. R. Astr. Soc., 57, 397–429, 1979.

Ben-Menahem, A., and S. J. Singh, Seismic Waves and Sources, Springer-Verlag Inc., New York, 1981.

Booth, D. C., and S. Crampin, Shear-wave polarizations on a curved wavefront at an isotropic free-surface, Geophys. J. R. Astr. Soc., 83, 31–45, 1985.

Booth, D. C., S. Crampin, J. H. Lovell, and J. M. Chiu, Temporal changes in shear-wave splitting during an earthquake swarm in Arkansas, J. Geophys. Res., 95, 11151–11164,1990.

Bowman, J. R., and M. Ando, Shear wave splitting in the upper-mantle wedge above the Tonga subduction zone, Geophys. J. R. Astr. Soc., 88, 25–41, 1987.

Chapin, C. E., The Rio Grande rift, Part I: Modifications and additions, New Mexico Geological Society, Guidebook 22, 191–201,1971.

Chapin, C. E., Evolution of the Rio Grande rift – a summary , in Riecker, R. E., ed., Rio Grande rift: Tectonics and magmatism, American Geophysical Union, 1–5, 1979.

Chapin, C. E., Volcanism along the Socorro accommodation zone, Rio Grande rift, New Mexico Bureau of Mines & Mineral Resources Memoir, 46, 46–57, 1989.

Chapin, C. E., and S. M. Cather, Eocene tectonics and sedimentation in the Colorado Plateau–Rocky Mountain area, in Lowell, J. E., ed., Rocky Mountain foreland basins and uplifts: Rocky Mountain Association of Geologists, Denver, Colorado, 33–56, 1983.

Chapin, C. E., and W. R. Seager, Evolution of the Rio Grande rift in the Socorro and Las Cruces areas, New Mexico Geological Society, Guidebook 26, 297–321,1975.

Chapin, C. E., R. M. Chamberlin, G. R., Osburn, A. R., Sanford, and D. W. White Exploration framework of the Socorro geothermal area, New Mexico, New Mexico Geological Society, Special Publication 7, 115–129,1978.

Cordell, L., Regional geophysical setting of the Rio Grande rift, Geological Society of America Bulletin, 89, 1073–1090, 1978.

Crampin, S., A review of the effects of anisotropic layering on the propagation of seismic waves, Geophys. J. R. Astr. Soc., 49, 9–27, 1977.

Crampin, S., A review of wave motion in anisotropic and cracked elastic media, Wave Motion, 3, 343–391, 1981.

Crampin, S., Effective anisotropic elastic constants for wave propagation through cracked solids, Geophys. J. R. Astr. Soc., 76, 135–145, 1984.

Crampin, S., Evaluation of anisotropy by shear–wave splitting, Geophysics,50, 142–152, 1985.

Crampin, S., Geological and industrial implications of extensive–dilatancy anisotropy, Nature, 328, 491–496, 1987.

Crampin, S., R. Evans, and S. B. Ucer, Analysis of records of local earthquakes: the Turkish Dilatancy Projects (TDP1 and TDP2), Geophys. J. R. Astr. Soc., 83, 1–16, 1985.

Decker, E. R., and S. B. Smithson, Heat flow and gravity interpretation across the Rio Grande rift in southern New Mexico and west Texas, J. Geophys. Res., 80, 2542–2552, 1975.

Forsyth, D. W., The early structural evolution and anisotropy of the oceanic upper–mantle, Geophys. J. R. Astr. Soc., 43, 103–162, 1975.

Fukao, Y., Evidence from core–reflected shear waves for anisotropy in the Earth's mantle, Nature, 309, 695–698, 1984.

Hales, A. L., and J. L. Roberts, The travel times of S and SKS, Bull. Seis. Soc. Ame., 60, 461–489, 1970.

Hermance, J. F., and J. Pederson, The deep structure of the Rio Grande rift: A magnetotelluric study, J. Geophys. Res., 85, 3899–3912, 1980.

Hess, H. H., Seismic anisotropy of the uppermost mantle under oceans, Nature, 203, 629–631, 1964.

Illies, J. H., Mechanism of graben formation, Tectonophysics, 73, 249–266, 1981.

Keith, C. M., and S. Crampin, Seismic body waves in anisotropic media: reflection and refraction at a plane interface, Geophys. J. R. Astr. Soc., 49, 181–208, 1977a.

Keith, C. M., and S. Crampin, Seismic body waves in anisotropic media: propagation through a layer, Geophys. J. R. Astr. Soc., 49, 209–223, 1977b.

Keith, C. M., and S. Crampin, Seismic body waves in anisotropic media: synthetic seismograms, Geophys. J. R. Astr. Soc., 49, 225–243, 1977c.

Kind, R., G. L. Kosarev, L. I. Makeyeva, and L. P. Vinnik, Observations of laterally inhomogeneous anisotropy in the continental litosphere, Nature, 318, 358–361, 1985.

Larsen, S. R., R. Reilenger, Recent measurements of crustal deformation related to the Socorro magma body, New Mexico, New Mexico Geological Society, Guidebook 34 , 119–121, 1983.

Mc Kenzie, D., and N. Weiss, Speculations on the thermal and tectonic history of the Earth, Geophys. J. R. Astr. Soc., 42, 131–174, 1975.

Milanovsky, E. E., Continental Rift zones: their arrangement and development, Tectonophysics, 15, 65–70, 1972.

Morgan, P., W. R. Seager, and M. D. Golombek, Cenozoic thermal, mechanical and tectonic evolution of the Rio Grande rift, J. Geophys. Res., 91, 6263–6276, 1986

Nuttli, O. W., The effect of the Earth's surface on the S wave particle motion, Bull. Seis. Soc. Ame., 51, 237–246, 1961.

Raitt, R. W., G. G. Shor, T. J. G. Francis, and G. B. Morris, Anisotropy of the Pacific upper mantle, J. Geophys. Res., 74, 3095–3109, 1969.

Reiter, M., C. L. Edwards, H. Hartman, and C. Weidman, Terrestrial heat flow along the Rio Grande rift, New Mexico and southern Colorado, Geological Society of America Bulletin, 86, 811–818, 1975.

Sanford, A. R., O. S. Alptekin, and T. R. Toppozado, Use of reflection phases on microearthquake seismograms to map an unusual discontinuity beneath the Rio Grande rift, Bull. Seis. Soc. Ame., 63, 2021–2034, 1973.

Sanford, A. R., R. P. Mott, P. J. Shuleski, E. J. Rinehart, F. J. Coravella, R. M. Ward, and T. C. Wallace, Geophysical evidence for a magma body in the crust in the vicinity of Socorro, New Mexico, in Heacock, J. G., ed., The Earth's crust: American Geophysical Union, Geophysical Monograph, 20, 385–403, 1977.

Sanford, A. R., K. H. Olsen, and L. H. Jaksha, Seismicity of the Rio Grande rift, in Riecker, R. E., ed., Rio Grande rift: Tectonics and magmatism: American Geophysical Union, 145–168, 1979.

Sanford, A. R., and P. Einarsson, Magma Chambers in rifts: American Geophysical Union Series, 8, 147–168, 1982.

Sanford, A. R., L. H. Jaksha, and D. J. Cash, Seismicity of the Rio Grande rift in New Mexico, Geological Society of America, 1990 (in press).

Savage, M. K., P. G. Silver, and R. P. Meyer, Observations of teleseismic shear wave splitting in the Basin and Range from portable and permanent stations, Geophysical Research Letters, 17, 21–24, 1990.

Savage, M. K., W. A. Peppin, and U. R. Vetter, Shear wave anisotropy in and near Long Valley Caldera, California, 1979–1989, J. Geophys. Res., 95, 11165–11177, 1990.

Schlue, J. W., and L. Knopoff, Shear wave polarization anisotropy in the Pacific Basin, Geophys. J. R. Astr. Soc., 49, 145–165, 1977.

Sengor, A. M. C., and K. Burke., Relative timing of rifting and volcanism on Earth and its tectonic implication, Geophysical Research Letters, 5, 419–421, 1978.

Shearer, P. M., and J. A., Orcutt, Compressional and shear wave anisotropy in the oceanic litosphere –the Ngendei seismic refraction experiment, Geophys. J. R. Astr. Soc., 87, 967–1003, 1986.

Shih, X. R., R. P. Meyer, and J. F. Schneider, An automated, analytical method to determine shear–wave splitting, Tectonophysics, 165, 271–278,1989.

Silver, P. G., and W. W. Chan, Implications for continental structure and evolution from seismic anisotropy, Nature, 335, 34–39, 1988.

Silver, P. G., and W. W. Chan, Shear wave splitting and subcontinental mantle deformation, J. Geophys. Res., 1990 (in press).

Spence, W., and R. S. Gross, Upper mantle source of magmas of the Jemez lineament, New Mexico, J. Geophys. Res., 1990 (in press).

Tanimoto, T., and D. L. Anderson, Lateral heterogenity and azimuthal anisotropy of the upper mantle: Love and Rayleigh waves 100–250 s., J. Geophys. Res., 90, 1842–1858, 1985.

Turcotte, D. L., and S. H. Emmerman, Mechanisms of active and passive rifting, Tectonophysics, 94, 39–50, 1983.

Vetter, U., and J. B., Minster, P_n velocity anisotropy in southern California, Bull. Seis. Soc. Ame., 71, 1511–1530, 1981.

Vinnik, L. P, G. L. Kosarev, and L. I. Makeyeva, Anisotropy of the litosphere from the observations of SKS and SKKS, Proc. Acad. Sci., USSR, 278, 1335–1339, 1984 (in Russian).

Vinnik, L. P, R. Kind, G. L. Kosarev, and L. I. Makeyeva, Azimuthal anisotropy in the litosphere from observations of long period S– waves, Geophys. J. Int., 99, 549–559, 1989.

Zoback, M. L., and M. Zoback, State of stress in the conterminous United States, J. Geophys. Res., 85, 6113–6156, 1980.

APPENDIX 1

This appendix contains the SKS seismograms used in splitting analysis from station WTX. A title page showing the event and estimated splitting parameters is included before the seismograms. The seismograms are given in the following order :

1. Three component seismograms of SKS, vertical, radial and transverse components top to bottom respectively. S and SKS arrivals are labelled.

2. Uncorrected (original) radial and transverse components top two traces and corrected transverse and radial component seismograms bottom two traces respectively.

3. Superimposed plot of Fast (solid) and slow (dotted) component SKS seismograms. Uncorrected (left) and corrected (right). At the bottom corresponding particle motion diagrams. The fast direction is along the vertical axis.

Only original three component seismograms (vertical, radial and transverse) are shown for the events that did not exhibit detectable splitting. On the seismograms, WTXI and WTXB indicate intermediate-period and broad-band seismograms respectively.

EVENT PARAMETERS

Event : 90133

Date : 90/05/13

Origin Time : 04 : 23

Magnitude : 6.0

Depth : 30 km

Latitude : 40.26S Longitude : 176.14E

STATION : WTXI

Δ = 102.4

BAZ = 229.7

SPLITTING PARAMETERS

ϕ = 50°

δt = 0.0s

Quality A

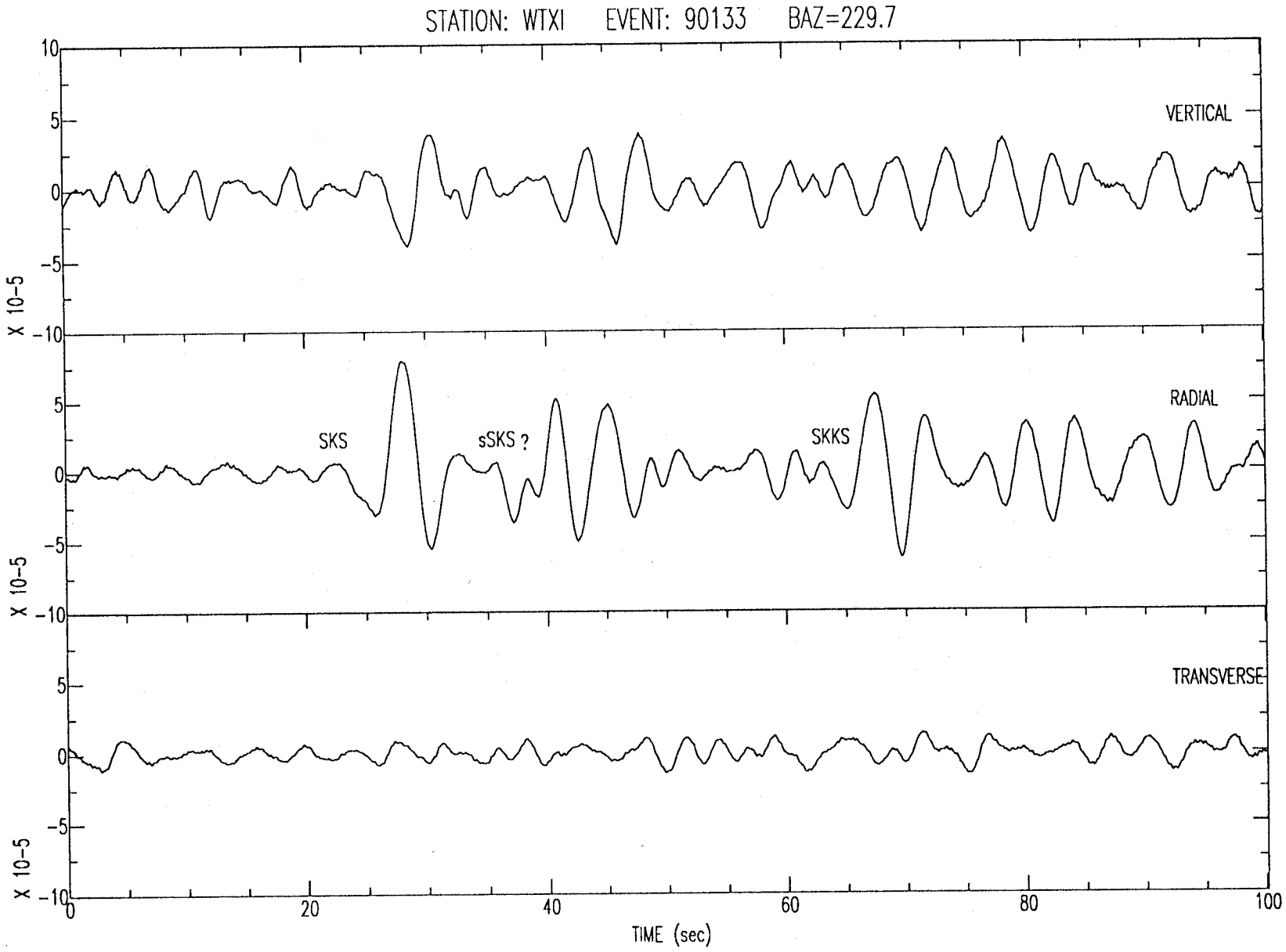
STATION: WTXI EVENT: 90133 BAZ=229.7
VERTICAL
RADIAL
TRANSVERSE
SKS
sSKS ?
SKKS
X 10-5
TIME (sec)
10
5
0
-5
-10
20
40
60
80
100

EVENT PARAMETERS

Event : 90148

Date : 90/05/28

Origin Time : 11:28

Magnitude : 5.8

Depth : 497 km

Latitude : 20.75S Longitude : 178.07W

STATION : WTXI

Δ = 86.8

BAZ = 242.4

SPLITTING PARAMETERS

ϕ = 62°

δt = 0.0s

Quality A

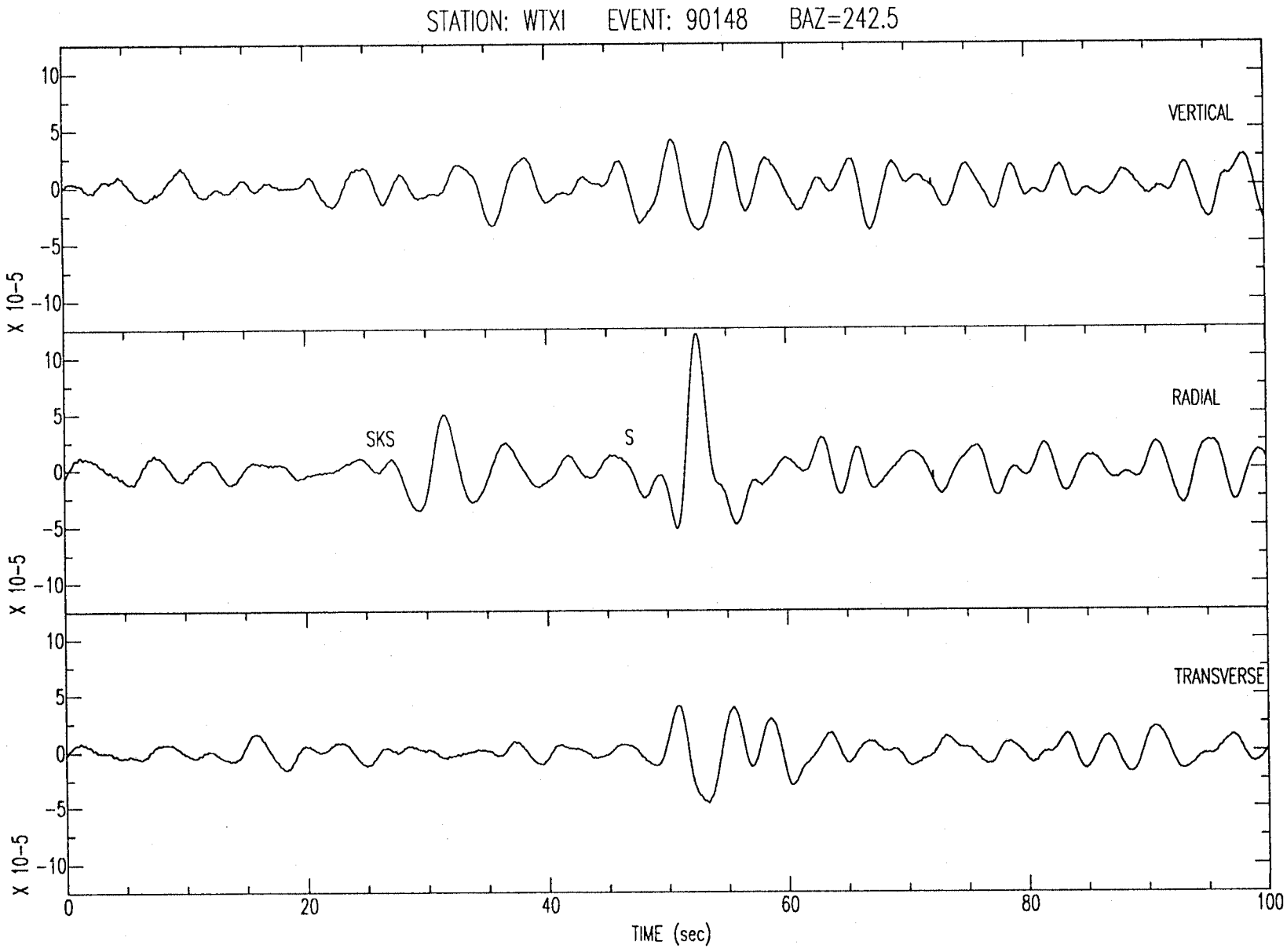
STATION: WTXI EVENT: 90148 BAZ=242.5
VERTICAL
RADIAL
TRANSVERSE
SKS
S
X 10-5
10
5
0
-5
-10
0
20
40
60
80
100
TIME (sec)

EVENT PARAMETERS

Event : 90150

Date : 90/05/30

Origin Time : 10:40

Magnitude : 6.7

Depth : 90 km

Latitude : 45.87N Longitude : 26.66E

STATION : WTXI

Δ = 90.0

BAZ = 30.4

SPLITTING PARAMETERS

ϕ = 55°

δt = 1.65s

Quality C

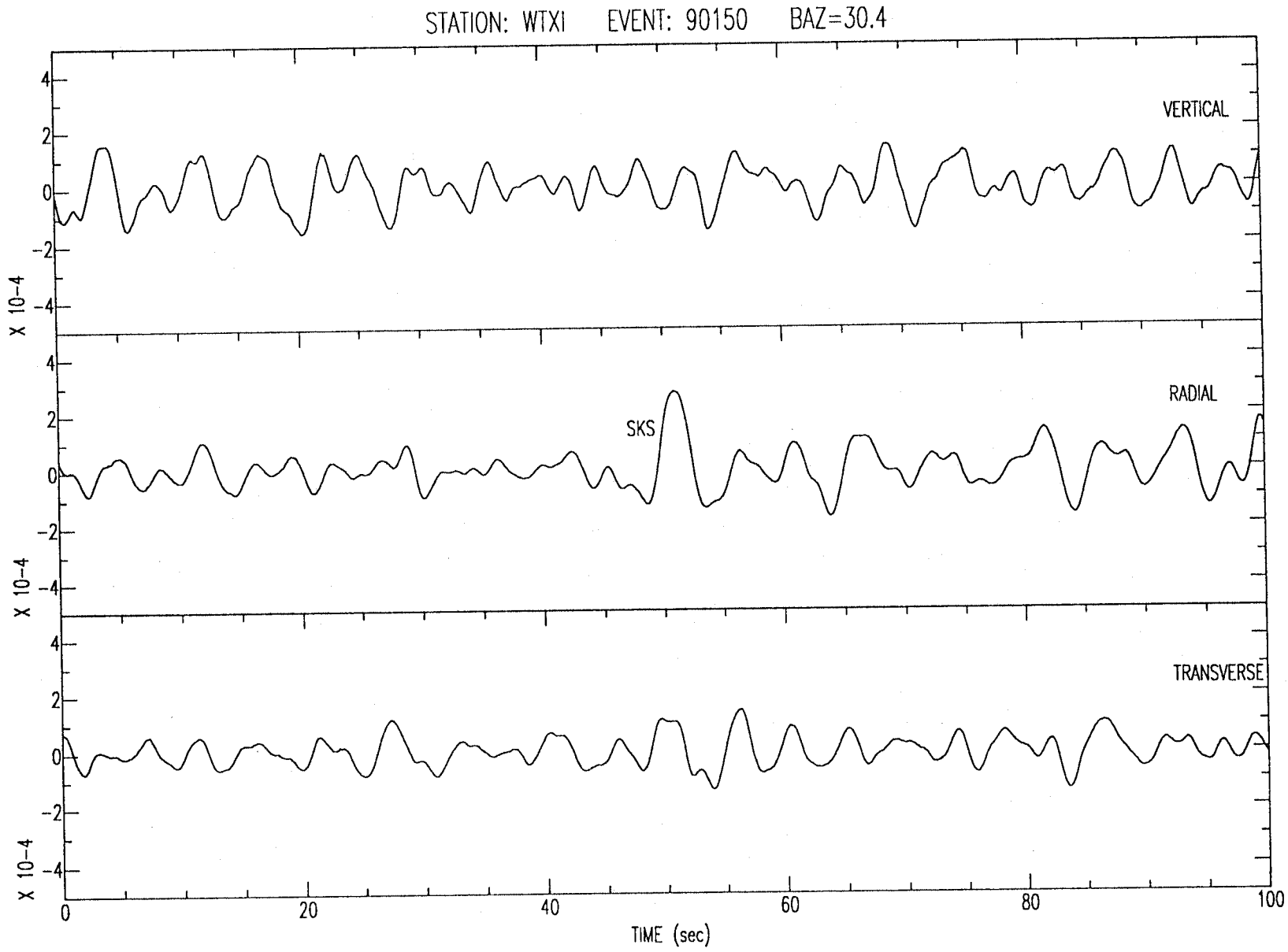
STATION: WTXI EVENT: 90150 BAZ=30.4
VERTICAL
RADIAL
SKS
TRANSVERSE
X 10-4
X 10-4
X 10-4
4
2
0
-2
-4
0
20
40
60
80
100
TIME (sec)

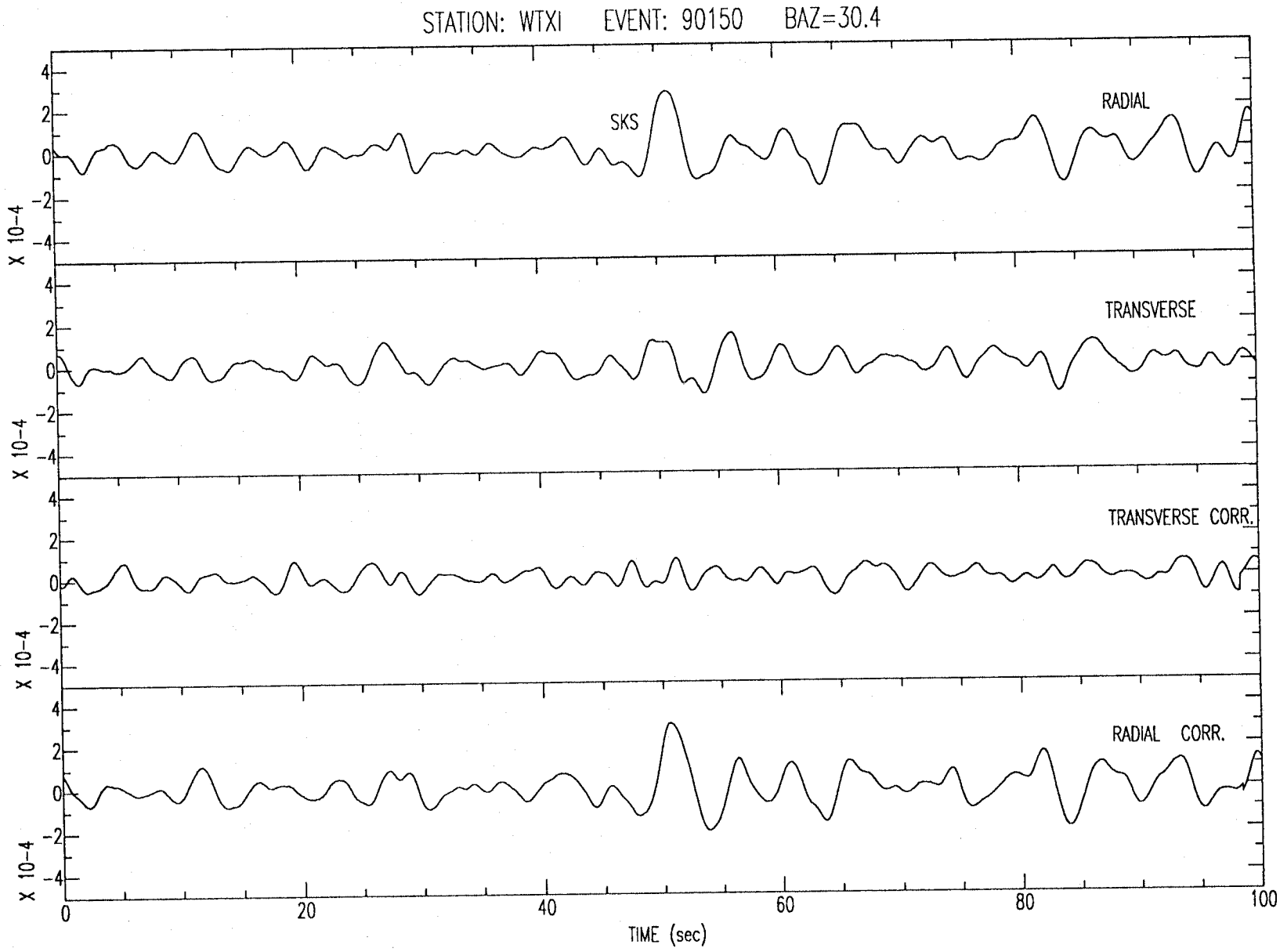
STATION: WTXI EVENT: 90150 BAZ=30.4
SKS
RADIAL
TRANSVERSE
TRANSVERSE CORR.
RADIAL CORR.
X 10-4
4
2
0
-2
-4
0
20
40
60
80
100
TIME (sec)

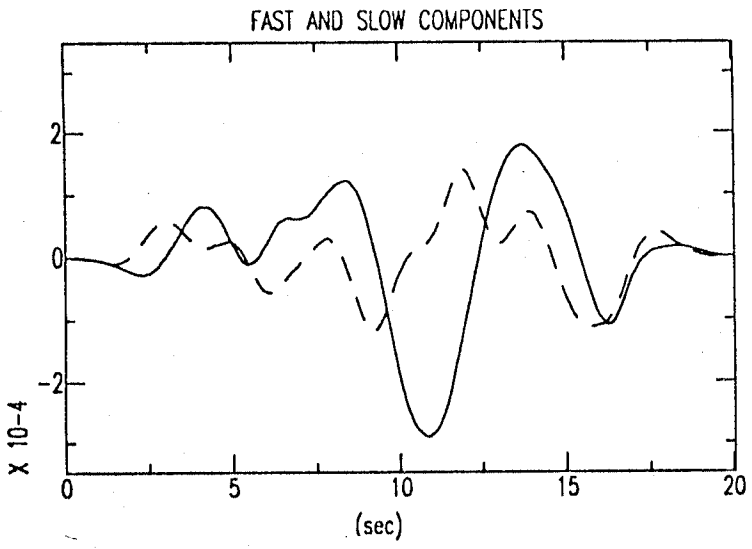
FAST AND SLOW COMPONENTS
X 10-4
2
0
-2
0
5
10
15
20
(sec)

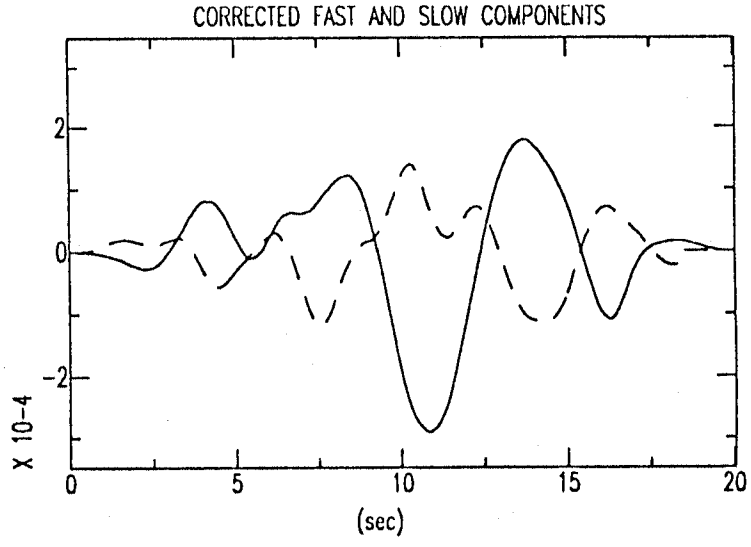
CORRECTED FAST AND SLOW COMPONENTS
X 10-4
2
0
-2
0
5
10
15
20
(sec)

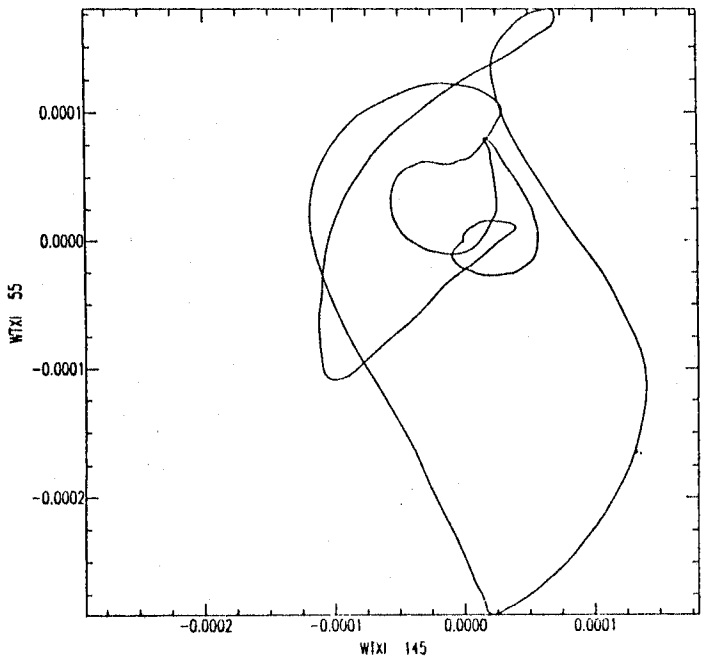
WIXI 55
0.0001
0.0000
-0.0001
-0.0002
-0.0002
-0.0001
0.0000
0.0001
WIXI 145

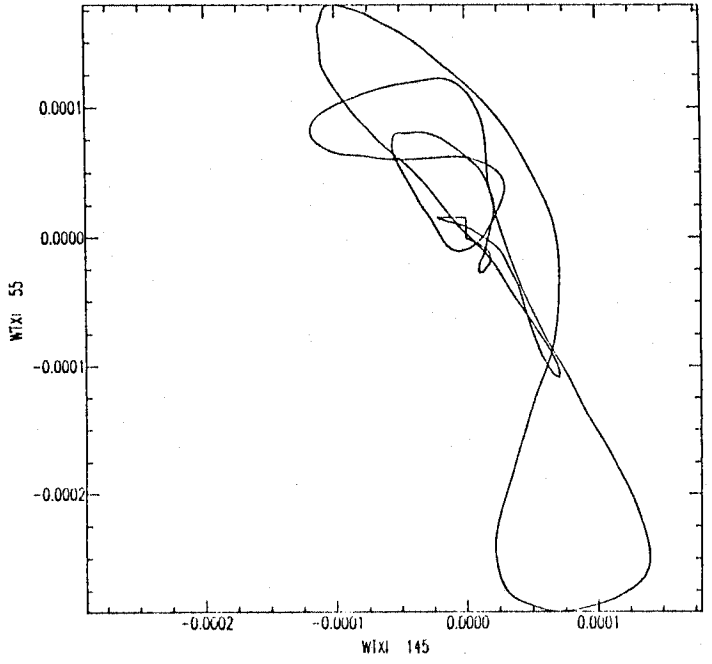
WIXI 55
0.0001
0.0000
-0.0001
-0.0002
-0.0002
-0.0001
0.0000
0.0001
WIXI 145

EVENT PARAMETERS

Event : 90150

Date : 90/05/30

Origin Time : 10:40

Magnitude : 6.7

Depth : 90 km

Latitude : 45.87N Longitude : 26.66E

STATION : WTXB

Δ = 90.0

BAZ = 30.4

SPLITTING PARAMETERS

ϕ = 94°

δt = 0.75s

Quality B

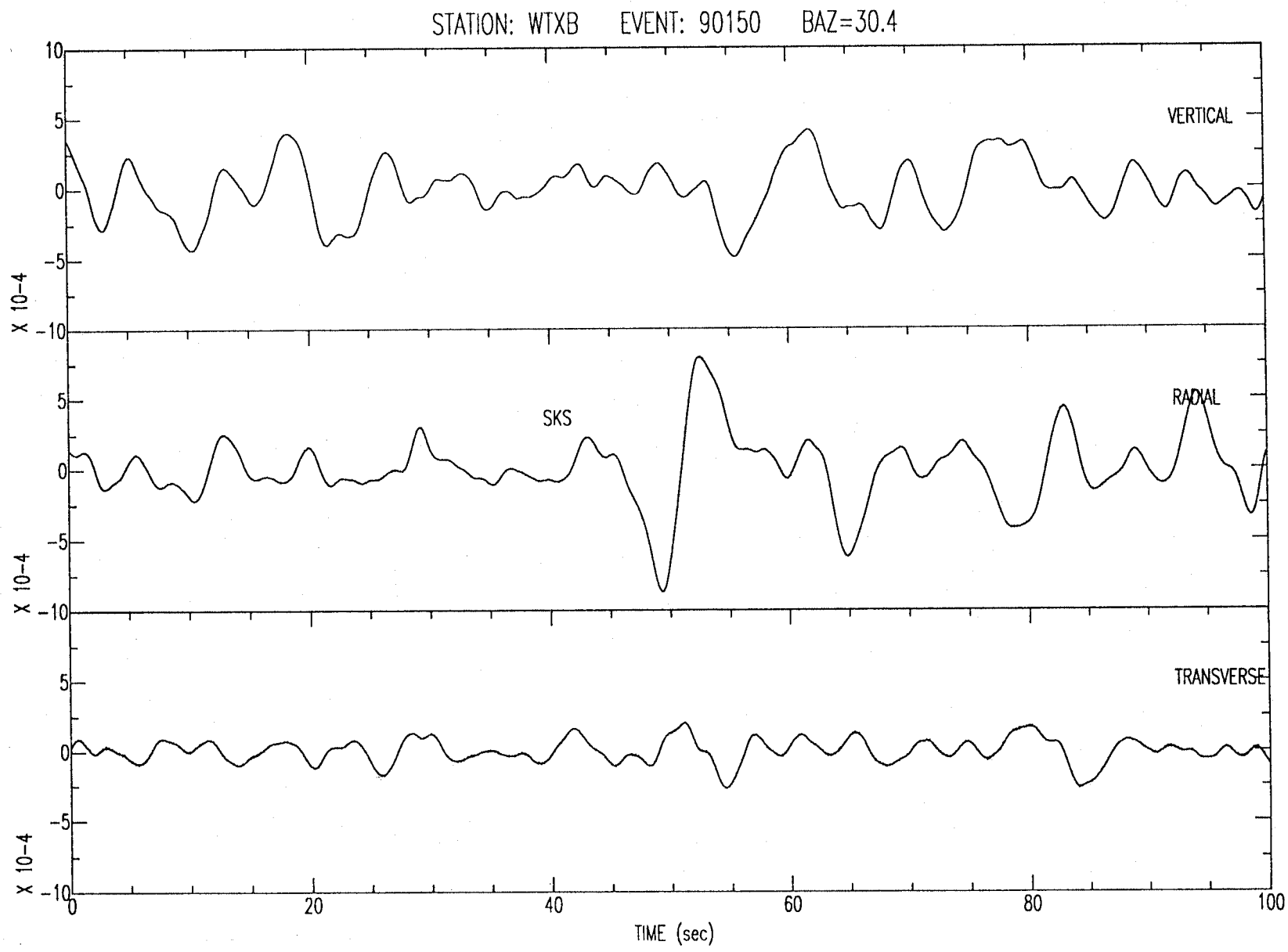
STATION: WTXB EVENT: 90150 BAZ=30.4
VERTICAL
RADIAL
SKS
TRANSVERSE
X 10-4
X 10-4
X 10-4
10
5
0
-5
-10
0
20
40
60
80
100
TIME (sec)

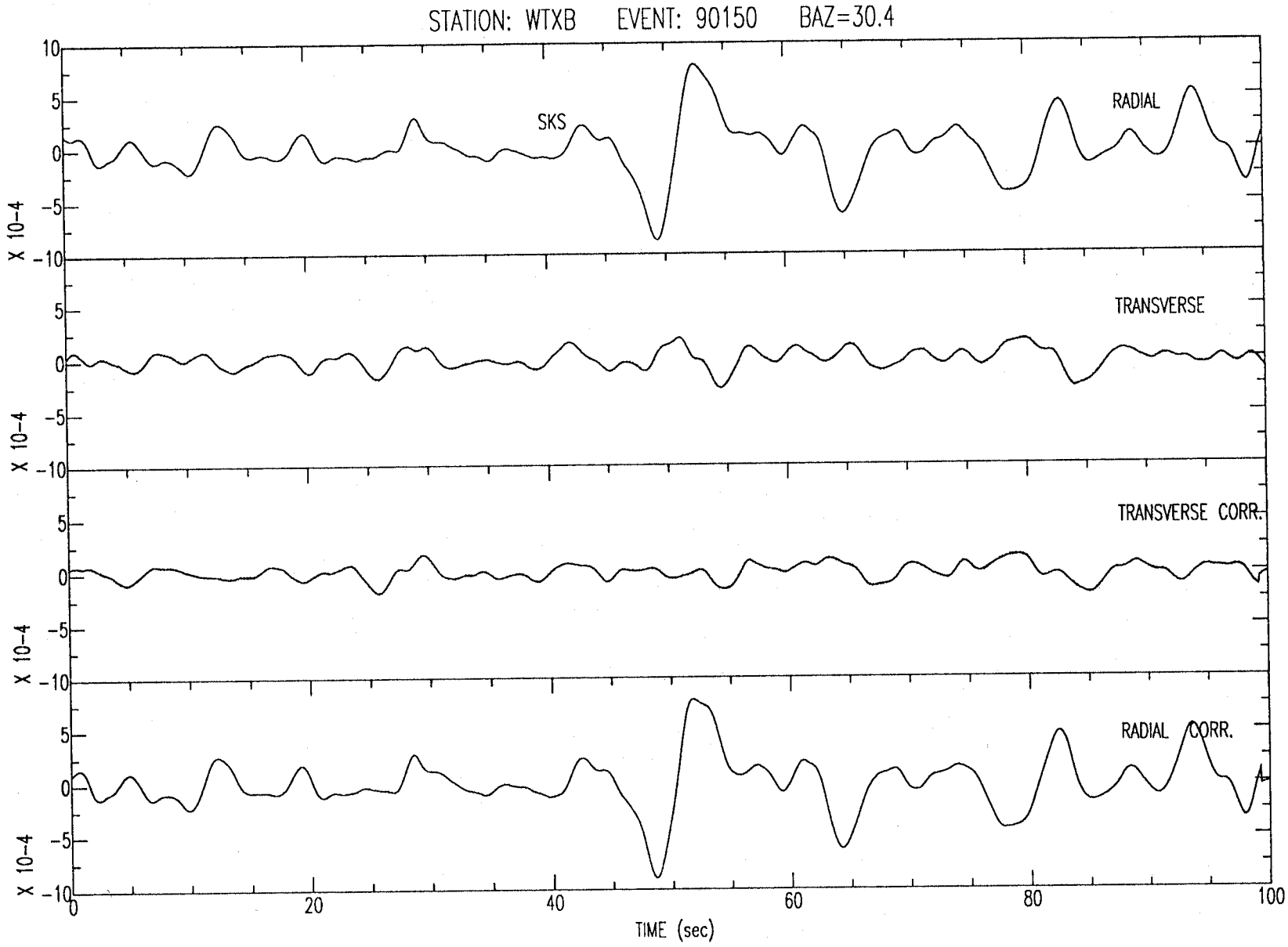
STATION: WTXB EVENT: 90150 BAZ=30.4
SKS
RADIAL
TRANSVERSE
TRANSVERSE CORR.
RADIAL CORR.
X 10-4
10
5
0
-5
-10
0
20
40
60
80
100
TIME (sec)

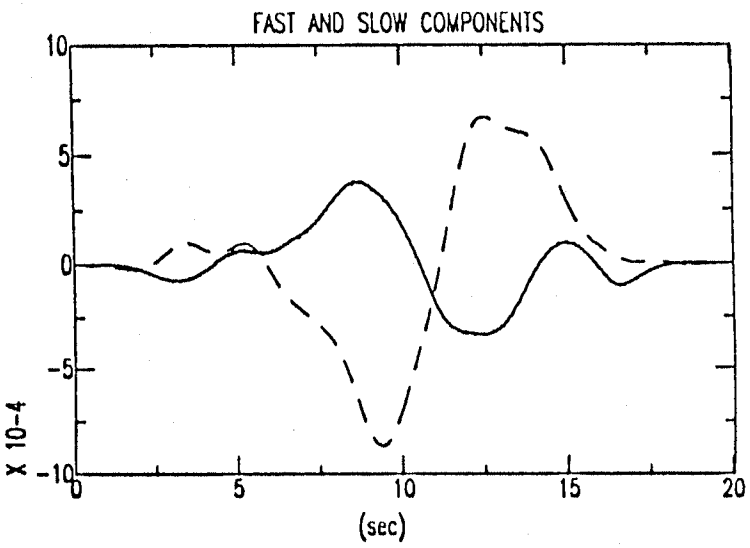
FAST AND SLOW COMPONENTS
X 10-4
(sec)

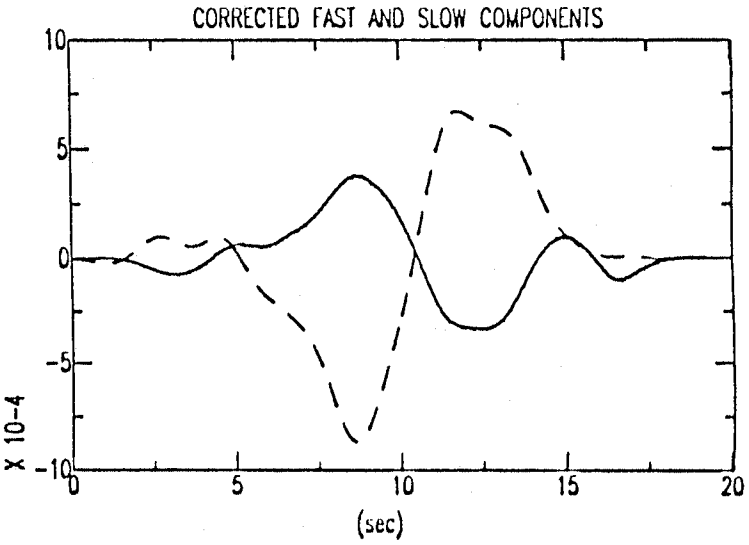
CORRECTED FAST AND SLOW COMPONENTS
X 10-4
(sec)

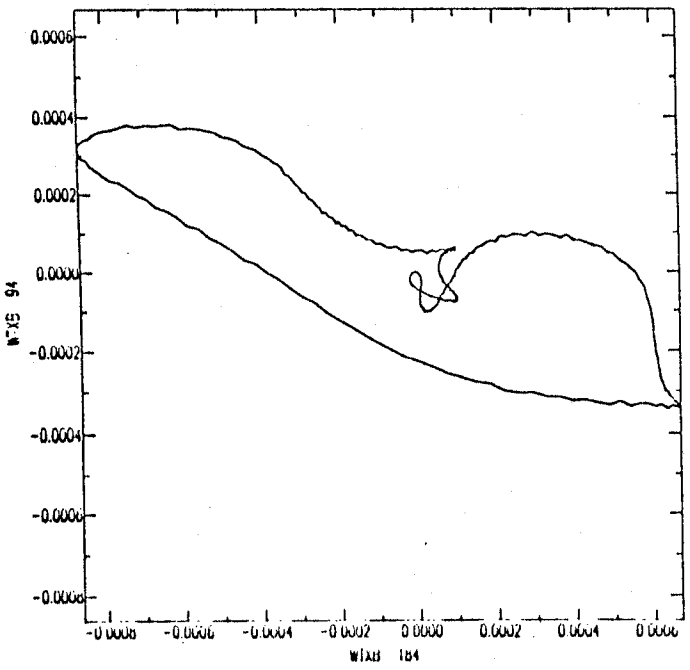

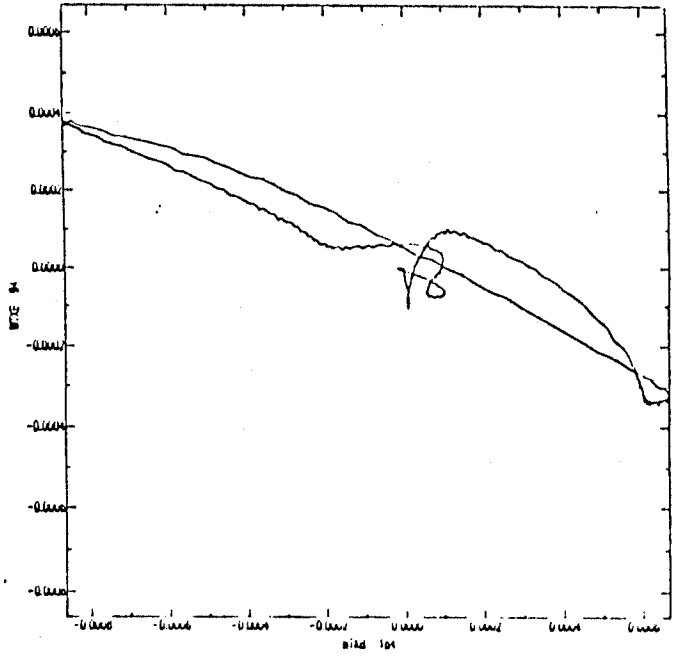

EVENT PARAMETERS

Event : 90177

Date : 90/06/26

Origin Time : 12:08

Magnitude : 5.8

Depth : 593 km

Latitude : 21.97S Longitude : 179.52W

STATION : WTXB

Δ = 88.7

BAZ = 242.5

SPLITTING PARAMETERS

ϕ = 53°

δt = 1.00s

Quality A

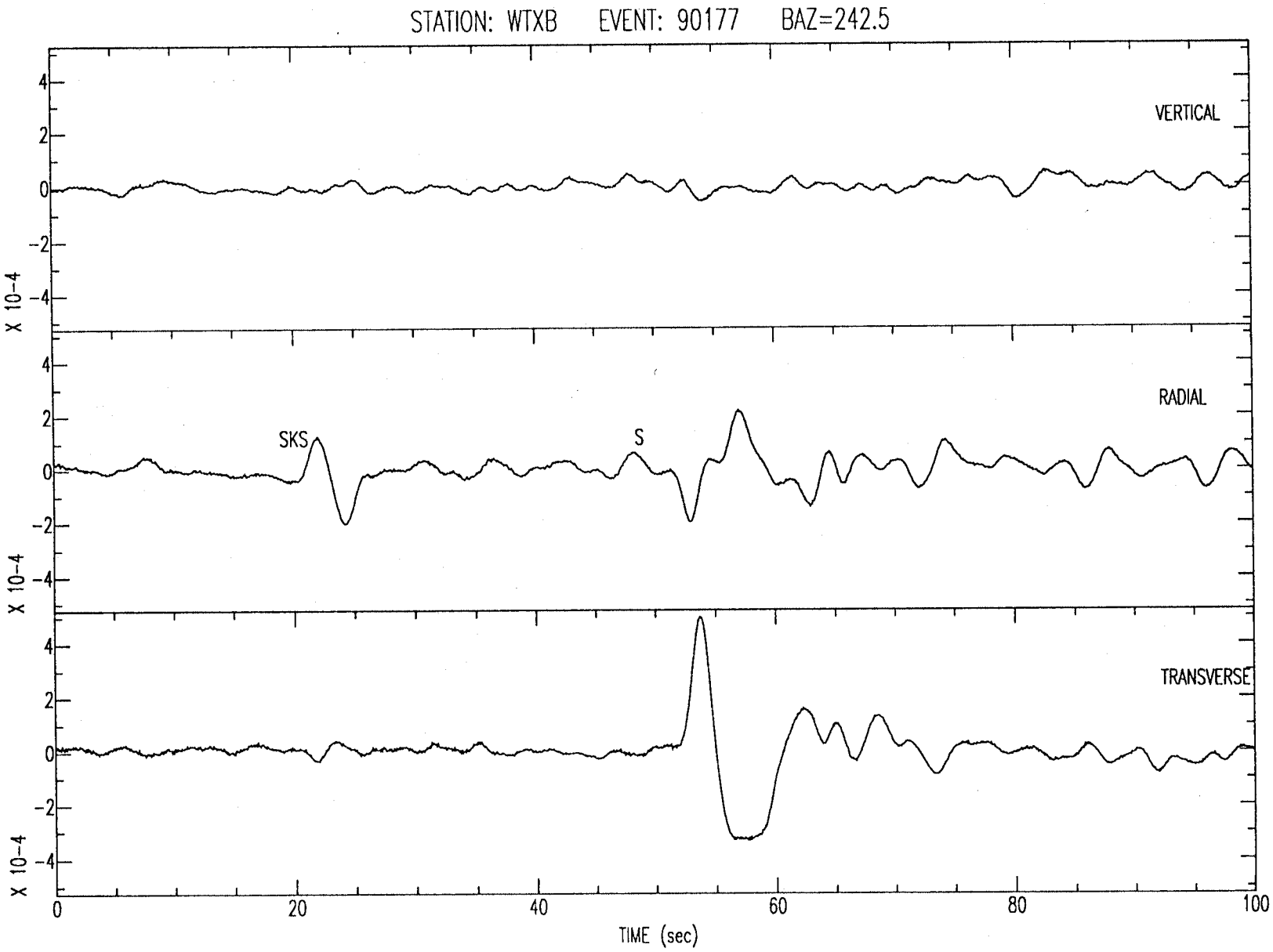
STATION: WTXB EVENT: 90177 BAZ=242.5
VERTICAL
RADIAL
TRANSVERSE
SKS
S
X 10-4
4
2
0
-2
-4
0
20
40
60
80
100
TIME (sec)

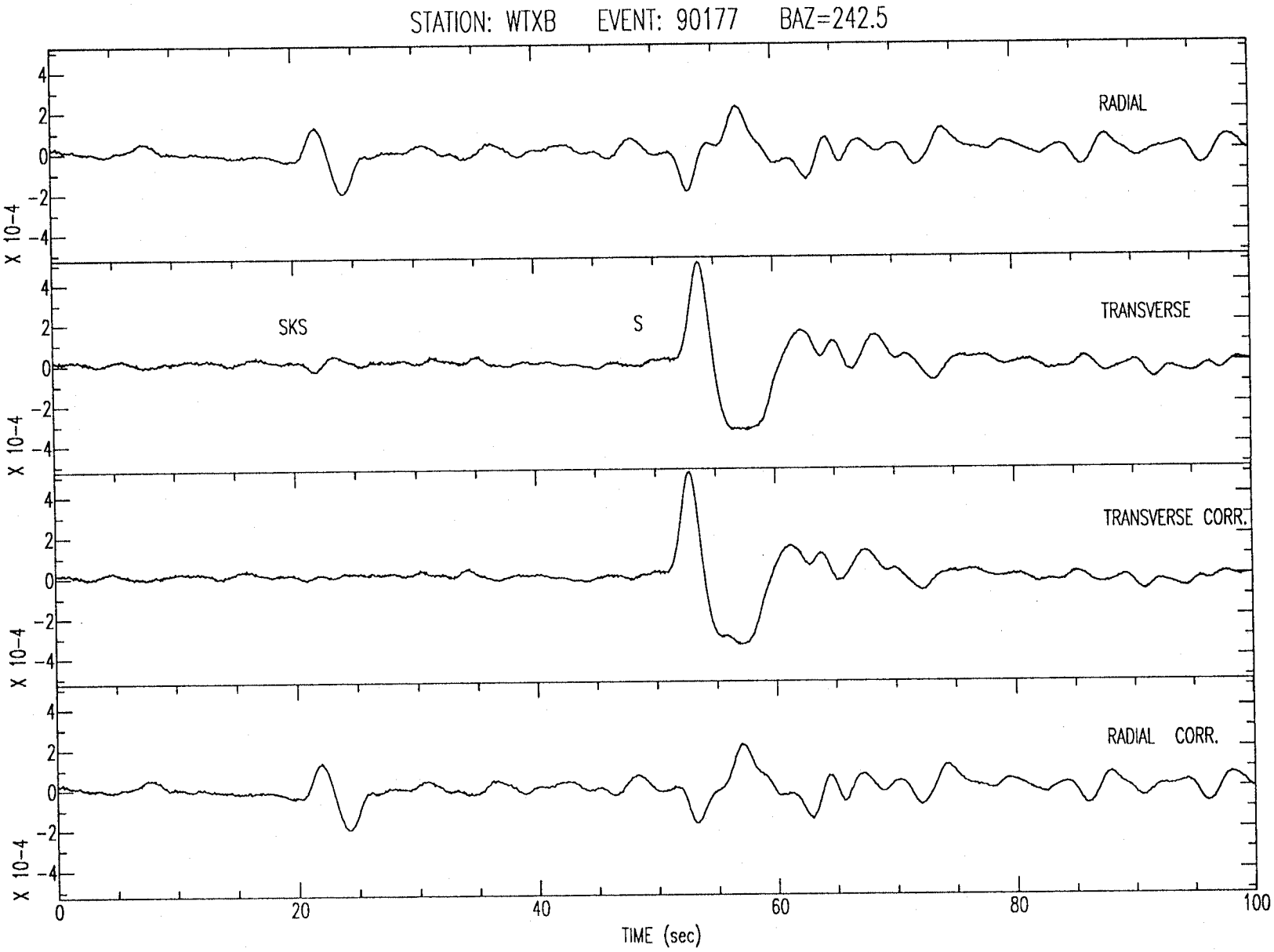
STATION: WTXB EVENT: 90177 BAZ=242.5
RADIAL
TRANSVERSE
SKS
S
TRANSVERSE CORR.
RADIAL CORR.
X 10-4
4
2
0
-2
-4
0
20
40
60
80
100
TIME (sec)

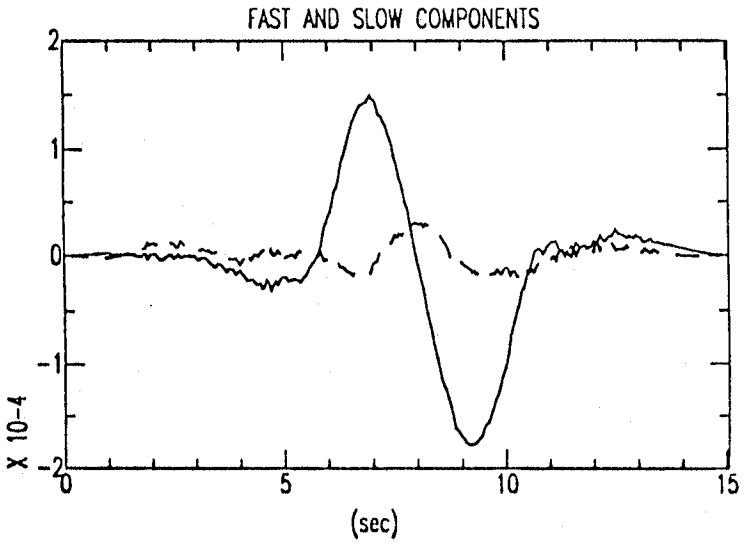
FAST AND SLOW COMPONENTS
X 10-4
(sec)

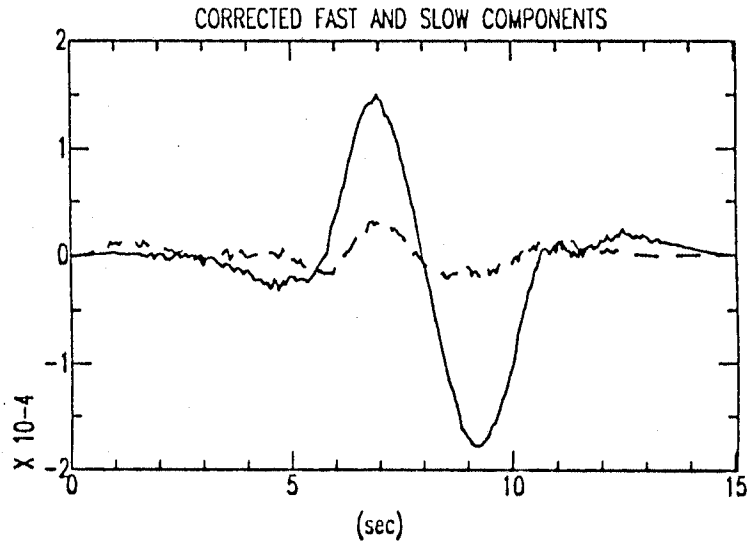
CORRECTED FAST AND SLOW COMPONENTS
X 10-4
(sec)

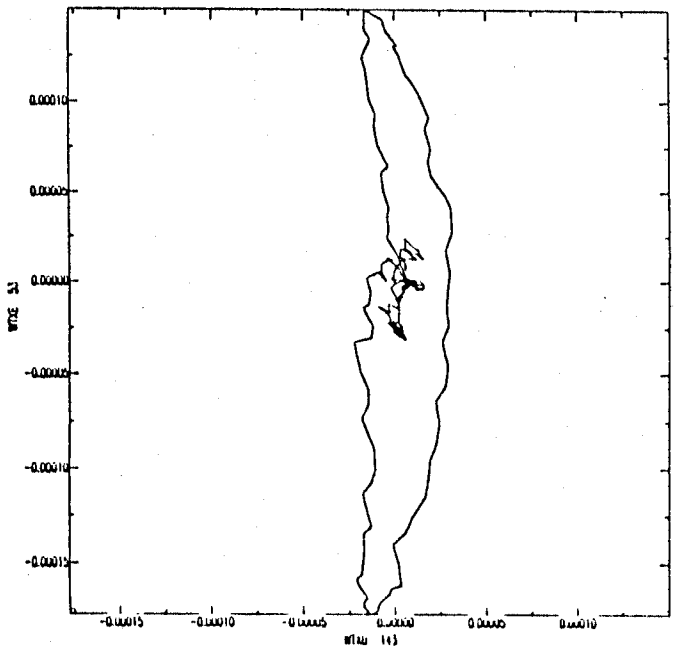

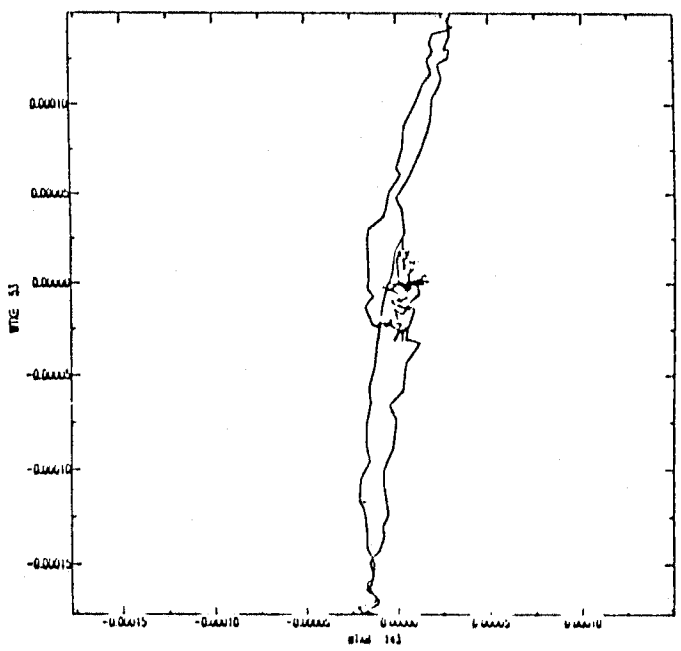

EVENT PARAMETERS

Event : 90191

Date : 90/07/10

Origin Time : 03:18

Magnitude : 5.8

Depth : 69 km

Latitude : 10.29S Longitude : 161.14E

STATION : WTXB

Δ = 97.3

BAZ = 262.5

SPLITTING PARAMETERS

ϕ = 52°

δt = 1.45s

Quality C

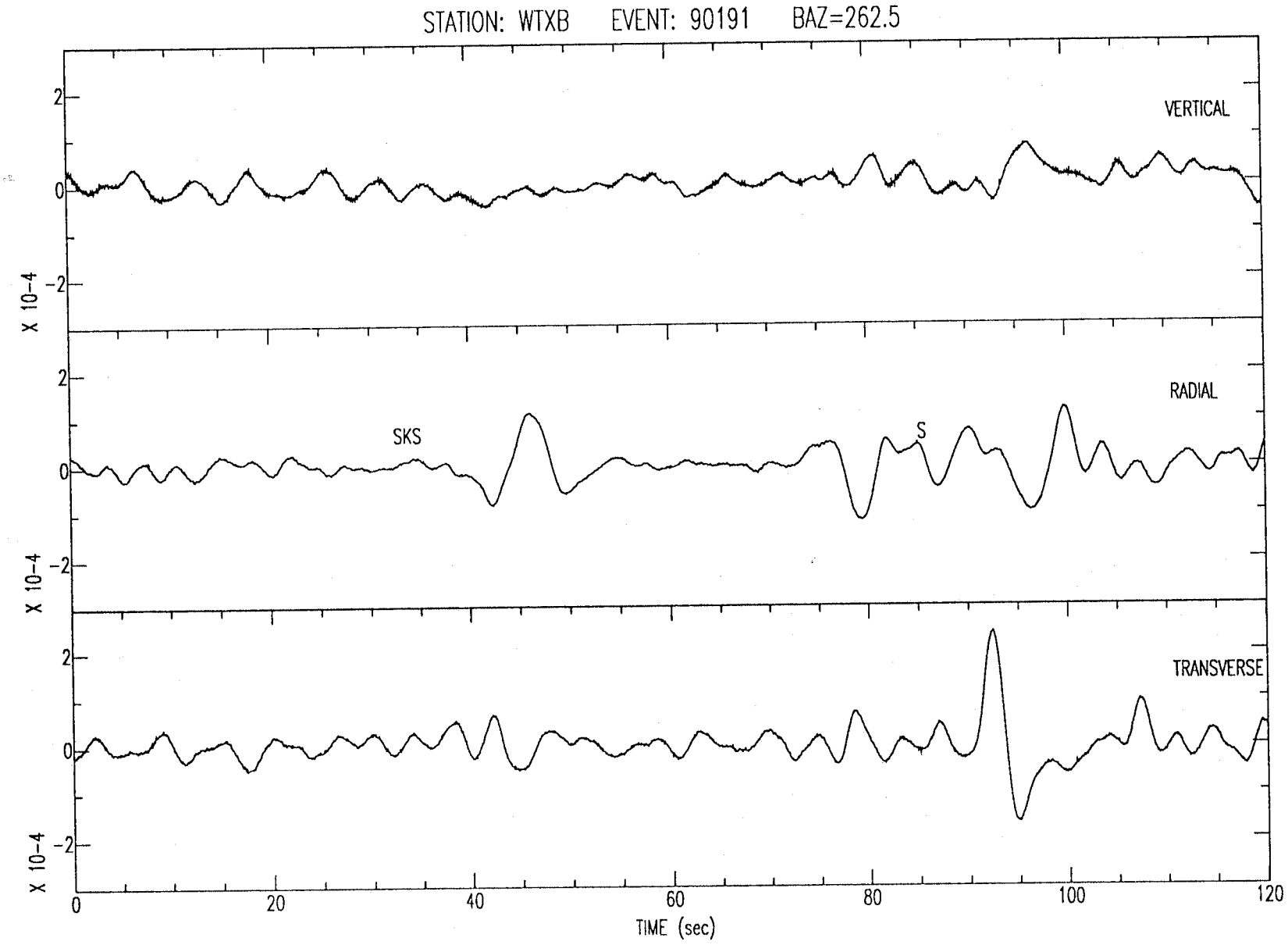
STATION: WTXB EVENT: 90191 BAZ=262.5
VERTICAL
RADIAL
TRANSVERSE
SKS
S
X 10-4
2
0
-2
0
20
40
60
80
100
120
TIME (sec)

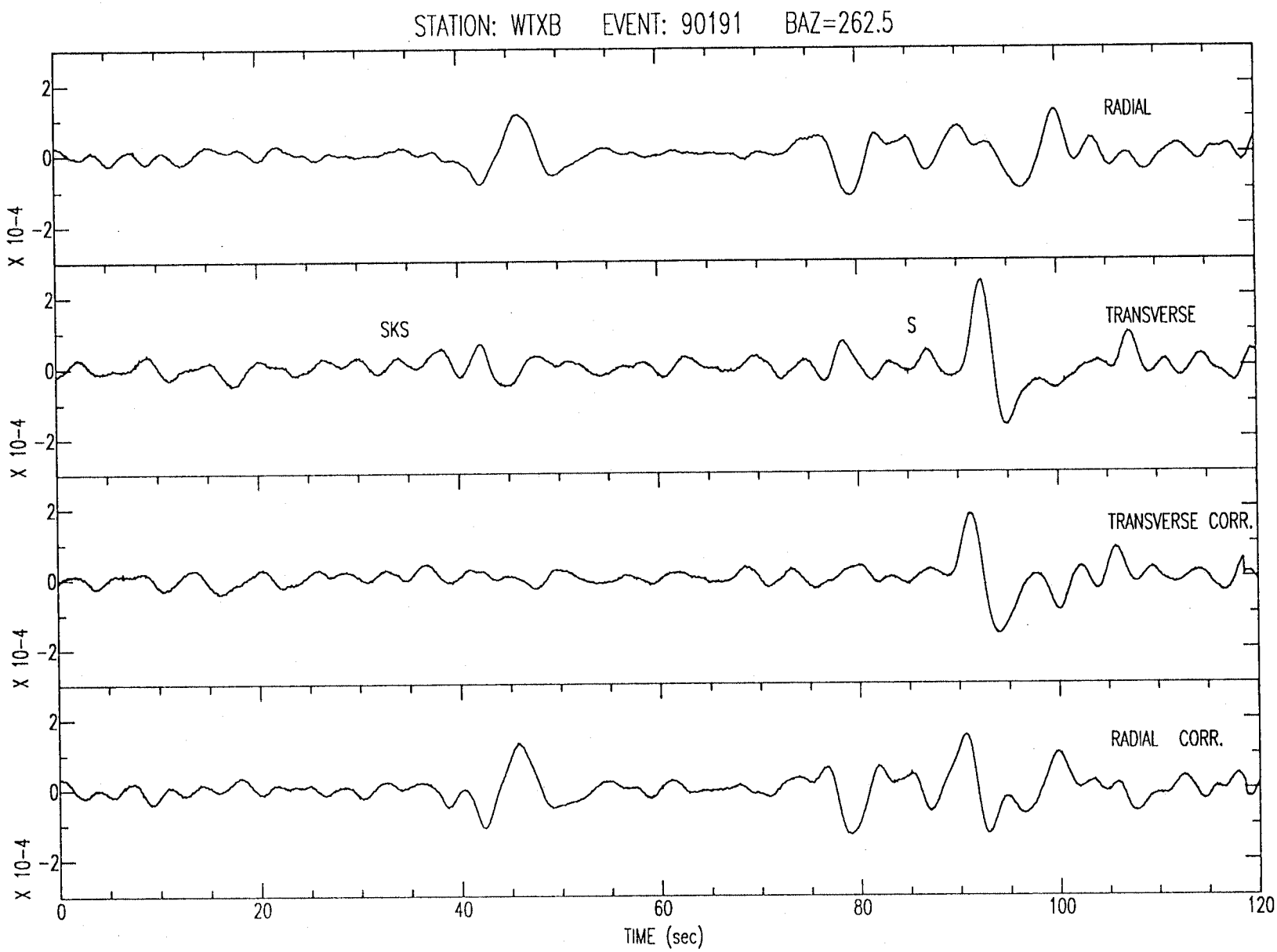
STATION: WTXB EVENT: 90191 BAZ=262.5
RADIAL
TRANSVERSE
SKS
S
TRANSVERSE CORR.
RADIAL CORR.
X 10-4
2
0
-2
0
20
40
60
80
100
120
TIME (sec)

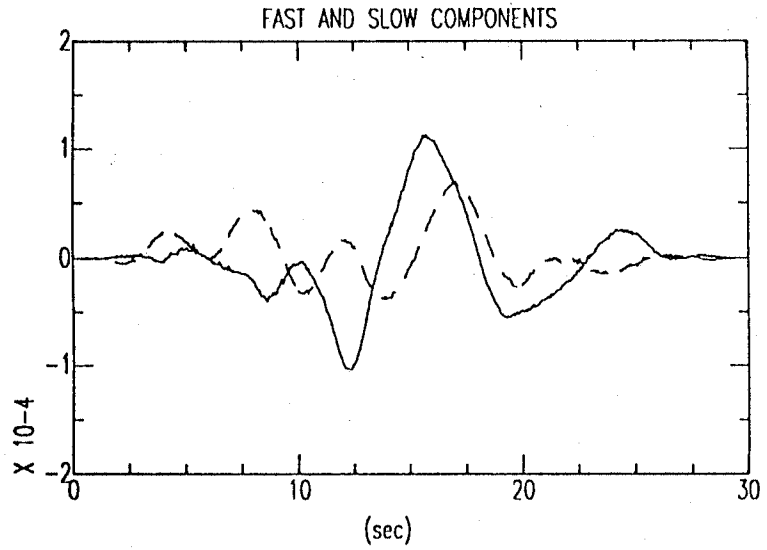
FAST AND SLOW COMPONENTS
X 10-4
(sec)

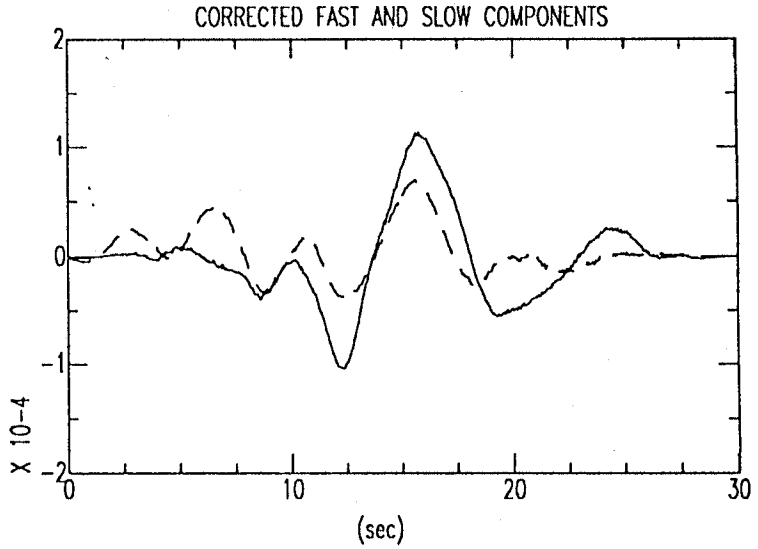
CORRECTED FAST AND SLOW COMPONENTS
X 10-4
(sec)

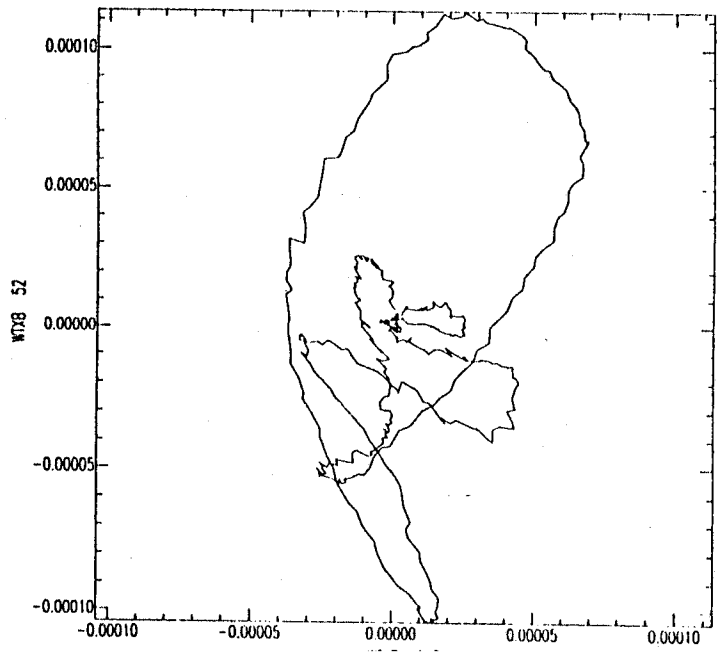
W03 52

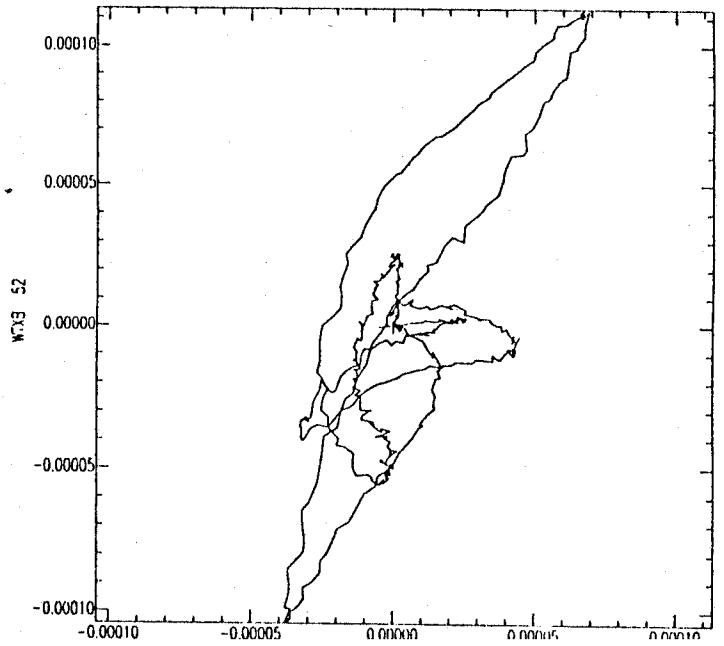
W03 52

EVENT PARAMETERS

Event : 90203

Date : 90/07/22

Origin Time : 09:26

Magnitude : 5.9

Depth : 565 km

Latitude : 23.45S Longitude : 179.92E

STATION : WTXI

Δ = 89.9

BAZ = 241.5

SPLITTING PARAMETERS

ϕ = 45°

δt = 0.65s

Quality A

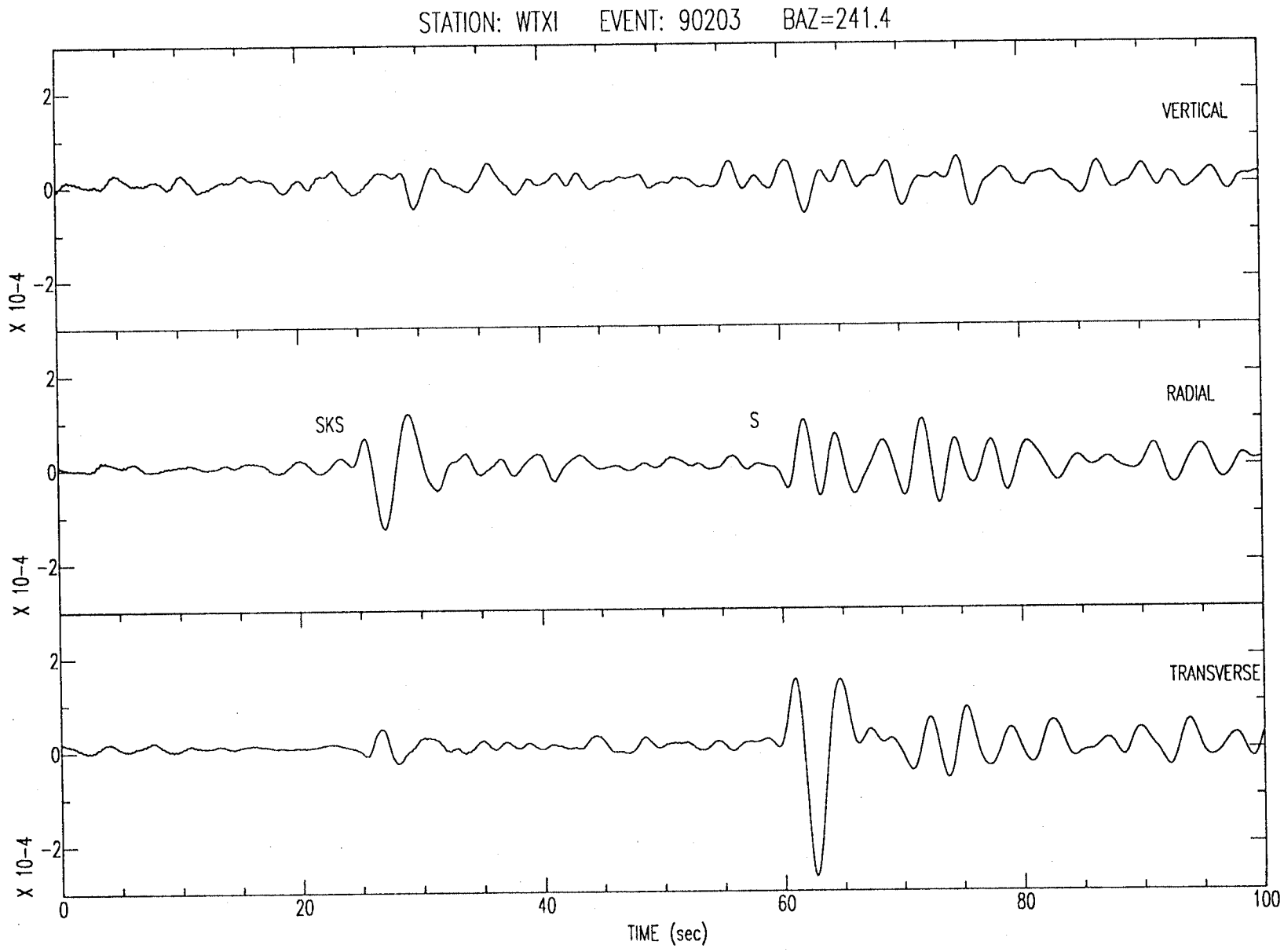
STATION: WTXI EVENT: 90203 BAZ=241.4
VERTICAL
RADIAL
TRANSVERSE
SKS
S
X 10-4
2
0
-2
0
20
40
60
80
100
TIME (sec)

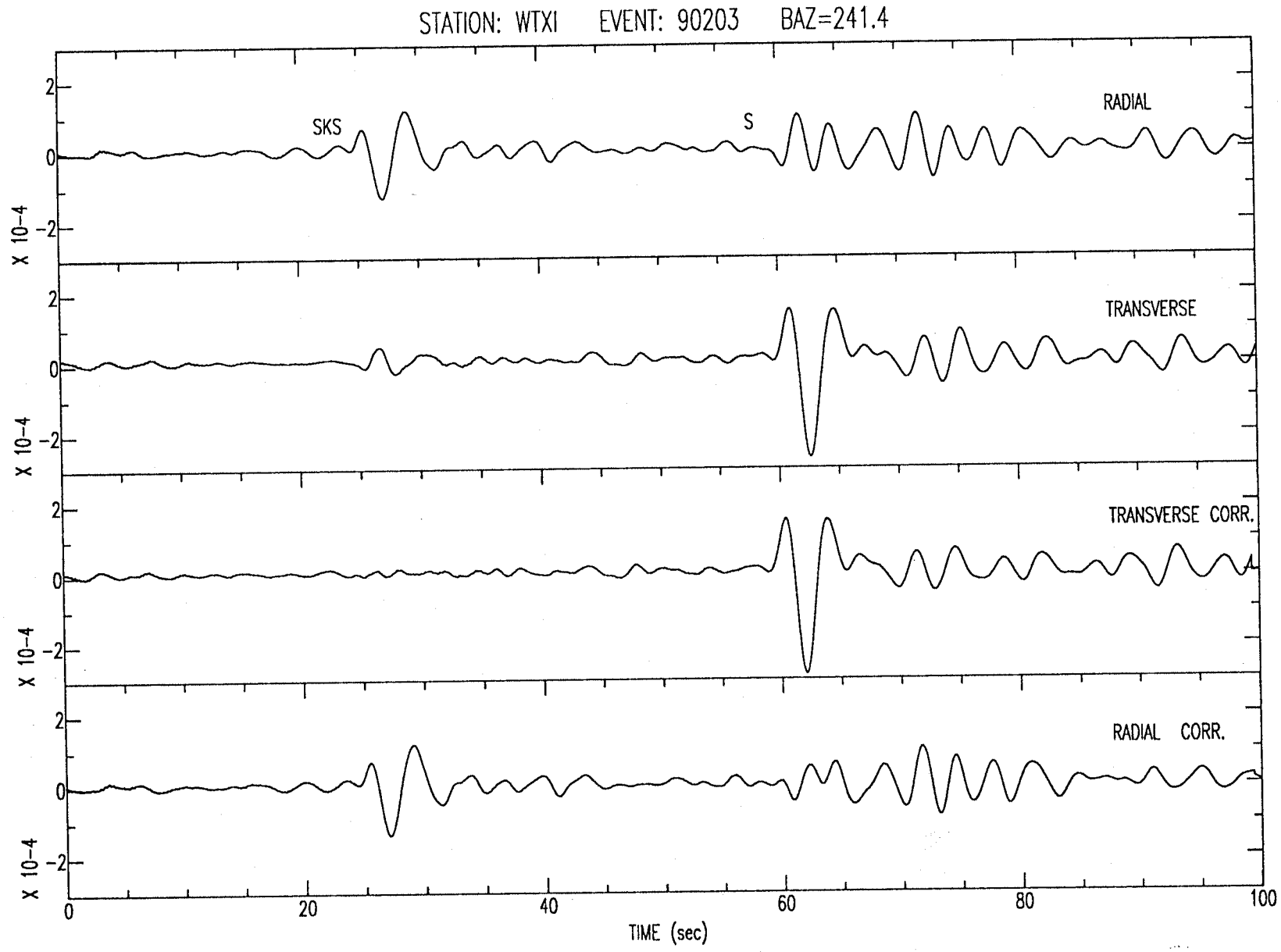
STATION: WTXI EVENT: 90203 BAZ=241.4
SKS
S
RADIAL
TRANSVERSE
TRANSVERSE CORR.
RADIAL CORR.
X 10-4
2
0
-2
0
20
40
60
80
100
TIME (sec)

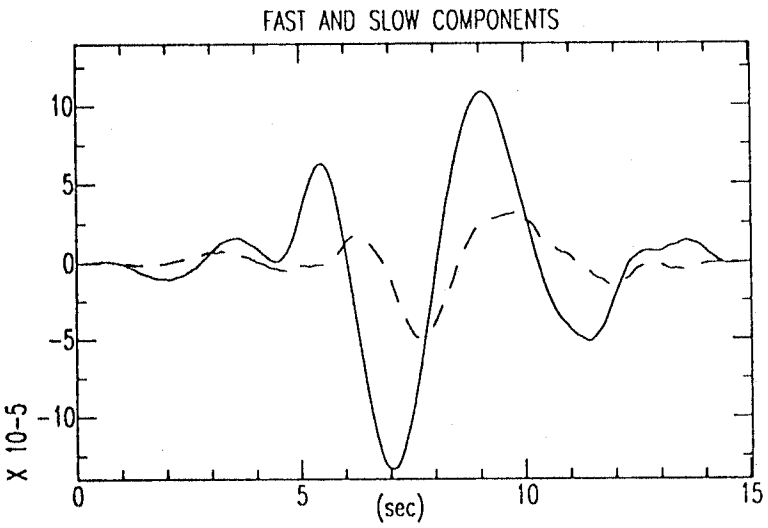
FAST AND SLOW COMPONENTS
X 10-5
10
5
0
-5
-10
0
5
(sec)
10
15

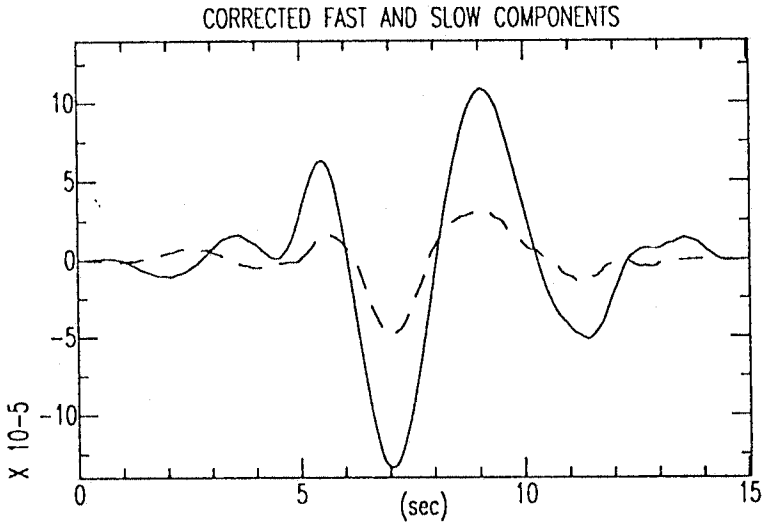
CORRECTED FAST AND SLOW COMPONENTS
X 10-5
10
5
0
-5
-10
0
5
(sec)
10
15

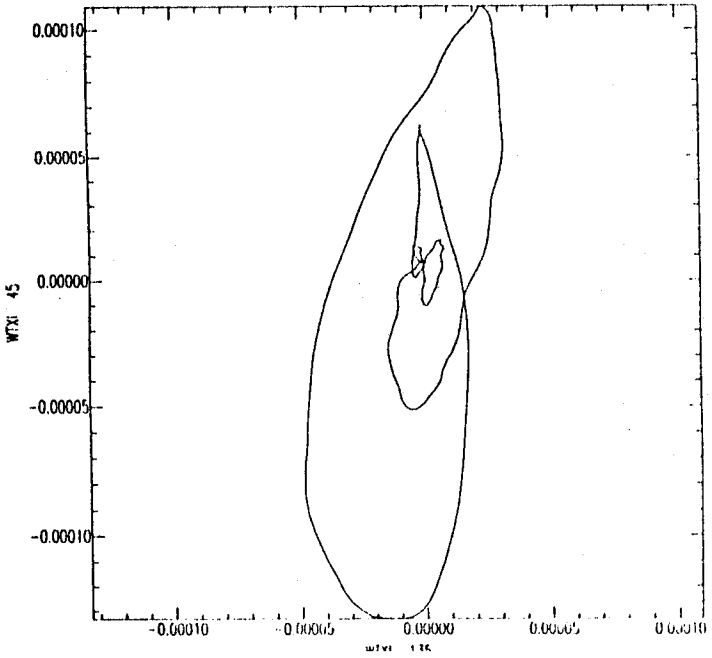
0.00010
0.00005
0.00000
-0.00005
-0.00010
-0.00010
-0.00005
0.00000
0.00005
0.00010

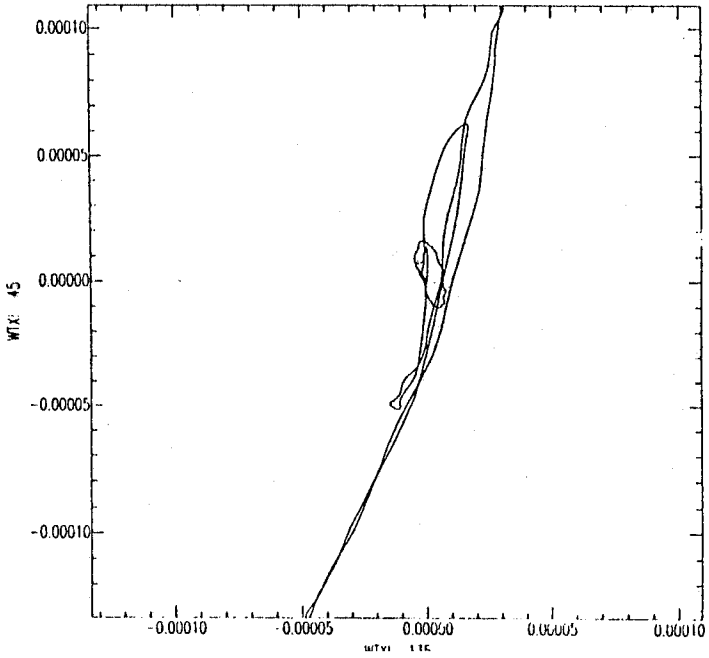
0.00010
0.00005
0.00000
-0.00005
-0.00010
-0.00010
-0.00005
0.00000
0.00005
0.00010

APPENDIX 2

This appendix contains the SKS seismograms used in splitting analysis from station ANMO. A title page showing the event and estimated splitting parameters is included before the seismograms. The seismograms are given in the following order :

1. Three component seismograms of SKS, vertical, radial and transverse components top to bottom respectively. S and SKS arrivals are labelled.

2. Uncorrected (original) radial and transverse components top two traces and corrected transverse and radial component seismograms bottom two traces respectively.

3. Superimposed plot of Fast (solid) and slow (dotted) component SKS seismograms. Uncorrected (left) and corrected (right). At the bottom corresponding particle motion diagrams. The fast direction is along the vertical axis.

Only original three component seismograms (vertical, radial and transverse) are shown for the events that did not exhibit detectable splitting.

EVENT PARAMETERS

Event : 90177

Date : 90/06/26

Origin Time : 12:08

Magnitude : 5.8

Depth : 593 km

Latitude : 21.97S Longitude : 179.52W

STATION : ANMO

Δ = 89.4

BAZ = 242.6

SPLITTING PARAMETERS

ϕ = -28^{o}

δt = 0.0s

Quality A

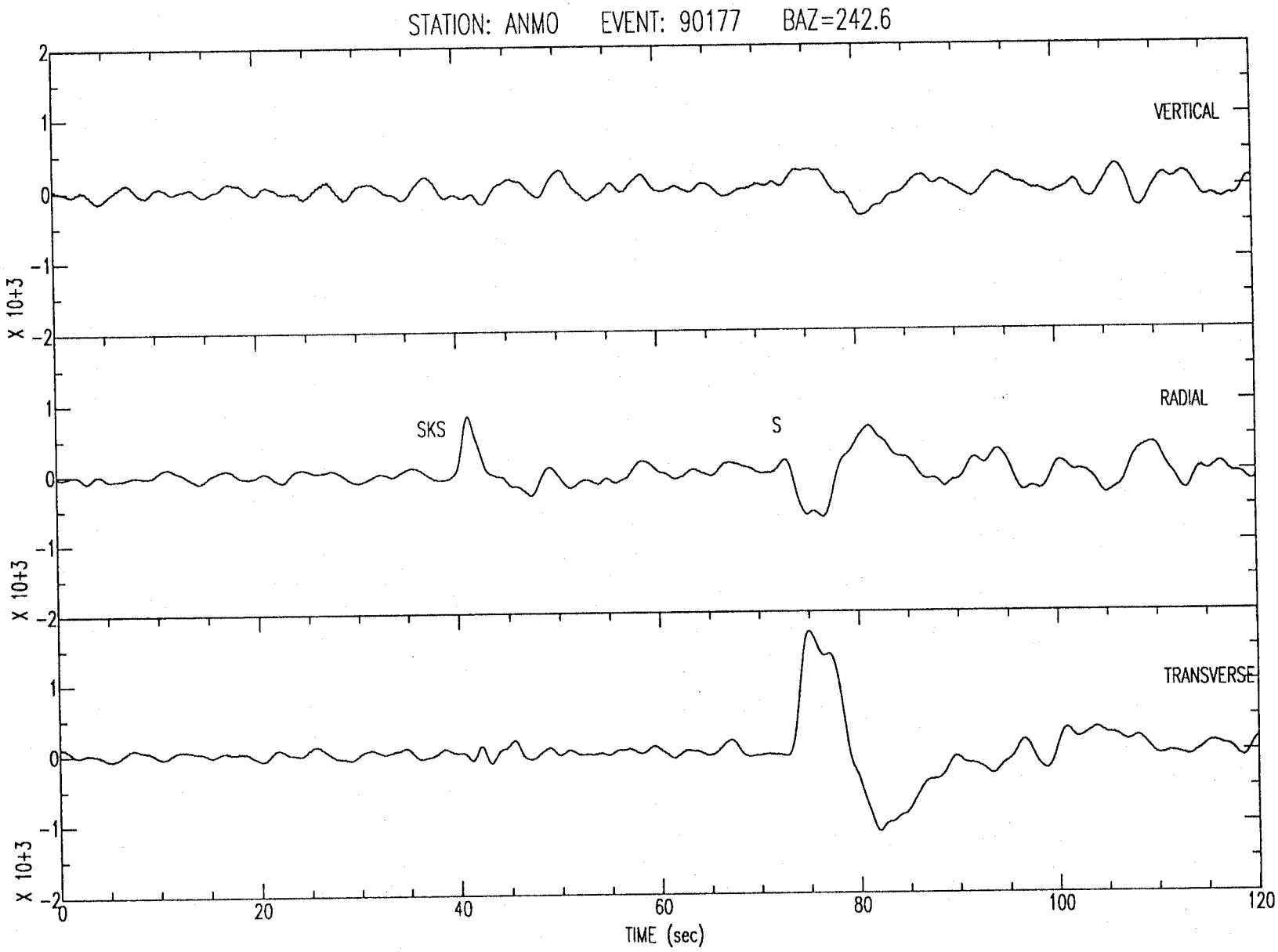
STATION: ANMO EVENT: 90177 BAZ=242.6
VERTICAL
RADIAL
TRANSVERSE
SKS
S
X 10+3
X 10+3
X 10+3
2
1
0
-1
-2
0
20
40
60
80
100
120
TIME (sec)

EVENT PARAMETERS

Event : 90191

Date : 90/07/10

Origin Time : 03:18

Magnitude : 5.8

Depth : 69 km

Latitude : 10.29S Longitude : 161.14E

STATION : ANMO

Δ = 97.7

BAZ = 262.9

SPLITTING PARAMETERS

ϕ = 20°

δt = 0.80s

Quality C

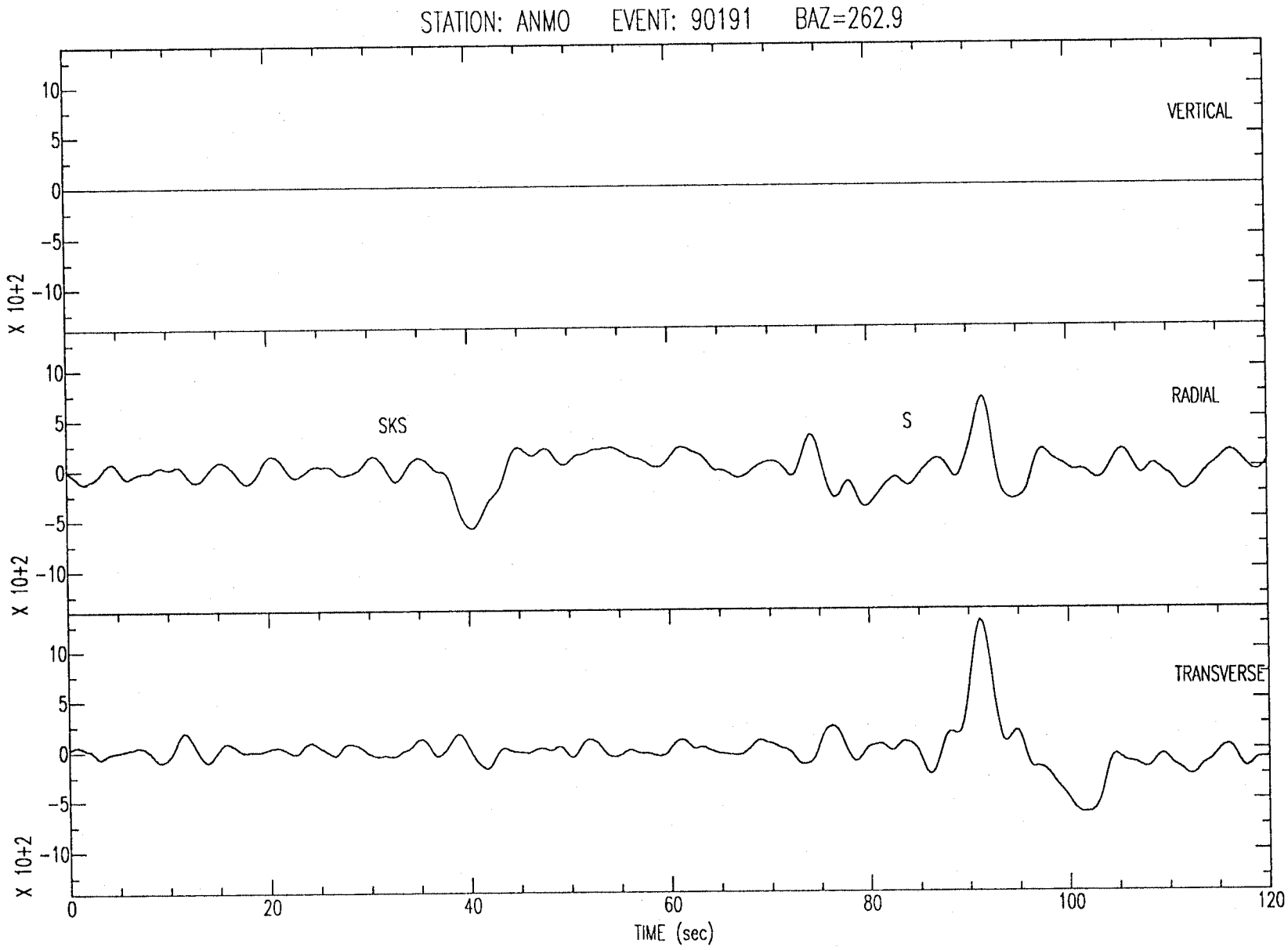
STATION: ANMO EVENT: 90191 BAZ=262.9
VERTICAL
RADIAL
TRANSVERSE
SKS
S
X 10+2
X 10+2
X 10+2
10
5
0
-5
-10
0
20
40
60
80
100
120
TIME (sec)

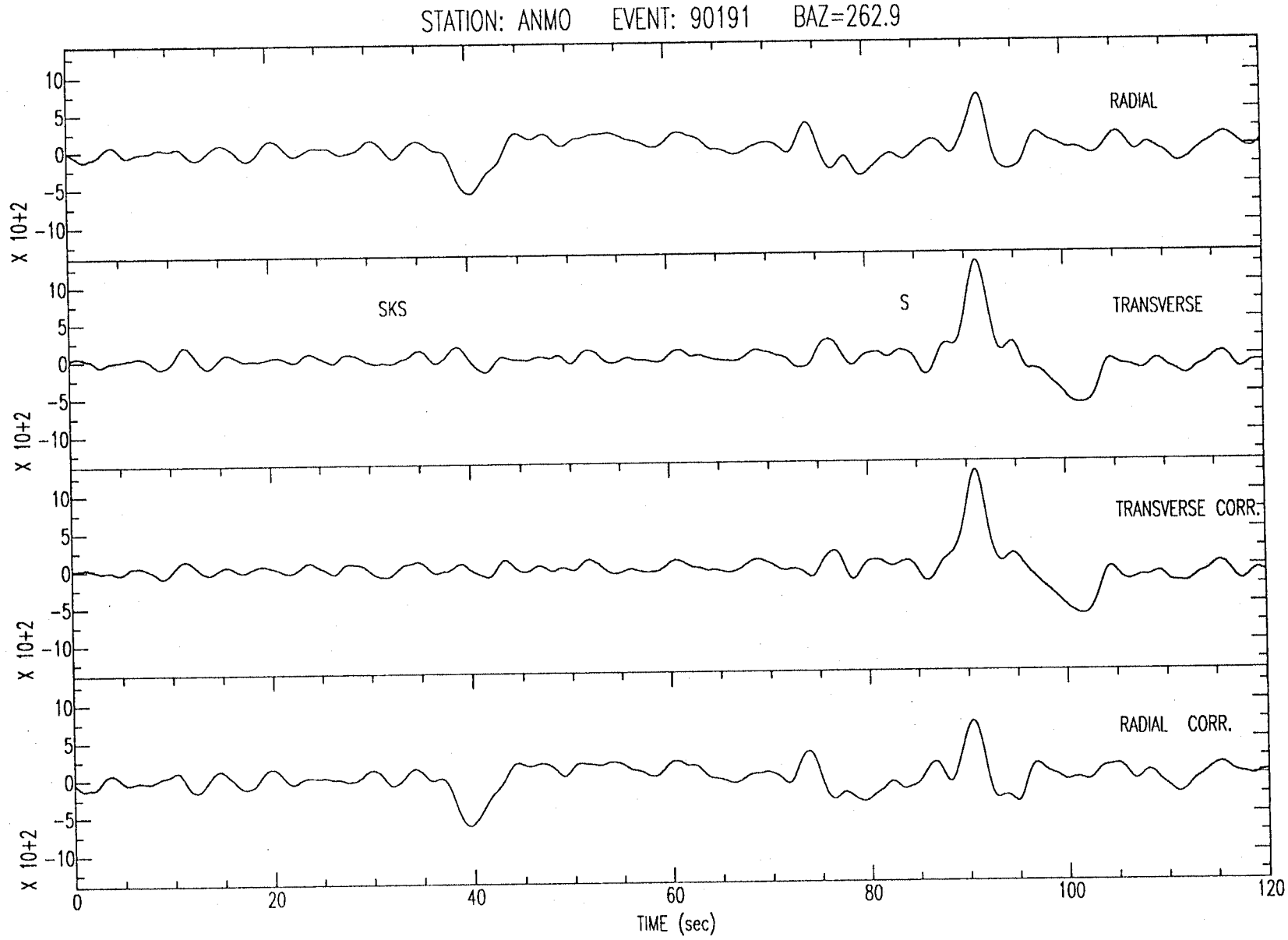
STATION: ANMO EVENT: 90191 BAZ=262.9
RADIAL
TRANSVERSE
SKS
S
TRANSVERSE CORR.
RADIAL CORR.
X 10+2
10
5
0
-5
-10
0
20
40
60
80
100
120
TIME (sec)

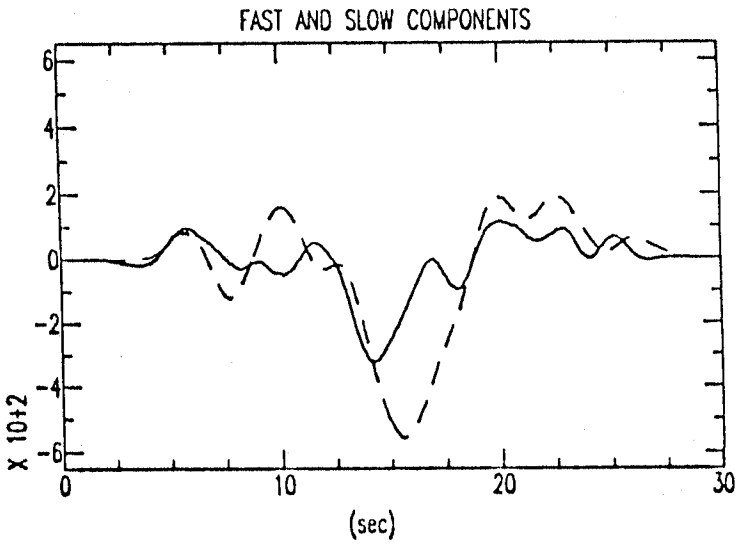
FAST AND SLOW COMPONENTS
X 10+2
6
4
2
0
-2
-4
-6
0
10
20
30
(sec)

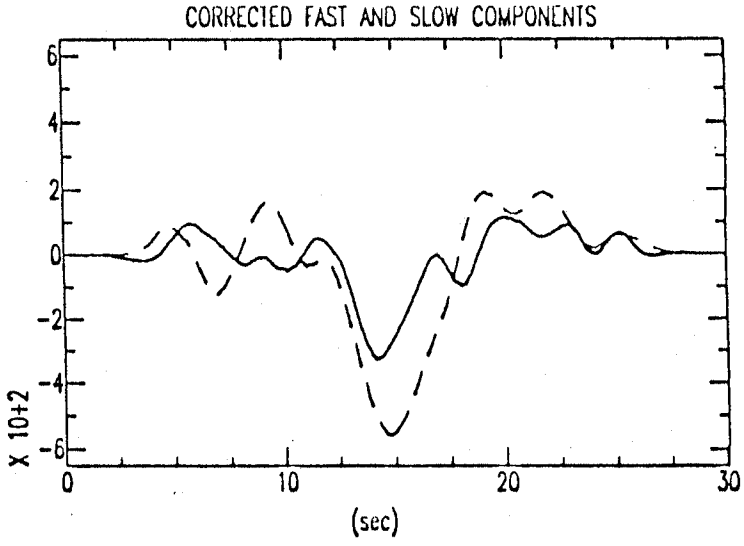
CORRECTED FAST AND SLOW COMPONENTS
X 10+2
6
4
2
0
-2
-4
-6
0
10
20
30
(sec)

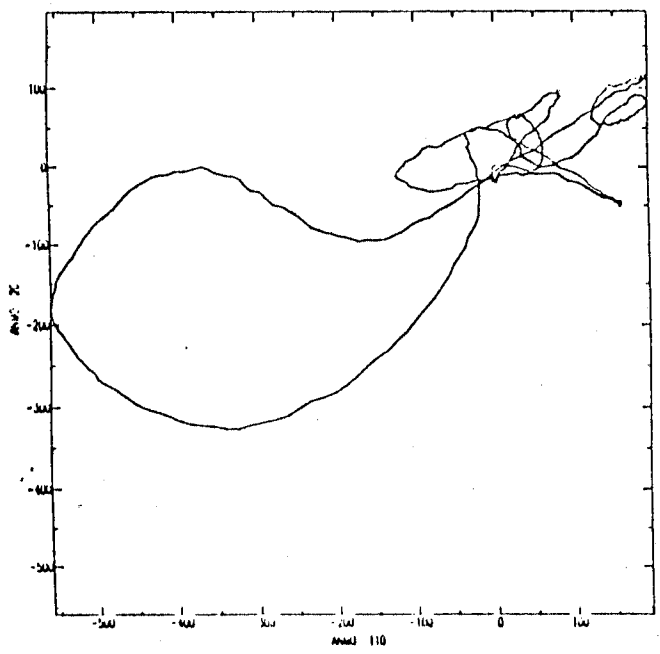

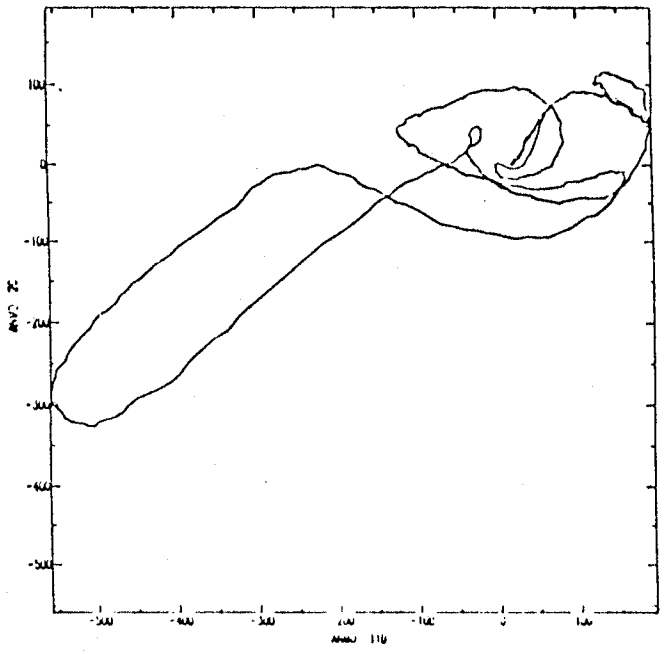

EVENT PARAMETERS

Event : 90217

Date : 90/08/05

Origin Time : 01:34

Magnitude : 5.9

Depth : 516 km

Latitude : 29.51N Longitude : 137.59E

STATION : ANMO

Δ = 92.0

BAZ = 308.3

SPLITTING PARAMETERS

ϕ = -28^{o}

δt = 0.60s

Quality A

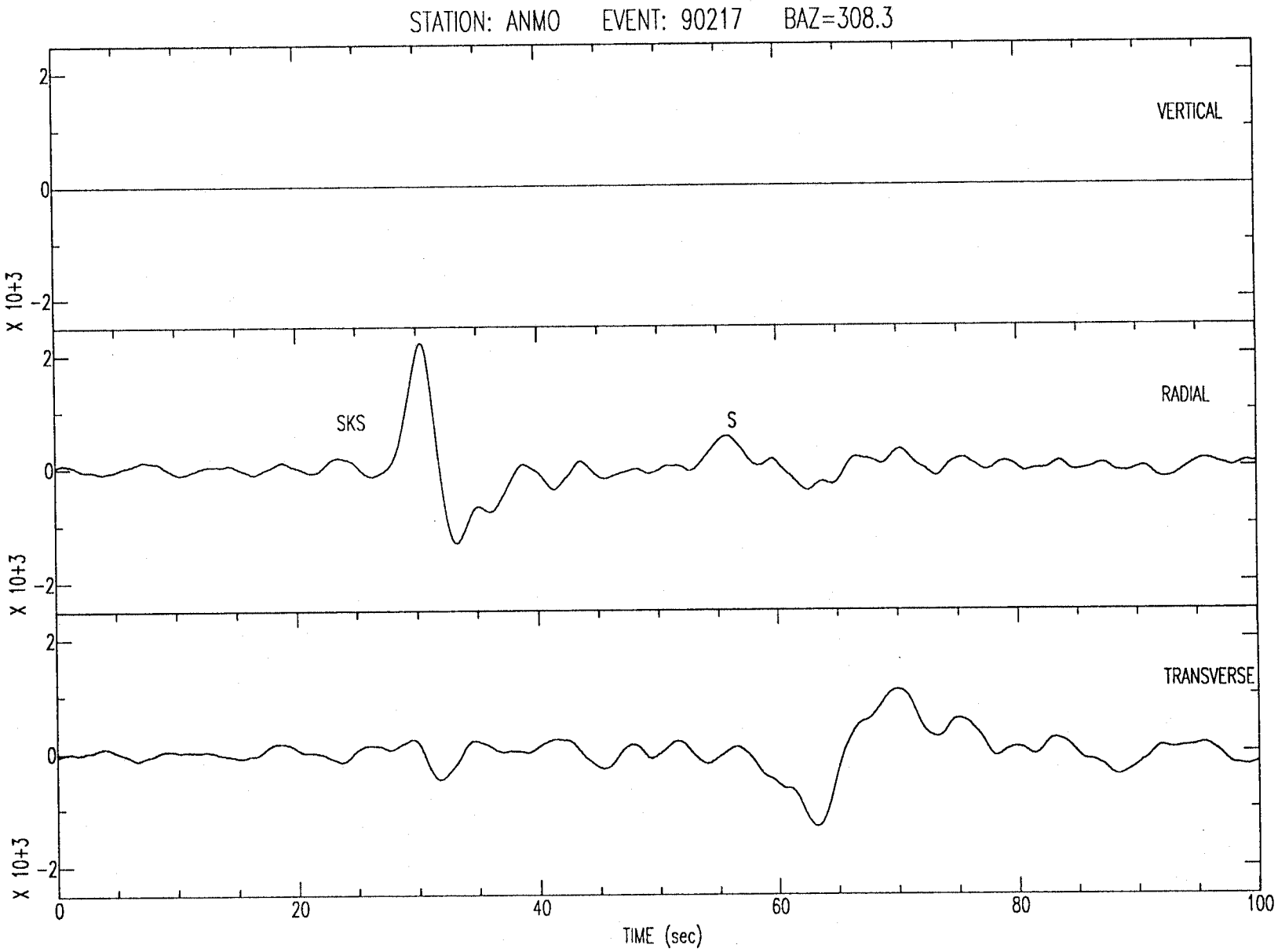
STATION: ANMO EVENT: 90217 BAZ=308.3
VERTICAL
RADIAL
TRANSVERSE
SKS
S
X 10+3
2
0
-2
0
20
40
60
80
100
TIME (sec)

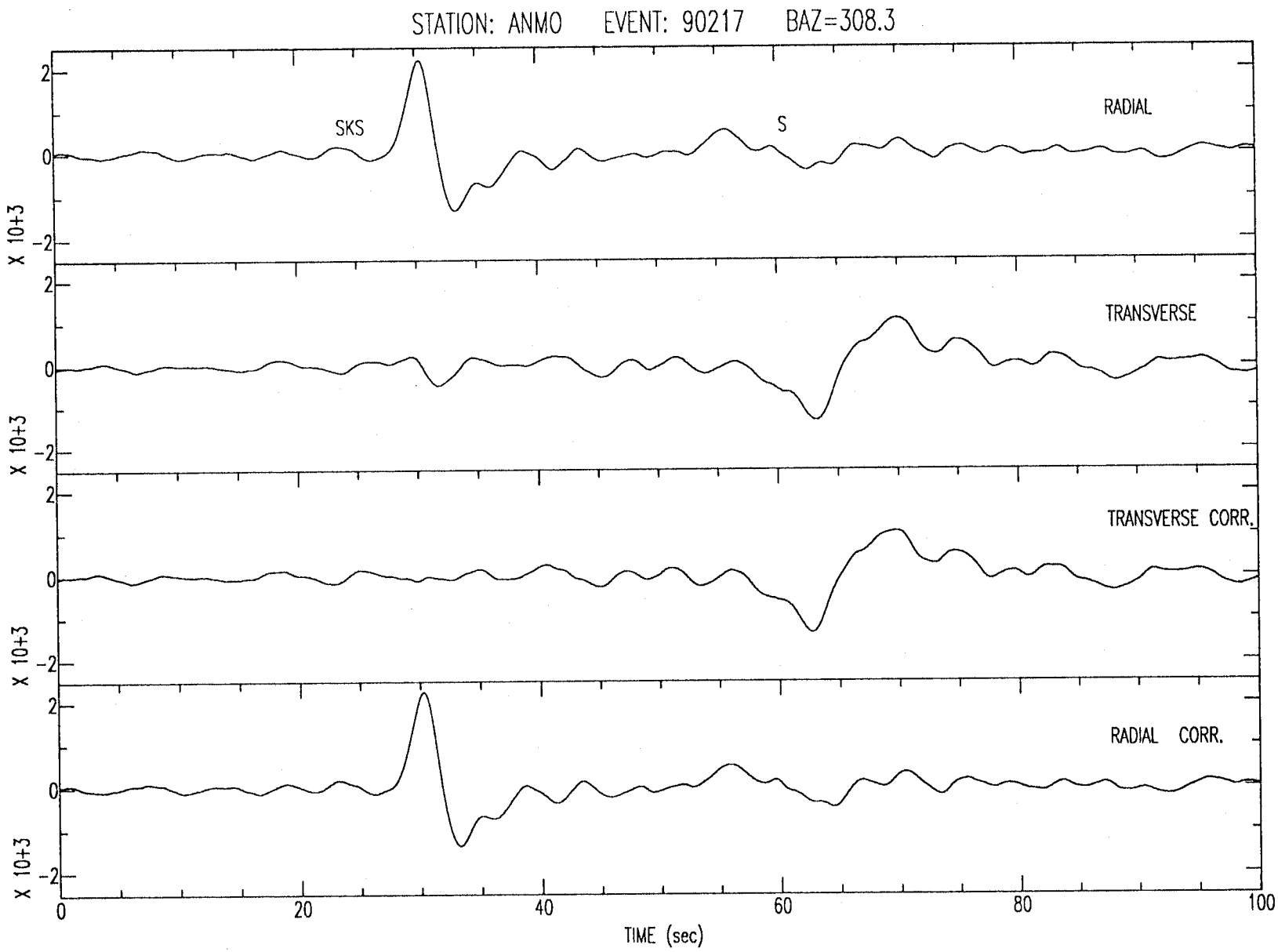
STATION: ANMO EVENT: 90217 BAZ=308.3
SKS
S
RADIAL
TRANSVERSE
TRANSVERSE CORR.
RADIAL CORR.
X 10+3
2
0
-2
0
20
40
60
80
100
TIME (sec)

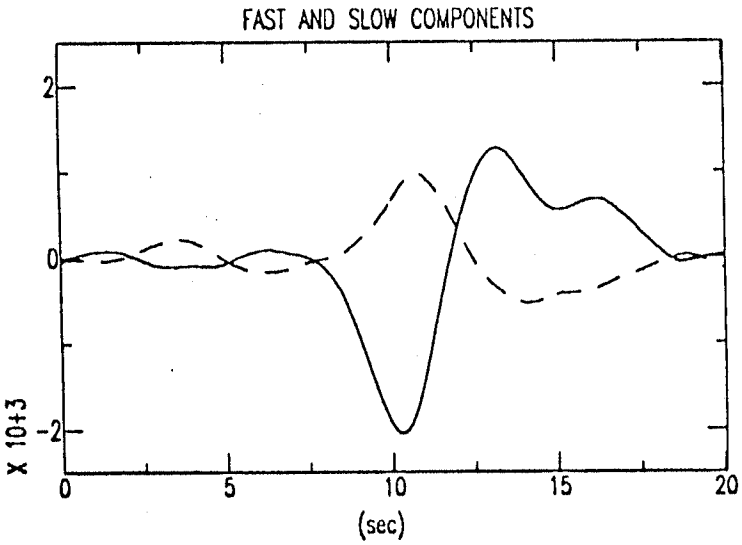
FAST AND SLOW COMPONENTS
X 10+3
2
0
-2
0
5
10
15
20
(sec)

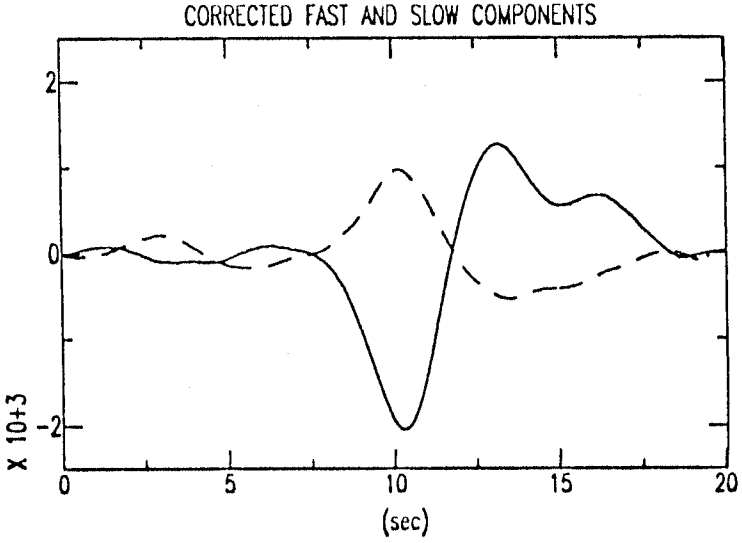
CORRECTED FAST AND SLOW COMPONENTS
X 10+3
2
0
-2
0
5
10
15
20
(sec)

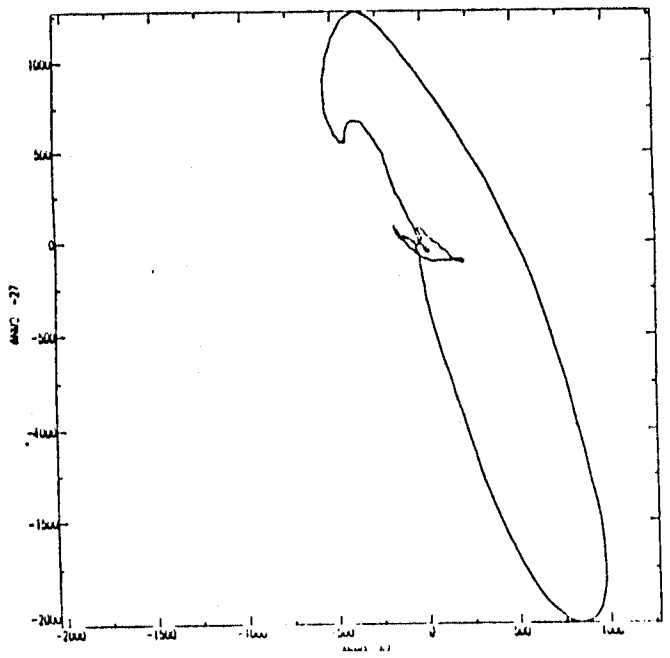

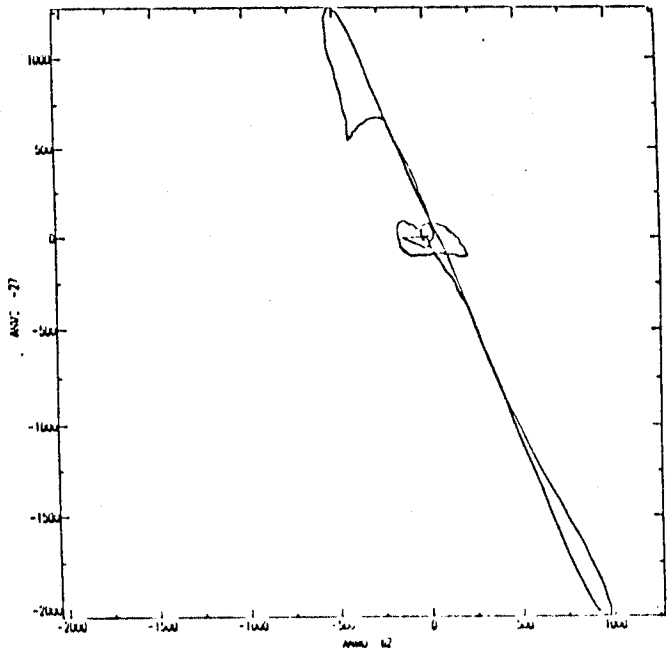

EVENT PARAMETERS

Event : 90217

Date : 90/08/05

Origin Time : 17:42

Magnitude : 5.6

Depth : 10 km

Latitude : 1.01S Longitude : 13.96W

STATION : ANMO

Δ = 92.6

BAZ = 89.4

SPLITTING PARAMETERS

ϕ = 21°

δt = 1.80s

Quality A

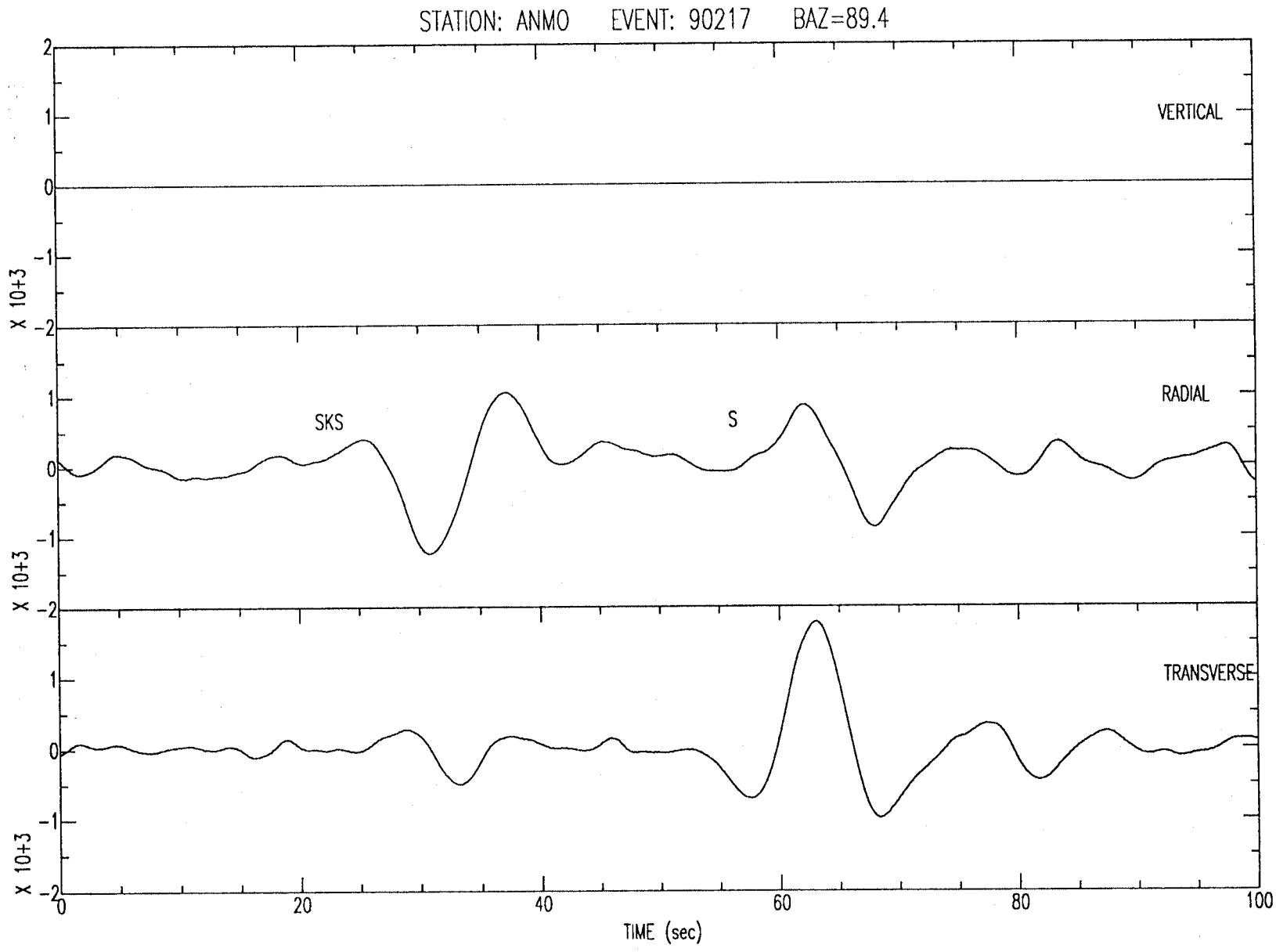
STATION: ANMO EVENT: 90217 BAZ=89.4
VERTICAL
RADIAL
TRANSVERSE
SKS
S
X 10+3
X 10+3
X 10+3
2
1
0
-1
-2
0
20
40
60
80
100
TIME (sec)

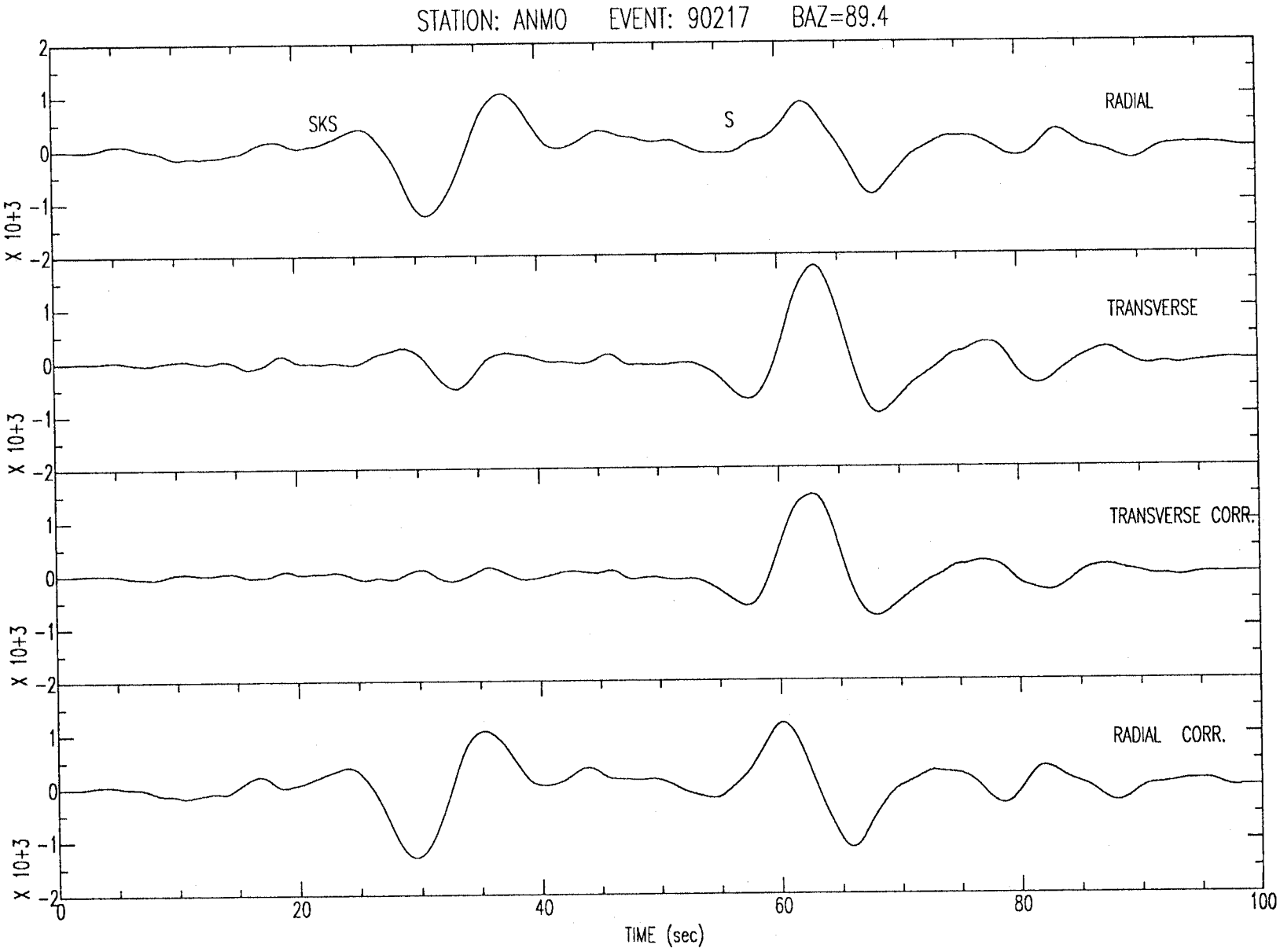
STATION: ANMO EVENT: 90217 BAZ=89.4
SKS
S
RADIAL
TRANSVERSE
TRANSVERSE CORR.
RADIAL CORR.
X 10+3
2
1
0
-1
-2
0
20
40
60
80
100
TIME (sec)

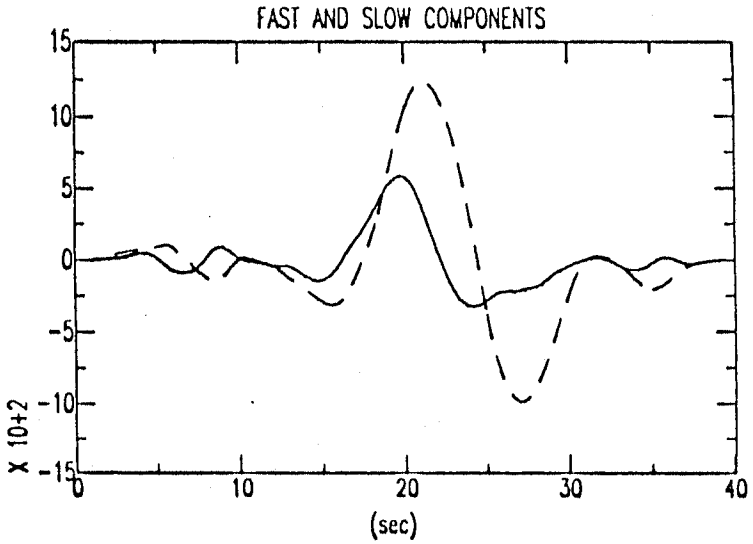
FAST AND SLOW COMPONENTS
X 10+2
(sec)

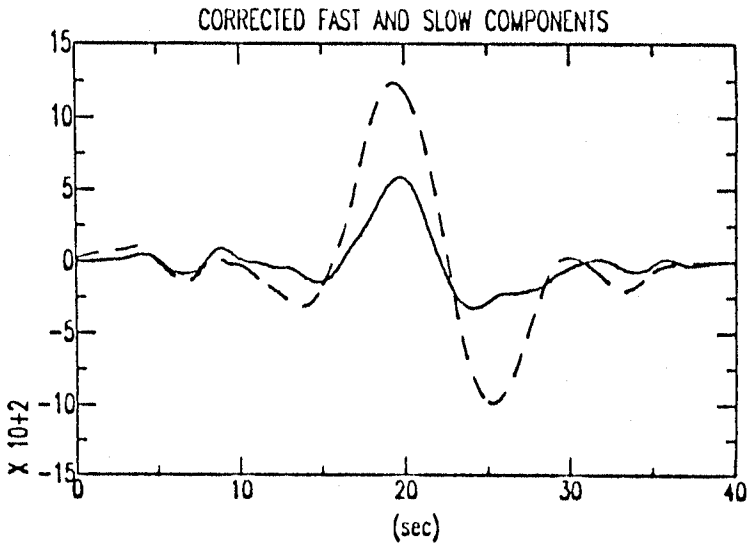
CORRECTED FAST AND SLOW COMPONENTS
X 10+2
(sec)

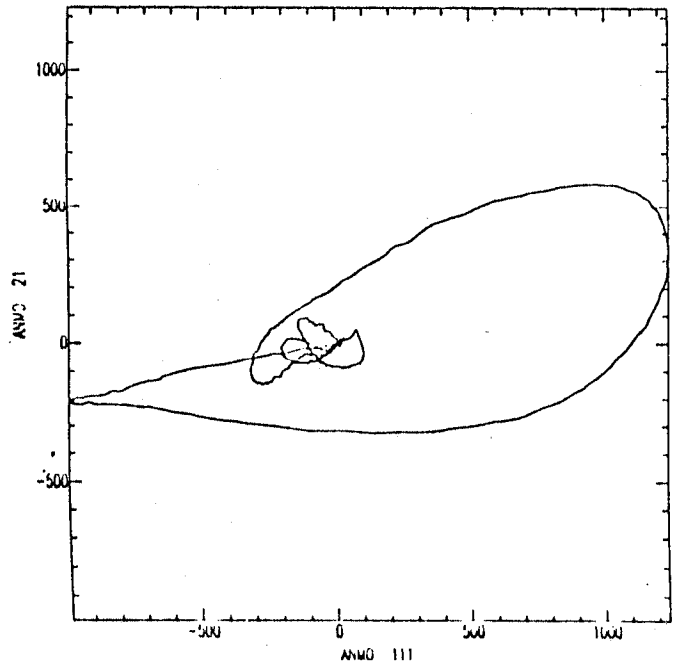
ANMO 21
ANMO 111

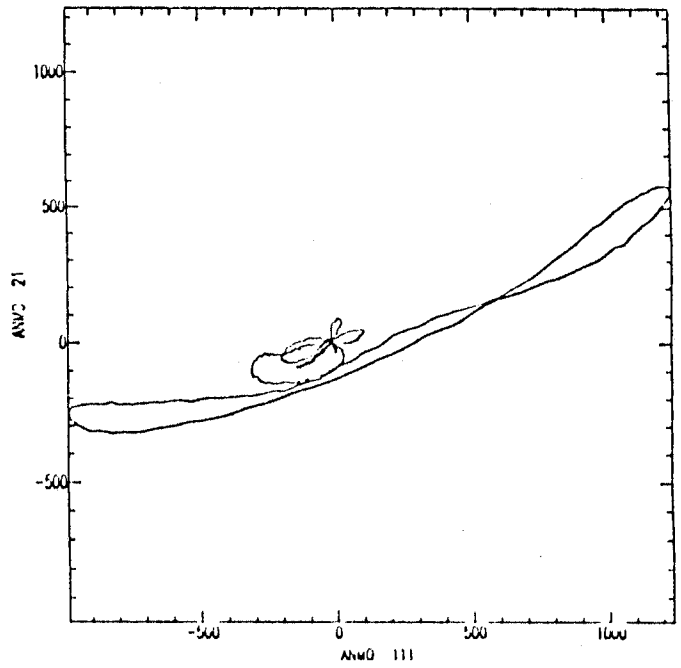
ANMO 21
ANMO 111

EVENT PARAMETERS

Event : 90229

Date : 90/08/17

Origin Time : 13:07

Magnitude : 5.9

Depth : 33 km

Latitude : 11.20S Longitude : 161.99E

STATION : ANMO

Δ = 97.3

BAZ = 262.0

SPLITTING PARAMETERS

ϕ = 16°

δt = 0.85s

Quality B

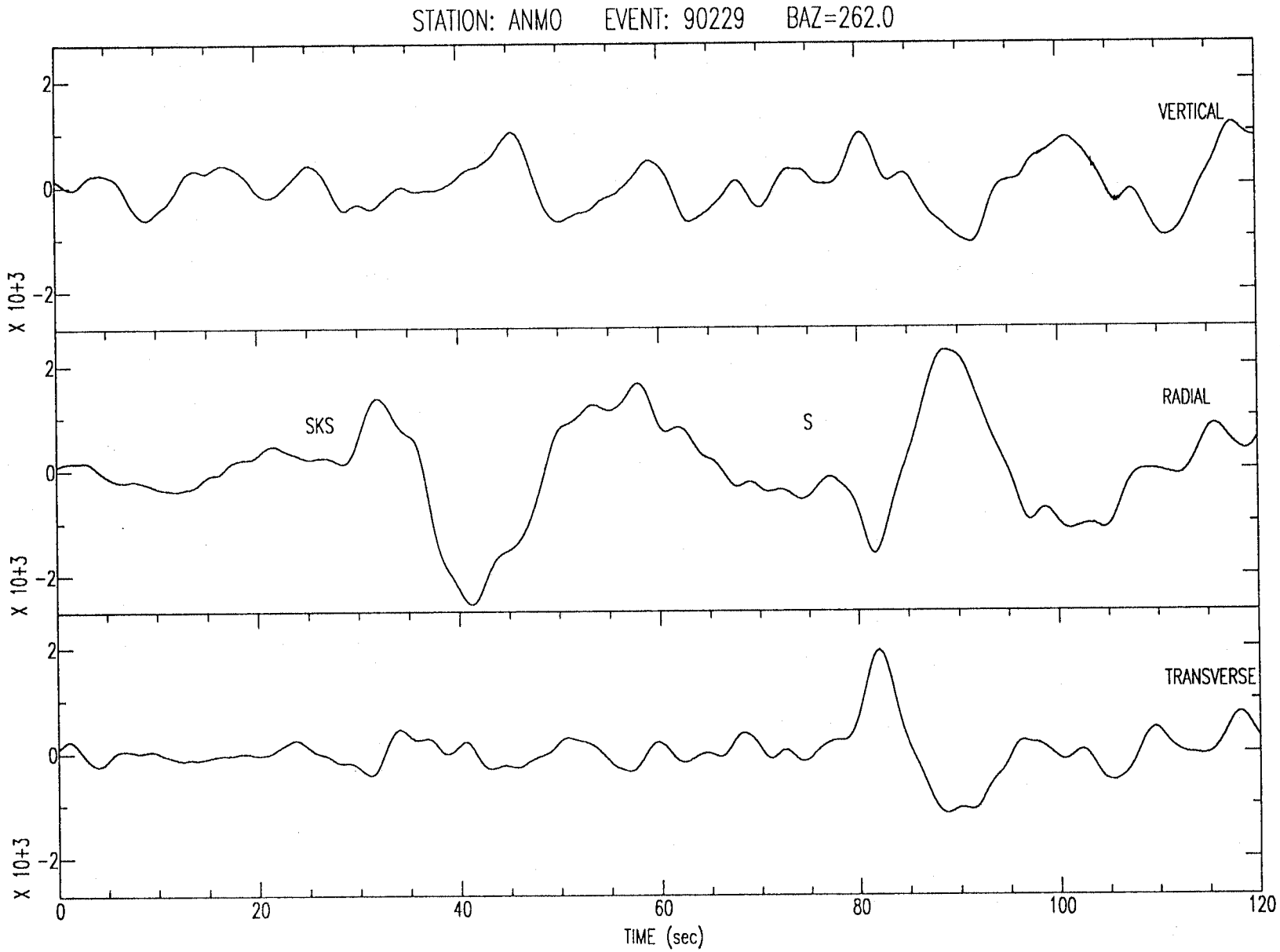
STATION: ANMO EVENT: 90229 BAZ=262.0
VERTICAL
RADIAL
TRANSVERSE
SKS
S
X 10+3
2
0
-2
0
20
40
60
80
100
120
TIME (sec)

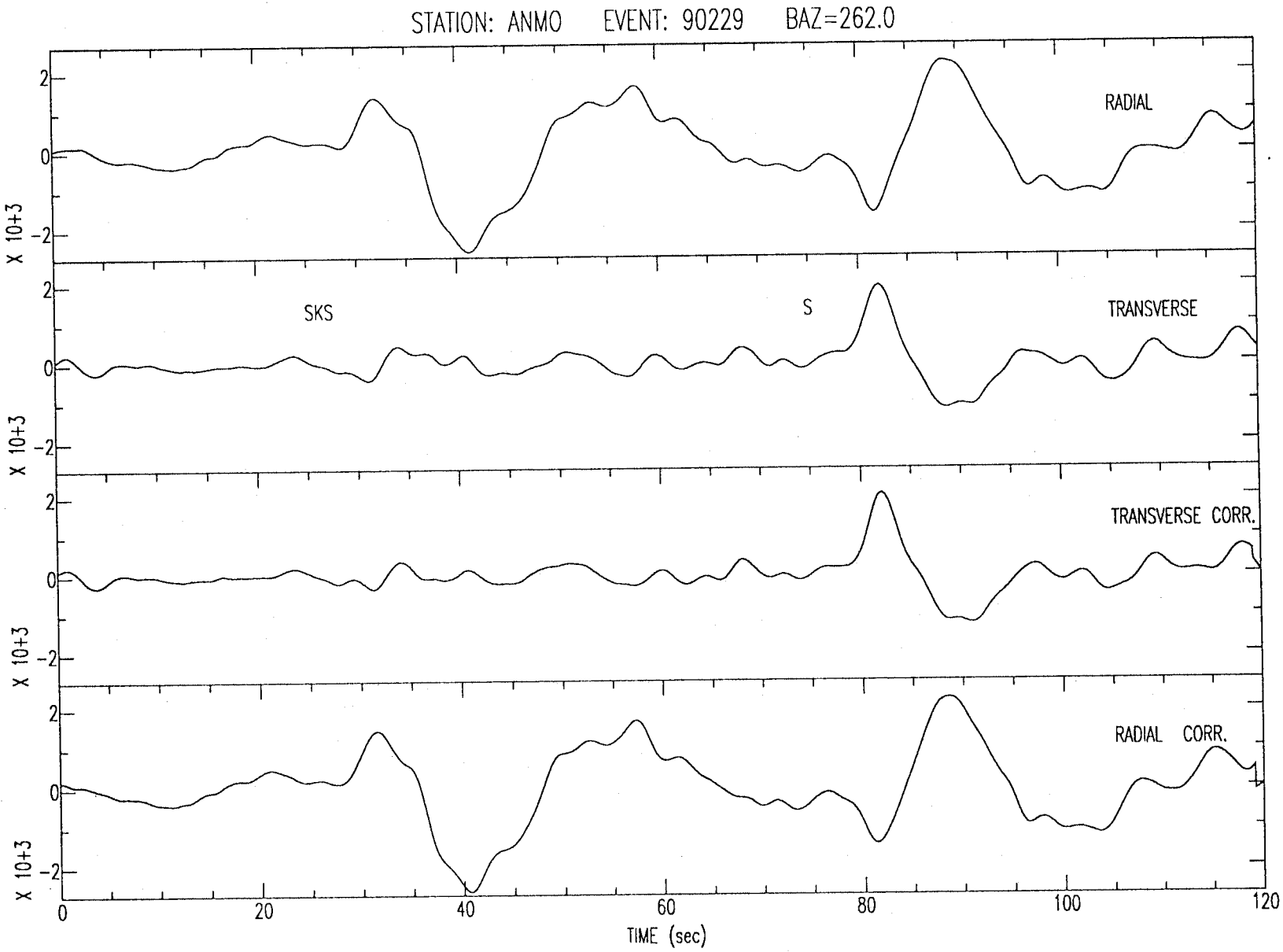
STATION: ANMO EVENT: 90229 BAZ=262.0
RADIAL
SKS
S
TRANSVERSE
TRANSVERSE CORR.
RADIAL CORR.
X 10+3
2
0
-2
0
20
40
60
80
100
120
TIME (sec)

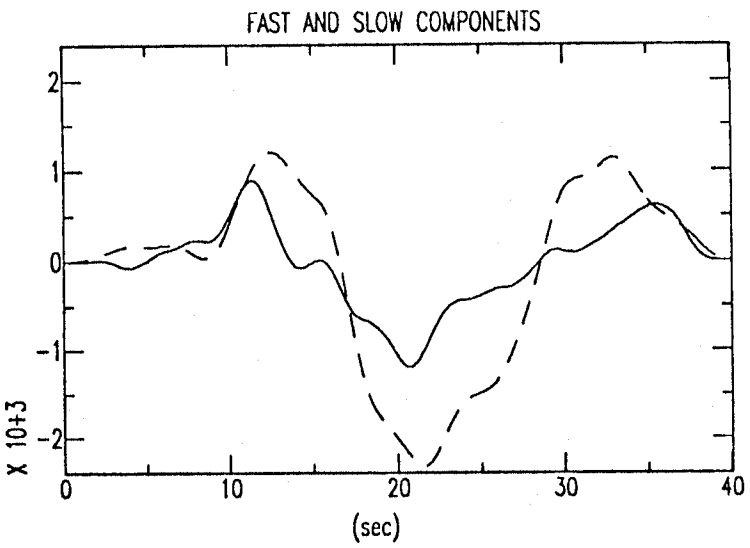
FAST AND SLOW COMPONENTS
X 10+3
(sec)

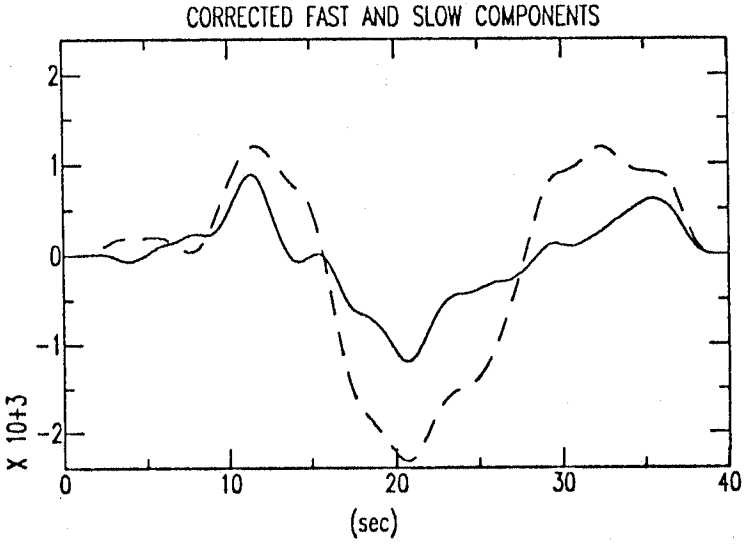
CORRECTED FAST AND SLOW COMPONENTS
X 10+3
(sec)

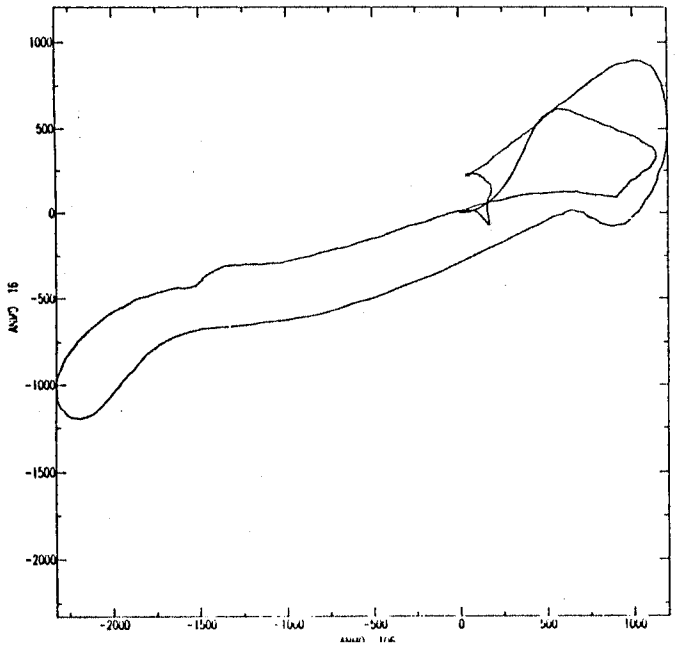

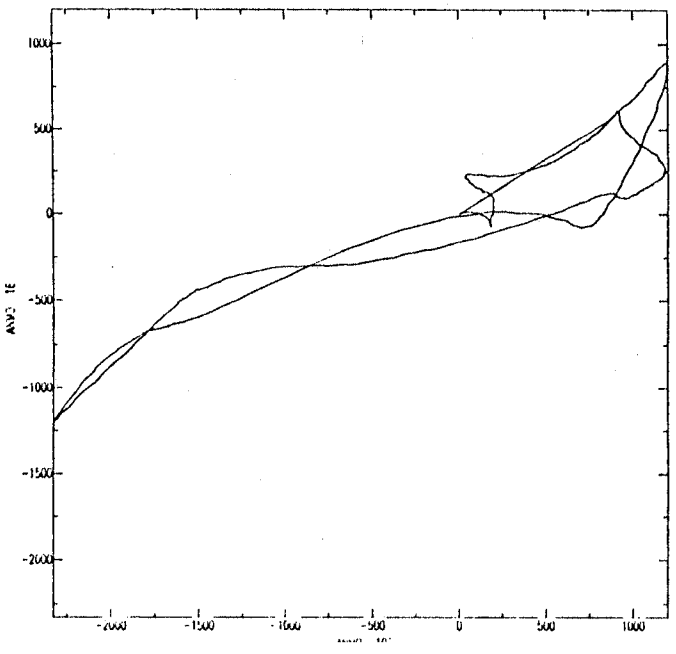

APPENDIX 3

This appendix contains the Fortran Code used to compute SKS splitting parameters : ϕ and δt .

```
c*************************************************************************
c                                                                        *
c    This code is written to compute                                     *
c                                                                        *
c    SHEAR WAVE SPLITTING PARAMETERS:  ϕ and δt                          *
c                                                                        *
c    from SKS data  using the method of Silver and Chan, 1988            *
c                                                                        *
c    Written by Serdar  Ozalaybey                                        *
c                                                                        *
c    August 31 1990                                                      *
c                                                                        *
c    Revised  in  September 3  1990                                      *
c                                                                        *
c*************************************************************************

     dimension cmp1(2000),cmp2(2000),x(2000),y(2000)
     dimension xx(2000),yy(2000)
     dimension tre(500,500)
     parameter(npad=2000,nshift=60)
     integer  ny,nd,nh,nm,ns,nm,npts,oun
     real b,e,cmpi,stla,stlo,evlo,evla,gcarc,baz,xaz,yaz,rota
     real caz1,caz2,dt
    character*16 kstnm,kval
    character evid*4,bb*1
    character f1*5
    common /saci/ b,e,cmpi,stla,stlo,evla,evlo,gcarc,baz,
    *ny,nd,nh,nm,ns,nms,kstnm,kval
c
c ... READ  ORIGINAL  HORIZONTAL  COMPONENTS  IN
c
     write(6,*)' TYPE  IN  EVENT  ID  (CHARACTER*4  e.g. e200)'
     read(5,*)evid
c
     bb='2'
     f1 = evid//bb
c
     call sacin(f1,cmp1,npts,dt,caz1)
c
     bb='3'
     f1 = evid//bb
c
     call sacin(f1,cmp2,npts,dt,caz2)
c
     write(6,100)
 100  format('type DROT: ROTATION  SAMPLING  INTERVAL
    *1.,2.,5. or 10.0 degrees')
```

```
      read(5,*)drot
c
      if(drot.eq.1.00) nrot = 180
      if(drot.eq.2.00) nrot =  90
      if(drot.eq.5.00) nrot =  36
      if(drot.eq.10.0) nrot =  18
c
      nro2 = (nrot / 2) + 1
      emin=1.0e10
      emax=1.0e-10
c
c ... START ROTATING ORIGINAL SEISMOGRAMS
c
      nrot  = nrot + 1
c
      do 12 i = 1,nrot
c
        call zero (x,npad)
        call zero (y,npad)
        call zero (xx,npad)
        call zero (yy,npad)
c
        call copy(npts,cmp1,xx)
        call copy(npts,cmp2,yy)
c
        xaz=caz1
        yaz=caz2
        rota = drot * float(nro2-i)
c
        call rotate(xx,yy,rota,npts,xaz,yaz,1)
c
c ... START SHIFTING ROTATED SEISMOGRAMS
c
        do 11 j = 1,nshift
c
        call copy(npts,xx,x)
        call copy(npts,yy,y)
c
        ide = j
c
       call  shift(y,npts,ide)
c
        call rotbaz(x,y,baz,npts,xaz,yaz)
c
        call energy(npts,y,en)
c
        tre(i,j) = en
c
        if(en.ge.emin) goto 123
        emin=en
```

```
      imin=i
      jmin=j
 123  if(en.le.emax) goto 11
      emax=en
      imax=i
      jmax=j
c
 11   continue
c
 12   continue
c
c ... FINDING  FAST  POLARIZATION  DIRECTION  AND  TIME  DELAY
c
     iang   = nro2-imin
     ang    = drot * float(iang)
     idel   = jmin
     delay  = float(idel)*dt
c
c ... SCALE  TRANSVERSE  ENERGY  SPACE
c
     scal = emax
     do 14 i =1,nrot
       do 13 j=1,nshift
         emm = tre(i,j)
 13      tre(i,j) = (emm / scal)*100.0
 14   continue
c
c ... TERMINAL  OUTPUT
c
     oun=6
     write(oun,66)
     write(oun,77)
     write(oun,67)kstnm,evid
     write(oun,78)
     write(oun,66)
     write(oun,79)ang,delay,idel
      write(oun,66)
      write(oun,77)
c
c ... FILE  OUTPUT
c
      oun=7
     open(unit=oun,file='MINOUT')
     write(oun,66)
 66  format(/)
     write(oun,67)kstnm,evid
 67  format(4x,'STNM    = ',a5,2x,'EVENT ID  = ',a4)
     write(oun,68)npts,dt
 68  format(4x,'NPTS    = ',i4,3x,'DELTA    = ',f6.3,' [sec]')
     write(oun,69)baz,gcarc
```

```
69  format(4x,'BAZ    = ',f5.1,2x,'GCARC  =',f6.2)
    write(oun,66)
    write(oun,77)
77  format(80('*'))
    write(oun,66)
    write(oun,78)
78  format(4x,'MINIMUM  TRANSVERSE  ENERGY  FOUND FOR ')
    write(oun,66)
    write(oun,79)ang,delay,idel
79  format(4x,'FAST ANGLE = ',f6.2,3x,'DELAY TIME = ',f5.2,1x,'sec.',
   *3x,'[',i4,']')
    write(oun,80)emin,tre(imin,jmin),imin,jmin
80  format(4x,'MIN ENERGY COEFF. = ',e15.4,3x,'NORMALISED = ',
   *f10.5,/,4x,'IMIN =',i5,3x,' JMIN = ',i5)
   write(oun,81)emax,tre(imax,jmax),imax,jmax
81  format(4x,'MAX ENERGY COEFF. = ',e15.4,3x,'NORMALIZED = ',
   *f10.5,/,4x,'IMAX =',i5,3x,' JMAX = ',i5)
    write(oun,66)
   write(oun,82)nrot,drot,nshift,dt
82  format(4x,'# OF ROTATIONS = ',i3,3x,
   *'ROTATION SAMPLE INTERVAL = ',f5.1,/,
   *4x,'# OF SHIFTS   = ',i3,3x,'SAMPLING INTERVAL = ',f6.3)
    write(oun,66)
   write(oun,77)
c
c ... WRITE  OUT TRANSVERSE  ENERGY  SPACE MATRIX
c
    write(oun,83)
 83 format(32(/))
    tre(imin,jmin)= -1
    tre(imax,jmax)= -9
   write(oun,84)(j,j=1,nshift)
 84  format(6x,60(i2))
    do 15 i =1,nrot
      rota=float((nro2-i))*drot
     write(oun,85)rota,(int(tre(i,j)),j=1,nshift)
 15  continue
 85 format(f5.1,1x,60(i2))
    close(unit=oun)
    stop
    end
```

```
c
c ************************ SACIN ************************************
c
c   READ SAC DATA INTO A FORTRAN CODE
c
c ********************************************************************
c
   subroutine sacin(fle,dat,npts,dt,cmpaz)
c
   parameter(max=2000)
    integer ny,nd,nh,nm,ns,nm
   real b,e,cmpi,stla,stlo,evlo,evla,gcarc,baz
   character*16 kstnm,kval
   character*5 fle
   common /saci/ b,e,cmpi,stla,stlo,evla,evlo,gcarc,baz,
  *ny,nd,nh,nm,ns,nms,kstnm,kval
c
   dimension dat(1)
c
   call rsac1(fle,dat,npts,beg,del,max,nerr)
c
    if(nerr.eq.0) goto 999
c
    write(6,*)' ATTENTION MAX DIMENSION IS EXCEEDED,/,
   *  TERMINATION .... '
    return
c
999 call getfhv('delta',dt,nerr)
    call getfhv('b',b,nerr)
    call getfhv('e',e,nerr)
    call getfhv('cmpinc',cmpi,nerr)
    call getfhv('cmpaz',cmpaz,nerr)
    call getfhv('stla',stla,nerr)
    call getfhv('stlo',stlo,nerr)
    call getfhv('evla',evla,nerr)
    call getfhv('evlo',evlo,nerr)
    call getfhv('gcarc',gcarc,nerr)
    call getfhv('baz',baz,nerr)
    call getnhv('nzyear',ny,nerr)
    call getnhv('nzjday',nd,nerr)
    call getnhv('nzhour',nh,nerr)
    call getnhv('nzmin',nm,nerr)
    call getnhv('nzsec',ns,nerr)
    call getnhv('nzmsec',nms,nerr)
    call getnhv('npts',npts,nerr)
    call getkhv('kstnm',kstnm,nerr)
    call getihv('iztype',kval,nerr)
    return
    end
```

```
c
c ************************ SACOU ************************************
c
c   WRITE DATA IN SAC FORMAT FROM A FORTRAN CODE
c
c ********************************************************************
c
      subroutine sacou(fil,dat,npts,dt,cmpaz)
c
       integer ny,nd,nh,nm,ns,nm
      real b,e,cmpi,stla,stlo,evlo,evla,gcarc,baz
      character*16 kstnm,kval
      character*4 fil
      common /saci/ b,e,cmpi,stla,stlo,evla,evlo,gcarc,baz,
       *ny,nd,nh,nm,ns,nms,kstnm,kval
c
       dimension dat(1)
c
       call newhdr
       call setfhv('delta',dt,nerr)
       call setfhv('b',b,nerr)
       call setfhv('e',e,nerr)
       call setnhv('nzyear',ny,nerr)
       call setnhv('nzjday',nd,nerr)
       call setnhv('nzhour',nh,nerr)
       call setnhv('nzmin',nm,nerr)
       call setnhv('nzsec',ns,nerr)
       call setnhv('nzmsec',nms,nerr)
       call setnhv('npts',npts,nerr)
       call setfhv('cmpinc',cmpi,nerr)
       call setfhv('cmpaz',cmpaz,nerr)
       call setfhv('stla',stla,nerr)
       call setfhv('stlo',stlo,nerr)
       call setfhv('evla',evla,nerr)
       call setfhv('evlo',evlo,nerr)
       call setfhv('gcarc',gcarc,nerr)
       call setfhv('baz',baz,nerr)
       call setkhv('kstnm',kstnm,nerr)
       call setihv('iztype',kval,nerr)
c
       call wsac0(fil,xdummy,dat,nerr)
c
        return
        end
```

```
c
c ************************ ROTATE ***********************************
c
c   ROTATE  TWO  ORTHOGONAL  COMPONENTS  THROUGH
c
c   REQUESTED  ANGLE  AND  POLARITY
c
c ********************************************************************
c
      subroutine rotate(x,y,ang,npts,azx,azy,kp)
c
      dimension x(1),y(1)
      rad(deg) = deg / 57.295779
      azx = azx + ang
      azy = azy + ang
      angr = rad(ang)
      s = sin(angr)
      c = cos(angr)
c
      do 10 i = 1,npts
        xc = x(i)*c + y(i)*s
        yc =-x(i)*s + y(i)*c
        x(i) = xc
 10     y(i) = yc
c
        if(kp.eq.-1) then
          do 11 i = 1,npts
 11          y(i)=-y(i)
            azy=180-azy
        else
        endif
      return
      end
```

```
c
c ************************ ROTBAZ ****************************************
c
c   ROTATE TWO ORTHOGONAL COMPONENTS TO BACKAZIMUTH
c
c ************************************************************************
c
    subroutine rotbaz(x1,x2,baz,npts,az1,az2)
c
c ... Rotates horizontal components, x1&x2 into radial&transverse components
c ... given backazimuth : baz
c ... and their orientations : az1 , az2
c ... Radial is positive away from the source
c ... Transverse is positive clockwise from + radial direction
c
    dimension x1(1),x2(1)
c
    rad(deg)=deg / 57.295779
    azck = az1 + 90.0
    diff = abs(azck-az2)
    if(diff.lt.0.01) goto 1
    if(diff.lt.179.)then
      write(6,*)' PROBLEM IN ROTATION '
      return
    else
    endif
 1  aa=sin(rad(baz)-rad(az1))
    bb=cos(rad(baz)-rad(az1))
    do 4 i = 1,npts
      radial = - x1(i)*bb - x2(i)*aa
      transv =   x1(i)*aa - x2(i)*bb
      x1(i)=radial
      x2(i)=transv
 4  continue
    return
    end
```

```
c ******************************  ZERO  ************************************
c
c                          ZERO  OUT  AN  ARRAY
c
c ***************************************************************************
c
      subroutine zero(x,lx)
c
      dimension x(1)
      data lunout/6/
c
      if (lx.le.0) go to 100
      do 20 i=1,lx
   20 x(i) = 0.0
c
      return
c
  100 write(lunout,6010) lx
 6010 format(1x,'*****error in subroutine zero***length of array x ',
     $           'was set to ',i8,' must be > 0')
      return
      end
c
c ************************ SHIFT  ***********************************
c
c                  SHIFT  AN  ARRAY
c
c ***************************************************************************
c
      subroutine shift(x,lx,ish)
c
c ... shift moves data in array x by ishft positions
c ... positive value of ishft moves data up the array : advance
c ... negative value of ishft moves data down the array : delay
c ... open holes are filled with zeroes
c ... data shifted off the ends will be lost
c
      dimension x(1)
c
      ishft = - ish
c
c ... check shift direction
c
      if (ishft.ge.0) then
c
c ... data will be shifted down the array : delay
c
        istp = lx - ishft
        do 100 i=1,istp
          k = lx + 1 - i
```

```
      x(k) = x(k-ishft)
 100    continue
      do 110 i=1,ishft
 110    x(i) = 0.0
     else
c
c ... data will be shifted up the array : advance
c
      istp = lx + ishft
      do 200 i=1,istp
       x(i) = x(i-ishft)
 200    continue
      istrt = istp + 1
      do 210 i=istrt,lx
 210    x(i) = 0.0
c
    endif
    return
    end
c
c ************************ COPY ***********************************
c
c          COPY AN ARRAY ONTO A NEW ARRAY
c
c ******************************************************************
c
    subroutine copy(np,x1,x2)
c
    dimension x1(1),x2(1)
    do 555 i =1,np
 555    x2(i)=x1(i)
    return
    end
c
c ************************ ENERGY *********************************
c
c          COMPUTE ENERGY OF AN ARRAY
c
c ******************************************************************
c
    subroutine  energy(nps,cc,sum)
c
    dimension cc(1)
    sum = 0.0
    do 666 i=1,nps
      tsq = cc(i)*cc(i)
      sum = sum + tsq
 666 continue
    return
    end
```